Fall 10-1-2021

Mechanisms of Pierce's disease resistance in grapevine (Vitis vinifera L.): from xylem structure to whole plant function

Ana Clara Fanton
Yale University Graduate School of Arts and Sciences, anaclarafanton@gmail.com

Abstract

Mechanisms of Pierce's Disease Resistance in Grapevine (*Vitis vinifera* L.): from Xylem Structure to Whole Plant Function

Ana Clara Fanton Borges

2021

Xylella fastidiosa (*Xf*) is a xylem-dwelling bacterium that causes Pierce's disease (PD) in grapevines (*Vitis vinifera* L.), and disease in a range of other ecologically and economically important woody plants. To successfully colonize the xylem network, *Xf* cells accumulate on the vessel walls and form a biofilm. The biofilm contains cell wall-degrading enzymes, allowing the bacteria to breach the intervessel pit membranes. Thus, *Xf* can move from one vessel to another and colonize the xylem network. Degraded intervessel pit membranes and the production of tyloses in response to the presence of *Xf* likely contribute to significant declines in both hydraulic conductivity and resistance to drought-induced embolism spread. Indeed, *Xf*-infected grapevines typically display a range of symptoms that are often associated with water transport dysfunction.

Despite the consensus that PD susceptibility is associated with *Xf* multiplication and systemic spread within the xylem network, there significant gaps in our understanding of the relationships between xylem structure and function that allow for *Xf* establishment and colonization still remain. For instance, although *Xf* can breach pit membranes to move from one vessel to another, the consequences of the breakdown of pit membranes within the context of embolism spread and

hydraulic conductivity, and the subsequent implications for whole-plant physiological decline, remain inconclusive. Furthermore, the physical structure of the xylem network, i.e. the spatial distribution of xylem connections that might facilitate the spread of *Xf*, are largely unknown because of the complex, three-dimensional nature of the network.

In my dissertation research, I explored the roles of the xylem structure and function related to the mechanisms of PD resistance. Throughout my work, I applied a holistic approach, coupling anatomical and physiological measurements across different grapevine genotypes with different levels of PD resistance -- from non-cultivated North American species to commercial European vinifera cultivars and their hybrids.

In the first chapter, I tested the hypothesis where if the 3D structure of the xylem network connectivity plays a significant role in *Xf* spread, then PD resistant grapevine genotypes should have fewer total connections in the lateral and radial directions, which thereby limits the total number of pathways. Given that the *Xf* spread is essentially dependent on the intervessel connections, comparing the number and orientation of connections was a logical step in the fundamental understanding of this host-pathogen relationship. The chapter concludes, however, that there was limited evidence to support this hypothesis, and network connectivity does not appear to be strongly correlated with PD resistance and *Xf* spread. While network connectivity in the radial and lateral directions is somewhat variable within the genus *Vitis*, no clear trends emerged linking connectivity with resistance to PD.

In the second chapter, I investigated the consequences of the extracellular cell wall-degrading enzyme released by *Xf* on pit membrane integrity and the downstream effects on water transport. The enzymatic breakdown of the pit membranes was relatively small, less than 10% of the pit aperture area, but enough to weaken pit membrane resistance to air-seeding by introducing pores into the membrane. Not only would larger pore diameters facilitate *Xf* movement, but they would subsequently increase the vulnerability of those vessels to drought-induced embolism spread. These factors would significantly affect the water transport capacity of infected grapevines and put them at greater risk to the effects of drought.

In the third chapter, my objective was to determine the key physiological mechanisms that lead to mortality in the *Xf* infection process. This chapter reveals the mechanistic cascade of events that occur after *Xf* inoculation, with a coordinated decline in hydraulic conductivity, photosynthesis, and starch storage in PD susceptible grapevine genotypes. The results support the theory that hydraulic failure and carbon starvation underlie plant mortality resulting from PD.

My dissertation explored the roles of the xylem structure and function on the PD mechanisms of resistance. Collectively, this work (1) identifies the variability in 3D xylem network traits in six different *Vitis* genotypes, representing the most complete analysis of its type for any plant group; (2) reveals that in young shoots the axial pathway appears to be the most important in determining the long-distance movement and systemic spread of *X*f in the xylem network, (3) and provides a more robust, mechanistic understanding of the timing and sequence of

events from initial *Xf* inoculation to ultimate death, as well as the variability in this mortality sequence in resistant and susceptible genotypes. As we do not have an effective remedy against the *Xf* bacterium, a more accurate understanding of how some grapevines resist to the infection process is one piece of this very important puzzle.

Mechanisms of Pierce's Disease Resistance in Grapevine (*Vitis vinifera* L.):

from Xylem Structure to Whole Plant Function

A Dissertation

Presented to the Faculty of the Graduate School

of

Yale University

in Candidacy for the Degree of

Doctor of Philosophy

By

Ana Clara Fanton Borges

Dissertation Director: Craig R. Brodersen

December 2021

Table of Content

List of Tables and Figures

Acknowledgements

First, I would like to thank my committee. My Advisor, Craig Brodersen for teaching me to navigate the complex world of academic publishing, for always promptly answering my questions, and for letting me take on a project that required BSL-2 certification in a lab new to disease. Andrew McElrone, thank you for opening the door to this Ph.D. and for showing me the vessel 3D network images that took me here. Graeme Berlyn, for all your kind words in the greenhouse and for the countless hours you spent helping me to run my large sample of Rubisco.

My time in graduate school was enriched by the friendship, support, and guidance of my colleagues in the several lab groups I have received through my Ph.D. years. Whether we spent time prolonging our lives on coffee breaks, hikes, and travels, or just banging our heads against lab equipment and computer screens: Aleca Bursuk, Cameron Musser, Joseph Zailaa, Julia Monk, Leila Fletcher, Martin Bouda, Meredith Martin, Morgan Furze, Rob Buchkowski, and Santiago Trueba. I am special grateful to Adam Roddy, Juan Penagos-Zuloaga, and Kyra Prats for always being there when I was lost. Furthermore, I would like to thank you Annise Dobson, Danica Doroski, and Eli Ward for the weekly dose of friendship and support on our dog hikes. I could not forget to mention, Adriana Rubinstein, thank you for all the help with endless microscope slides and for encouraging me when I needed cheering on.

I am grateful to my family support and specially to my sister, Ana Julia Fanton Borges, for always being kind and patiently listening to me on endless phone calls. An especially enormous thank you for my therapist, who changed my life. I also want to thank my dog, Rubisco, who literally sat next to me while I did data analyses and wrote this dissertation. Finally, I want to thank my husband, Peter Marcouillier, this work truly would not have been possible without his love, patience, and support.

Dissertation Overview

Xylella fastidiosa (*Xf*; Wells et al., 1987) is a xylem-limited bacterium transmitted by sap-feeding hemipteran insects (e.g., sharpshooters and spittlebugs; (Redak et al., 2004). *Xf* causes diseases in economically important crops, including grapevines (Pierce's Disease), citrus (Citrus Variegated Chlorosis), coffee (Coffee Leaf Scorch), peach (Phony Peach Disease) and olive (Olive Quick Decline Syndrome), and other ecologically important species, such as *Quercus* spp., *Nerium* spp. and *Acer* spp. (EFSA, 2020). Pierce's Disease (PD) of grapevine (*Vitis vinifera* L.) is chronic in the USA, and is responsible for the limited production of European vinifera wine grapes in the Southern States, and has led to significant yield declines in California vineyards (Hopkins and Purcell, 2002).

After *Xf* is introduced into a xylem vessel by sap-feeding insect vectors, it migrates within the transpiration stream or against it by pili-movement (Meng et al., 2005). Given that a vessel has a finite surface area, *Xf* cells accumulate within the intervessel pit fields in vessel endings and lateral walls, where they develop a biofilm that produces extracellular cell wall-digesting enzymes that breach intervessel pit membranes (Roper et al., 2007; Ingel et al., 2019). The bacteria can then migrate between adjacent vessels, colonizing the xylem network. The ability of *Xf* to multiply and migrate long distances through the xylem network is believed to be a key weakness of susceptible grapevines, as PD-

susceptible genotypes have been shown to have bacterial cells present further from the inoculation site when compared to PD-resistant genotypes (Krivanek and Walker, 2005; Baccari and Lindow, 2011; Sun et al., 2013). The overall redundancy, tortuosity, and resistance of the pathway that *Xf* cells must traverse when spreading through the xylem network should, therefore, influence the ability of the bacterium to become systemic.

Symptomatic grapevines typically show hydraulic transport dysfunctions, with differences in the genotype or the level of PD-resistance, yet PD-susceptible genotypes generally have a greater hydraulic conductivity reduction (Sun et al., 2013; Deyett et al., 2019). While hydraulic conductivity reductions have been associated with xylem occlusions, such as air-embolisms and tyloses (Sun et al., 2013; Pérez-Donoso et al., 2016), the implication of this hydraulic decline at the whole organism level and the mechanisms behind grapevines plants mortality remains inconclusive.

When I started my dissertation, I set out to explore these unresolved questions regarding the xylem structural traits and hydraulic transport dysfunctions that lead to PD progression and, consequently, plant mortality. My overarching goal in this dissertation is to explore the roles of the xylem structure and function on the PD mechanisms of resistance. I have applied a resistance/susceptibility framework to study the (1) the role of the 3D structure of the xylem network connectivity plays on the *Xf* cells spread, (2) the consequences of the enzymatic breakdown on the xylem hydraulic transport safety, and (3) the key physiological mechanisms behind grapevines mortality due to *Xf*-infection.

My first chapter focuses on the 3D structure of the xylem network connectivity and its implications for xylem-dwelling pathogen movement. PD resistance is associated with both lower bacterial cell count and the restriction of movement within the xylem. While xylem anatomy is not the only component of PD resistance, it was a logical part of a resistance mechanism that can easily be targeted and compared, thus building on a growing body of knowledge characterizing PD resistance traits. The aim of this work was to investigate whether there is a link between the number and orientation of the intervessel connections with PD resistance since the *Xf* systemic spread is essentially dependent on these connections. While I found limited evidence correlating these xylem traits to PD resistance, I found that the 3D organization of the xylem is instead highly conserved within the genus *Vitis*.

In my second chapter (published in *Plant Physiology*), I explored the effects of a cell wall-degrading enzyme on the pit membrane integrity and the consequences of this breakdown on xylem water transport. *Xf* produces a biofilm on the vessel walls, and then secretes extracellular cell wall-degrading enzymes onto the intervessel connections --breaching the pit membranes -- and thus is able to move from one vessel to another. By isolating a single component of this pathosystem -- pit membrane breakdown – my goal was to disentangle the mechanisms behind known declines in stem water transport following Xf inoculation and the subsequent development of symptoms in grapevines. Although the enzymatic breakdown resulted in seemingly small proportions of the total pit area, less than 10% of the pit aperture area, the enzymatic activity resulted in the

production of pores in the pit membrane large enough to significantly decrease the resistance of the membrane to embolism spread. Introducing these pores into the membrane shifted pit membrane resistance to air-seeding to a more vulnerable state. Thus, the degradation of the pit membranes that produces holes of sufficient diameter to allow the bacteria to move between vessels leaves in its wake a more porous membrane that which would be more vulnerable to embolism spread during drought. Infected plants would then contend with not only an *Xf* infection, but also be at a greater risk to the effects of drought, which may help explain why PD symptoms often overlap with those of drought and hydraulic dysfunction.

In my third chapter (currently *under review*), I addressed the fundamental question: What is the mechanistic sequence of events that leads to grapevine mortality after *Xf*-inoculation? By applying the carbon-starvation and hydraulic-failure frameworks, I tested the hypothesis that susceptible grapevines would show a coordinated decline in stem hydraulics, photosynthesis, and starch accumulation in response to *Xf*-inoculation comparing to control and PD-resistant grapevines. The results show a conclusive relationship between *Xf*-infection and a coordinated decline in photosynthesis, starch storage, and stem hydraulics only in the PD-susceptible grapevines genotypes. This work builds on a growing body of knowledge characterizing *Xf*-induced mortality as a coordinated whole-plant response to the *Xf*-infection process.

References

Baccari C, Lindow SE (2011) Assessment of the process of movement of *Xylella fastidiosa* within susceptible and resistant grape cultivars. Phytopathology 101: 77–84

Deyett E, Pouzoulet J, Yang J -I., Ashworth VE, Castro C, Roper MC, Rolshausen PE (2019) Assessment of Pierce's disease susceptibility in *Vitis vinifera* cultivars with different pedigrees. Plant Pathol 68: 1079–1087

EFSA (2020) Update of the *Xylella* spp. host plant database. EFS2. doi: doi: 10.2903/j.efsa.2020.6114

Hopkins DL, Purcell AH (2002) *Xylella fastidiosa*: cause of Pierce's disease of grapevine and other emergent diseases. Plant Disease 86: 1056–1066

Ingel B, Jeske DR, Sun Q, Grosskopf J, Roper MC (2019) *Xylella fastidiosa* endoglucanases mediate the rate of Pierce's disease development in *Vitis vinifera* in a cultivar-dependent manner. MPMI 32: 1402–1414

Krivanek AF, Walker MA (2005) *Vitis* resistance to Pierce's disease is characterized by differential *Xylella fastidiosa* populations in stems and leaves. Phytopathology 95: 44–52

Meng Y, Li Y, Galvani CD, Hao G, Turner JN, Burr TJ, Hoch HC (2005) Upstream migration of *Xylella fastidiosa* via pilus-driven twitching motility. Journal of Bacteriology 187: 5560–5567

Pérez-Donoso AG, Lenhof JJ, Pinney K, Labavitch JM (2016) Vessel embolism and tyloses in early stages of Pierce's disease. Australian Journal of Grape and Wine Research 22: 81–86

Redak RA, Purcell AH, Lopes JRS, Blua MJ, Mizell III RF, Andersen PC (2004) The biology of xylem fluid–feeding insect vectors of *Xylella fastidiosa* and their relation to disease epidemiology. Annual Review of Entomology 49: 243–270

Roper MC, Greve LC, Warren JG, Labavitch JM, Kirkpatrick BC (2007) *Xylella fastidiosa* requires polygalacturonase for colonization and pathogenicity in *Vitis vinifera* grapevines. MPMI 20: 411–419

Sun Q, Sun Y, Walker MA, Labavitch JM (2013) Vascular occlusions in grapevines with Pierce's disease make disease symptom development worse. Plant Pathology 161: 1529–1541

Wells JM, Raju BC, Hung H-Y, Weisburg WG, Mandelco-Paul L, Brenner DJ (1987) *Xylella fastidiosa* gen. nov., sp. nov: gram-negative, xylem-limited,

fastidious plant bacteria related to *Xanthomonas* spp. International Journal of Systematic Bacteriology 37: 136–143

Chapter 1

Three-dimensional xylem network connectivity of six grapevines (*Vitis* spp.): implications for xylem-dwelling pathogen movement

Abstract

PREMISE OF THE STUDY: *Xylella fastidiosa* (*Xf*) is the xylem-dwelling bacterium associated with Pierce's disease, responsible for declines in productivity in agriculturally important species like grapevines (*Vitis vinifera* L.). The ability of *Xf* to multiply and migrate long distances through the xylem network is believed to be a key weakness of susceptible grapevines. The systematic spread of *Xf* is then necessarily dependent on the number and orientation of the interconduit connections within the xylem network.

METHODS: We used high-resolution X-ray micro-computed tomography (microCT) imaging to identify and describe the type, number, and spatial orientation of the intervessel connections for six different grapevine genotypes with different levels of PD-resistance (four PD-resistant and two PD-susceptible). Our objective was to investigate whether there is a link between the number and orientation of the intervessel connections with PD resistance.

KEY RESULTS: Number of pit fields varied from 8 ±1 SD to 22 ±9 SD connections mm^{-3}; and the number of vessel relays varied from 0.28 ± 0.10 to 0.57 ±0.16 elements mm^{-3} among the six genotypes. Despite the variability in xylem traits among the studied genotypes, there was no link with PD resistance.

CONCLUSIONS: While we found limited evidence correlating number and orientation of the intervessel connections to PD resistance, we found that the 3D organization of the xylem is instead highly conserved within the genus *Vitis*.

Introduction

Xylem tissue transports water through a network of pipe-like cells from the roots to the leaves. While bulk flow occurs predominantly in the axial direction, anatomical configurations within xylem networks of plants like grapevine (*Vitis* spp.) provide both radial and lateral pathways for water movement (Brodersen et al., 2013a; McElrone et al., 2021; Wason et al., 2021). These alternative pathways are thought to increase the redundancy of the network and allow for water to be rerouted around dysfunctional sections of the xylem (Tyree and Zimmermann, 2002), where drought-induced embolism (Choat et al., 2018) and xylem-dwelling pathogens (Newbanks, 1983; Pérez-Donoso et al., 2016) can disrupt the flow of water.

Most water flowing between adjacent xylem vessels occurs through intervessel pits, minute perforations in the lateral walls bearing a thin pit membrane that represents a physical barrier to flow (Choat et al., 2008). While water moves readily through the tortuous nanometer-scale pit membrane matrix (Kaack et al., 2019), this interface can temporarily prevent the movement of both air-embolism and xylem-dwelling pathogens. These connections and their spatial distribution have recently been shown to strongly influence the overall flow of water through the xylem network (Loepfe et al., 2007; Bouda et al., 2019), how drought-induced embolism spreads through the network (Brodersen et al., 2013b; Wason et al., 2021) and how traits at the cellular level scale up to influence canopy physiology (McElrone et al., 2021). Within the xylem of *Vitis* a recently described anatomical feature can link adjacent vessels via vessel relays, chains of short and narrow

diameter vessel elements, which provide additional complexity to the possible pathways for the propagation of embolisms or xylem-dwelling organisms through the network (Brodersen et al., 2013a). Such features may result in increasing xylem network redundancy resulting from increased intervessel contact, but may also increase the susceptibility to the spread of both air-embolism and xylem-dwelling pathogens since they also depend on the same pathways (Tyree and Zimmermann, 2002; Newman et al., 2003; Brodersen et al., 2013b). Analyzing xylem networks should therefore allow us to better understand how the distribution of intervessel connections influences the movement of air-embolisms and xylem-dwelling pathogens, and consequently, the ability to respond or acclimate to biotic and abiotic stresses.

The systematic spread of xylem-dwelling pathogens is necessarily dependent on the number and orientation of the interconduit connections within the xylem network. *Xylella fastidiosa* (*Xf*; Wells et al., 1987) is a bacterium transmitted by insects that feed on xylem sap (e.g., leafhopper sharpshooters; Redak et al., 2004) causing Pierce's Disease (PD) in grapevines (*Vitis vinifera* L.). In the plant, *Xf* resides exclusively in the xylem conducting elements since it lacks a Type III secretion system (a structure that delivers protein effectors into living parenchyma cells; Chatterjee et al., 2008). Given that a vessel has a finite surface area, *Xf* cells accumulate within the intervessel pit fields in vessel endings and lateral walls, where they develop a biofilm containing cell wall-digesting enzymes that breaches intervessel pit membranes (Roper et al., 2007; Ingel et al., 2019), creating pores large enough to allow the individual bacterial cells to move across

the membrane. Once the bacteria migrate between adjacent vessels, they can colonize the xylem network. The ability of *Xf* to multiply and migrate long distances through the xylem network is believed to be a key weakness of susceptible grapevines, as PD-susceptible genotypes have been shown to have bacterial cells present further from the inoculation site when compared to PD-resistant genotypes (Krivanek and Walker, 2005; Baccari and Lindow, 2011; Sun et al., 2013). Indeed, Riaz et al., (2008) suggested that a yet unidentified anatomical differences between grapevines genotypes may play a role in their differential resistance to PD.

Given that PD-resistance has been associated with both lower bacterial cell count levels and restricted movement within the xylem, our objective was to investigate whether there is a link between the xylem network connectivity and reported resistance to the *Xf* spread and PD symptoms. Recently, Fanton and Brodersen (2021) found evidence that artificial pit membrane degradation, as a proxy for *Xf* mechanisms of spread, affected PD-susceptible and resistant grapevine genotypes and highlighted the implication to for both the spread of bacteria and embolism in the axial direction. Subtle differences in the maximum vessel length distributions and pit membrane properties (Sun et al., 2011; Sun et al., 2017; Fanton and Brodersen, 2021) appear to play a role in how easily *Xf* may spread over long distances, but possibilities for radial and lateral movement through the network is not well understood. This knowledge gap exists because of the complex, three-dimensional (3D) nature of grapevine xylem networks.

While recent work has established a new suite of tools for studying xylem networks in 3D (Brodersen et al., 2011; Lee et al., 2013; Wason et al., 2021), our understanding of the variability within the genus *Vitis* is still limited. The aforementioned studies utilize synchrotron based X-ray micro-computed tomography (microCT) as a means of obtaining digital serial sections of the xylem networks, in combination with recently developed software packages for extracting and quantifying the spatial distribution of vessels and their connections (Brodersen et al., 2011). This methodology significantly reduces the overall time involved in analyzing networks using previously established methods employing serial sectioning and light microscopy (Zimmermann and Tomlinson, 1966; Chatelet et al., 2006).

We aimed to identify key anatomical traits that could support the systemic spread of the xylem-dwelling pathogen *Xf*. We dedicated special attention to the radial and tangential pathways by analyzing vessel networks of six grapevine genotypes with different PD resistance levels, thereby extending the work on this same group of genotypes studied in (Fanton and Brodersen, 2021). We developed the study with two working hypotheses. First, if *Xf* movement is dependent on radial or lateral movement in the stem, then PD-resistant genotypes would have fewer network connections, thereby limiting *Xf* systemically spread. Second, more connections could have a similar effect, where multiple points of resistance in the form of the physical barrier represented by the pit membranes, could also prevent the rapid spread of *Xf* through the network. Finally, the null hypothesis was tested, where radial and lateral connections in the xylem have no effect or correlation with

susceptibility, and other traits (including axial pathways like vessel length or biochemical immune responses) play a greater role. While xylem anatomy would not be the only component of PD-resistance, it is a logical part of resistance that can easily be targeted and compared with new methodology, and can build on a growing body of knowledge characterizing the PD resistance traits (Sun et al., 2011; Brodersen et al., 2013a; Sun et al., 2013; Fanton and Brodersen, 2021).

For this study, we selected grapevines with different degrees of reported *Xf*-resistance from discrete genetic pools: two *Xf*-resistant genotypes from the Pierce's Disease breeding program, (1) American native b43-17 *Vitis arizonica/candicans* (Krivanek et al., 2006) and its daughter (2) hybrid 502-20, which is 88% *V. vinifera* cv. Chardonnay (A. Walker, 2016; personal communication). We then selected two commercial *Xf*-resistant hybrids with *Vitis aestivalis* parentage, (3) Lenoir (syn. Jacques or Black Spanish) and (4) Blanc du Bois, which are both popular in the American Southern wine industry where PD is problematic (Krivanek and Walker, 2005; Buzombo et al., 2006). Lastly, we selected two commercial wine grape varieties with reported *Xf*-susceptibility, *Vitis vinifera* L. cv. (5) Syrah and (6) Chardonnay (Varela et al., 2001).

Materials and Methods

1) Plant material and sample preparation

We selected six grapevines (*Vitis* spp.) genotypes with different reported degrees of resistance to PD: four PD-resistant (1) b43-17 *Vitis arizonica/candicans* hereafter designated as Arizonica, (2) Hybrid 502-20, 88% V.

vinifera cv Chardonnay, hereafter designated as Hybrid, (3) Lenoir and (4) Blanc du Bois; and two PD-susceptible *V. vinifera* L. cv (5) Syrah and (6) Chardonnay. All cuttings were kindly provided by Dr. Andrew Walker (Department of Viticulture and Enology, University of California Davis). The grapevine plants were grown and maintained in a glasshouse on the Yale University campus from self-rooted cuttings in 4 L pots filled with a peat-based growing medium with perlite and vermiculite (Premier Pro-Mix BX, Premier Horticulture Inc). Plants were fertilized with slow-release fertilizer (Scotts Miracle-Gro, Osmocote Plus Outdoor and Indoor, 15-09-12), irrigated daily, and provided with supplemental lighting (1,000 μmol (photons) m^{-2} s^{-1} at the top of canopy) on a 16 h day - 8 h night cycle. The grapevines had same age and were trained with a primary trunk with one vertical cane, a lignified year-old-shoot (one growth ring). We excised the third internode, with mean segment length of 4 $\pm$0.19 cm, from 24 plants and dehydrated them in a drying oven at 70 ^{o}C for 48h, until the samples were dried (n=4 stem segments per genotype).

We used internode segments in this study to avoid (a) terminal vessels that supply water to tendrils, leaves, and developing fruit that frequently occur in the nodes (Chatelet et al., 2006; Brodersen et al., 2011; Brodersen et al., 2013a) and (b) smaller diameter vessels in nodes that lead to a challenging determination of vessel wall boundaries (Brodersen et al., 2011). In addition, large diameter nodes increase scanned volume beyond the field of view for the microCT instrument, and which also extend the computational cost beyond the capabilities of our hardware and software.

2) The 3D xylem network

The dried stem sections were scanned at the X-ray micro-computed tomography (microCT) facility at the Lawrence Berkeley National Laboratory Advanced Light Source, beamline 8.3.2, in Berkeley, CA, USA. Stem segments were scanned at 15 keV yielding series of two-dimensional (2D) projection images captured while the segment was rotated over 180°. The 2D projection images were reconstructed into a 3D data set using TomoPy (Gürsoy et al., 2014) where we averaged reconstructions with and without phase contrast image processing to clearly differentiate between vessel lumen and other stem cell types. The scanned segments lengths were 2.8 ±0.6 SD mm yielding a mean xylem volume of 25 ±10 SD mm^3 (excluding the bark and the pith). The final 3D data sets had a voxel (volumetric pixel element) size of 3.3 μm^3 (Fig. 1 A) and included approximately 860 ±175 (mean ±SD) seamless transverse serial slices that can be viewed in any orientation. While it is possible to measure one long stem and understand the internal variability of that segment (Brodersen et al., 2011; Bouda et al., 2019; Wason et al., 2021), we chose to a greater number of shorter stem samples to better capture the variability between plants of the same genotype, and between genotypes.

The reconstructed microCT images were processed into an anatomically accurate vessel network using Avizo Software 2020.2 (FEI Co., Hillsboro, OR, USA) (Fig. 1 B-D) and custom software (TANAX, described in detail in Brodersen et al., 2011; Lee et al., 2013). Briefly, vessel lumens were segmented

from the surrounding xylem tissue using the “magic wand” tool in Avizo, which is constrained by a user-defined pixel intensity minimum and maximum threshold. This process creates a 3D representation of each vessel lumen, with x, y, and z coordinates for each voxel within the lumen. Once all the vessels were segmented, the vessel network provides a spatially explicit set of coordinates for each vessel, which can be used to determine the spatial relationship between network components. The custom software package TANAX (Brodersen et al., 2011) was used to determine whether adjacent vessels were connected by measuring the distance between their vessel wall boundary voxels. If the intervessel distance was less than 14 µm (e.g., radial, or tangential) for at least 56 µm of axial length the vessels were considered to be connected, and these connections were recorded as a pit field that could be measured as an area of intervessel contact with pitting and the potential for the flow of water between conduits. This threshold was empirically verified for *Vitis* by Brodersen et al., 2011 using a combination of microCT, scanning electron microscopy, and light microscopy. The TANAX software also measured vessel diameters, and the surface area of the connections among two vessels and vessel to vessel relay connections. We also measured the total volume of each scanned segment to normalize traits between samples. We then measured vessel density using the traditional two-dimensional metric (number of vessels per mm^2 of xylem area) from single transverse cross sections, and then compared those values to the total number of vessels found in the entire scanned tissue volume. The TANAX analysis also includes information about the

total number of connections per vessel, similar to the vessel grouping index (Carlquist, 1984) but incorporates all of the connections in the scanned volume.

Xylem vessel relays (here after referred to as relays; Brodersen et al., 2013a) were spatially mapped and characterized by scrolling through the image slices within 3D data sets using Avizo 2020.2, which allowed for virtual slices in any orientation (e.g., transverse and longitudinal). Once a relay was identified, we rendered its volume in 3D and then determined the number of relay elements linking two large-diameter vessels and the distance between bridged vessels. Lastly, the x, y, and z coordinates of the axial center of each chain of relay elements were determined in relation to the stem center and the edge of the pith using the “PointProbe” tool in Avizo. These two reference coordinates were used to compare the spatial distribution of the relays and vessels between scans where the total volume or shape of the pith were variable.

We performed a one-way ANOVA to determine whether the (a) total pit field area, (b) mean vessel diameter and (c) maximum vessel diameter, and (d) number of relays were different among the six grapevine genotypes, followed by a Tukey’s HSD post hoc test. We added xylem volume (segment volume excluding the bark and the pith) for each stem segment as an actional predictor. Variables were considered significant with a $p < 0.05$. Statistical analyses and graphics were prepared in R Studio (Version 1.4.1717) and 3D images were generated with Avizo 2020.2.

Results

Our analysis of the 24 grapevine internodes scanned with microCT (Fig. 1A-D) showed the mean total number of vessels varied from 269 ±30 SD vessels in Lenoir to 377 ±77 SD vessels in Syrah, but no significant difference was found between genotypes, with significant differences in vessels number among the six genotypes (Table 1, p= 0.212). In fact, we found a strong relationship between the number of vessels measured in a single, two-dimensional transverse cross section and the total number of vessels in the entire 3D volume (R^2 = 0.986, p< 0.001; Fig. 2). Within the 2.8 ±0.6SD mm in length of our microCT sections, the majority of the vessels were classified as solitary (60% ±8 SD, p= 0.07; Table 1) followed by vessel pairs (30% ±6 SD, p= 0.109; Table 1) and finally vessels with connections to three or more adjacent vessels (8% ±3 SD, p= 0.126; Table 1) for all genotypes.

We used the variability in stem segment volume scanned with microCT (25.06 ±10 mm^3; mean ±SD across all samples) to determine the relationship between tissue volume and the frequency of detected pit field area. Variability in stem segment volume arose from differences in stem diameter despite using identical aged material from identical positions on the stem (third internode), although it was not significant different across all samples (p= 0.232). We found a positive linear relationship between measured internode volume and pit field area, indicating that pit field distribution in the internode is relatively constant (R^2 = 0.637, p< 0.001; Fig. 3 A). Therefore, we used the total pit field area per mm^3 of xylem volume as a variable to compare whether this xylem network

trait differed among the genotypes. Despite the number of pit fields differ among the genotypes, they were not associated with the PD resistance levels (p= 0.003; Fig. 3 B). B. du Bois (PD- resistant) had 22 ±9 SD connections mm^{-3} (Fig. 3 B; Table 1), which was 50% more than the PD-susceptible Chardonnay (11 ±2 SD connections mm^{-3}, p< 0.05; Fig. 3 B; Table 1), and 64 and 58% greater than the other PD-resistant genotypes, Hybrid (8 ±1 SD connections mm^{-3}, p< 0.05; Fig. 3 B; Table 1) and Lenoir (9 ±2 SD connections mm^{-3}, p< 0.05; Fig. 3 B; Table 1), respectively. Likewise, the differences in pit field area did not correspond to PD resistance (p= 0.0207; Fig. 3 C). The PD-resistant B. du Bois and Lenoir had contrasting outcomes, where B. du Bois had the largest total pit field area of 0.132 ±0.053 SD μm^2 mm^{-3}, 58% greater than Lenoir (p< 0.05; Fig. 3 C, Table 1). However, it is worth to noting that Hybrid and Chardonnay had similar total pit field areas, 0.075 ±0.031 and 0.074 ±0.014 μm^2 mm^{-3} (Fig. 3 C, Table 1), respectively.

Our investigation on the anatomical characteristics of relays revealed the chains of relays elements composed of 2-9 elements connecting two or more vessels radially within a wedge of xylem tissue, or laterally across ray parenchyma (Fig. 4 A-L). The chains of relay elements bridged transverse distances of 35.87 to 544.06 µm (Fig. 5) between pair vessels within xylem sectors delineated by rays (i.e., in the radial direction, Fig 4 A-D) and less frequent across ray sectors (i.e., lateral connections; Fig. 4 E-H). Lateral connections across rays are likely composed of perforated ray cells along with the relay elements (Chalk and Chattaway, 1933; Nagai et al., 1994; Merev et al., 2005). We observed a general trend in which the number of relay elements increased as the distance between

the bridged vessels expanded (R^2 = 0.339, p< 0.05; Fig. 5 A). Mean relay element diameters (RD) were relatively constant among the grapevine genotypes (27.5 ±13.1 SD µm, p= 0.233; Table 1), whereas relay element numbers extended to span increasing distances between bridged vessels. However, we note that some relay elements were not always in a 'conventional' vessel element shape (e.g. straight axial line) and sometimes presented a 'zigzag' shape (term defined by Tyree and Zimmermann, 2002) that would be contorting the large-vessel and increase the bridged distance in a non-proportional way (Fig. 4 I-L and Fig. 5 A). We did find, however, a positive linear relationship between the mean vessel diameter (VD) and RD (R^2 = 0.364, p< 0.05; Fig. 5 B). Despite the mean RD being smaller than the mean VD, their diameter size and proportionality happen in the same fashion.

In grapevine canes (one-year growth ring), the vessels located in both lateral sectors of the stem (Fig. 6 A-B) are associated with water transport to the leaves, tendrils, and fruit clusters, while the dorsal/ventral sectors (Fig. 6 A-B) transport water over longer axial distances and do not generally terminate in the nodes (Chatelet et al., 2006; Brodersen et al., 2011; Brodersen et al., 2013a). Most relays were found in the dorsal or ventral sectors, with fewer relays occurring in the lateral sectors (Fig 6 C-H). This distribution pattern was clearly visualized in the PD-resistant Hybrid and Lenoir (Fig. 6 D-E, respectively); on both genotypes, the presence of relays in the lateral sectors corresponded to 5% and 4% of the total number of relays, respectively. In the PD-susceptible Syrah (Fig. 6 G), the relay distribution appeared to be more homogenous, where the lateral sectors had

20% of relays. The other genotypes, Arizonica, B. du Bois, and Chardonnay, the lateral sectors had ~14% of relays. This concentration of relays in the dorsal/ ventral sectors would produce a more connected xylem network and possibly increase number of potential pathways for *Xf* spread (and other xylem-dwelling pathogens). We found a positive relationship between the total number of relays per unit xylem volume ($R^2 = 0.328$, $p < 0.05$; Fig. 5 C). Grapevine stems with larger xylem volume would hold a greater number of vessel relays, suggesting that the vessel relays are evenly distributed along with the xylem network. For the same reasons, perhaps, the total number of vessel relays per mm^3 did not significantly differ among the grapevine genotypes ($p = 0.208$; Fig 5 D, Table 1). However, it is worth noting, the PD-resistant Arizonica and Hybrid have a divergent number of vessel relays per mm^3 (0.57 ± 0.16 and 0.28 ± 0.10, respectively; Fig 5 D, Table 1), where Arizonica had 51% more vessel relays than Hybrid.

While mean vessel diameters (VD) are not directly linked with *Xf* spread, it is a trait that may influence the *Xf* colonization process. Vessels with large lumen could harbor a greater number of colonies and maintaining bacterial cells in an adhesive state for longer--versus planktonic (non-adhesive) state where they would spread to an adjacent vessel. We found a heterogeneous distribution of VD in each xylem network among the six grapevine genotypes (Fig. 7 A). The mean maximum vessel diameter (MVD) was different among the grapevine genotypes ($p < 0.05$; Fig. 7 B, Table 1). The largest mean MVD we observed in the PD-resistant Arizonica (136.0 ±16 SD µm) and Hybrid (138.5 ±11 SD µm), while

the also PD-resistant Lenoir had the smallest mean MVD (99.9 ±15 SD µm; Fig 8 B, Table 1).

Discussion

Intervessel connections, such as pit fields and xylem relays, are responsible for xylem connectivity, thus critical in maintaining hydraulic transport since they rerouted around dysfunctional part of the network. Our data build on a growing body of knowledge characterizing the 3D xylem network (Brodersen et al., 2013b; Brodersen et al., 2013a; Lee et al., 2013; Bouda et al., 2019; Wason et al., 2021), allowing us to better understand how the distribution of vessel connections influences the movement of water (Bouda et al., 2019), air-embolism spread (Mrad et al., 2018; Mrad et al., 2021; Wason et al., 2021), and xylem-dwelling pathogens (Newbanks, 1983; Fanton and Brodersen, 2021).

Our results show that within the genus *Vitis* several proportionalities among the xylem anatomical traits exist. First, the number of vessels counted in the 3D scanned volumes and measured using 2D transverse images was close to a 1:1 line. The strong relationship between both measurements (Fig. 2) indicates that routine vessel density measurements from 2D slices accurately predict vessel density in the 3D xylem volume, at least for species with long vessels such as grapevines. Species with shorter vessels may require additional transverse sections to capture the total number of vessels and the vessel endings therein. Second, the pit field area (Fig. 3 A) increased with analyzed xylem volume across the 24 samples from the six genotypes. Our data on the number of pit fields and

pit filed area per mm^3 (Fig 3 B-C and Table 1) were consistent with a microCT analysis of a 2.7 mm stem segment of field-grown Chardonnay (16.63 pits mm^{-3} 0.04 μm^2 mm^{-3}; Wason et al., 2021), suggesting that the pit number and area are likely conserved due to the regularity of xylem development in this species. Despite that vessel connections increase as a function of stem length (Wason et al., 2021), the proportion of solitary vessels and vessels with ≥1 connection found here (Table 1), for all grapevines genotypes, were equivalent to a microCT of a 2.7 mm stem segment of Chardonnay (67% and 33%, respectively; Wason et al., 2021). Our method for scanning stem material with microCT and then processing the resulting datasets with custom software still has limitations, with stem diameter and total scanned volume being the primary limitations. Still, the similarity in data generated for Chardonnay growing in two different environments (vineyard vs. greenhouse, California vs. Connecticut) suggest that some xylem traits are highly conserved and show a low degree of plasticity in response to the growing environment.

We found that relays were distributed in the xylem similarly in the six genotypes; they were concentrated in the dorsal/ ventral sectors, with fewer relays occurring in the lateral sectors (Fig. 7). Since the dorsal/ ventral sectors transport water over longer axial distances, this arrangement of relays suggests that they may play a key role in maintaining xylem redundancy and providing alternate pathways for long-distance water transport. Their lower relative abundance in the lateral zones is noteworthy. McElrone et al., (2021) found that by partially removing the canopy on vineyard grown grapevines, water can be transported laterally around the trunk, which is dependent on the lateral connections within the xylem.

That analysis, however, was restricted to trunk xylem, which apparently has a significantly different organization that xylem found in one year old stems. This dichotomy of xylem organization (sectored, less connected xylem in young stems, and more highly integrated xylem in the trunk) suggests that certain traits, such as lateral connections, may be a disadvantage when stems are young, but beneficial in older growth.

The linear relationship between the mean diameter of vessels and relays (Fig. 5) and the uniformity in the relay element diameter among all genotypes (Table 1) suggests that the relay elements are formed by the fusiform cells as part of normal cambial activity. However, further investigation on grapevines' trunks (many growth rings) may reveal if the relays are still present in other growth rings and support the xylem redundancy. Our values on the number of relays per mm^3 were lower than found in other studies that measure the number of relays on longer stems (2.78 relays mm^{-3} in Chardonnay; Wason et al., 2021; and 29 and 23 relays cm^{-1} in Chardonnay and Arizonica, respectively; Brodersen et al., 2013a). Our scanned length was probably too short since the probability of finding intervessel connections via relays increases as a function of sample length (Wason et al., 2021). Nevertheless, this increase in relays would probably happen uniformly to all six genotypes, and the lack of statical significance would remain.

We found limited evidence to support our hypothesis that a link exists between PD-resistance and xylem network properties related to radial and lateral connectivity. Instead, we find that the organization of the xylem is instead highly conserved within the study species, with some exceptions for specific traits. This

negative result decreases the probability that the genes associated with PD resistance, present in the PdR1 region of Arizonica and Hybrid genotypes (Krivanek et al., 2006; Riaz et al., 2008) have any function in concerning xylem characteristic or development.

With the understanding that *Xf* cells do not reach xylem's systemic in the PD-resistant genotypes (Krivanek and Walker, 2005; Baccari and Lindow, 2011; Sun et al., 2013) and that cell-wall degrading enzymes released within the biofilm can degrade the pit membranes regardless of the PD-resistance level (Fanton and Brodersen, 2021). However, the chemical configuration of the pit membranes is different and that could be a temporary barrier to the *Xf* spread (Sun et al., 2017; Ingel et al., 2019). Consequently, the mechanisms of resistance are more like to be connected to the living cells of the xylem, the parenchyma cells, the production of the volatile signaling hormone ethylene (Pérez-Donoso et al., 2007), and the subsequent production of tyloses that follows *Xf* infection (Sun et al., 2013). Future studies on the mechanism of PD resistance should focus on flavonoids or proteins present in the xylem sap, comparing whether a new production of those secondary compounds followed inoculation among different grapevines genotypes.

Acknowledgements

I would like to thank the coauthors: Martin Bouda and Craig R. Brodersen. I thank Adriana Rubinstein for her help with Avizo segmentation.

References

Baccari C, Lindow SE (2011) Assessment of the process of movement of *Xylella fastidiosa* within susceptible and resistant grape cultivars. Phytopathology 101: 77–84

Bouda M, Windt CW, McElrone AJ, Brodersen CR (2019) In vivo pressure gradient heterogeneity increases flow contribution of small diameter vessels in grapevine. Nat Commun 10: 5645

Brodersen CR, Choat B, Chatelet DS, Shackel KA, Matthews MA, McElrone AJ (2013a) Xylem vessel relays contribute to radial connectivity in grapevine stems (*Vitis vinifera* and *V. arizonica* ; Vitaceae). American Journal of Botany 100: 314–321

Brodersen CR, Lee EF, Choat B, Jansen S, Phillips RJ, Shackel KA, McElrone AJ, Matthews MA (2011) Automated analysis of three-dimensional xylem networks using high-resolution computed tomography. New Phytologist 191: 1168–1179

Brodersen CR, McElrone AJ, Choat B, Lee EF, Shackel KA, Matthews MA (2013b) In Vivo Visualizations of Drought-Induced Embolism Spread in *Vitis vinifera*. Plant Physiol 161: 1820–1829

Buzombo P, Jaimes J, Lam V, Cantrell K, Harkness M, McCullough D, Morano L (2006) An American hybrid vineyard in the Texas Gulf Coast: analysis within a Pierce's disease hot zone. Am J Enol Vitic 57: 347–355

Carlquist S (1984) Vessel grouping in dicotyledon wood: significance and relationship to imperforate tracheary elements. Aliso: A Journal of Systematic and Evolutionary Botany 10: 505–525

Chalk L, Chattaway MM (1933) Perforated ray cells. The Royal Society London 113: 82--92

Chatelet DS, Matthews MA, Rost TL (2006) Xylem Structure and Connectivity in Grapevine (Vitis vinifera) Shoots Provides a Passive Mechanism for the Spread of Bacteria in Grape Plants. Annals of Botany 98: 483–494

Chatterjee S, Almeida RPP, Lindow S (2008) Living in two worlds: the plant and insect lifestyles of *Xylella fastidiosa*. Annu Rev Phytopathol 46: 243–271

Choat B, Brodribb TJ, Brodersen CR, Duursma RA, López R, Medlyn BE (2018) Triggers of tree mortality under drought. Nature 558: 531–539

Choat B, Cobb AR, Jansen S (2008) Structure and function of bordered pits: new discoveries and impacts on whole-plant hydraulic function. New Phytologist 177: 608–626

Fanton AC, Brodersen C (2021) Hydraulic consequences of enzymatic breakdown of grapevine pit membranes. Plant Physiology kiab191

Fanton AC, Furze ME, Brodersen CR Pathogen-induced hydraulic decline limits photosynthesis and nonstructural carbohydrate storage in grapevines (*Vitis* spp.). in review

Gürsoy D, De Carlo F, Xiao X, Jacobsen C (2014) TomoPy: a framework for the analysis of synchrotron tomographic data. J Synchrotron Rad 21: 1188–1193

Ingel B, Jeske DR, Sun Q, Grosskopf J, Roper MC (2019) *Xylella fastidiosa* endoglucanases mediate the rate of Pierce's disease development in *Vitis vinifera* in a cultivar-dependent manner. MPMI 32: 1402–1414

Kaack L, Altaner CM, Carmesin C, Diaz A, Holler M, Kranz C, Neusser G, Odstrcil M, Jochen Schenk H, Schmidt V, et al (2019) Function and three-dimensional structure of intervessel pit membranes in angiosperms: a review. IAWA J 40: 673–702

Krivanek AF, Riaz S, Walker MA (2006) Identification and molecular mapping of PdR1, a primary resistance gene to Pierce's disease in *Vitis*. Theor Appl Genet 112: 1125–1131

Krivanek AF, Walker MA (2005) *Vitis* resistance to Pierce's disease is characterized by differential *Xylella fastidiosa* populations in stems and leaves. Phytopathology 95: 44–52

Lee EF, Matthews MA, McElrone AJ, Phillips RJ, Shackel KA, Brodersen CR (2013) Analysis of HRCT-derived xylem network reveals reverse flow in some vessels. Journal of Theoretical Biology 333: 146–155

Loepfe L, Martinez-Vilalta J, Piñol J, Mencuccini M (2007) The relevance of xylem network structure for plant hydraulic efficiency and safety. Journal of Theoretical Biology 247: 788–803

McElrone AJ, Manuck CM, Brodersen CR, Patakas A, Pearsall KR, Williams LE (2021) Functional hydraulic sectoring in grapevines as evidenced by sap flow, dye infusion, leaf removal and micro-computed tomography. AoB PLANTS 13: plab003

Merev N, Gerçek Z, Serdar B (2005) Wood anatomy of some Turkish plants with special reference to perforated ray cells. Turkish Journal of botany 29: 269–281

Mrad A, Domec J-C, Huang C-W, Lens F, Katul G (2018) A network model links wood anatomy to xylem tissue hydraulic behaviour and vulnerability to cavitation. Plant, Cell & Environment 41: 2718–2730

Mrad A, Johnson DM, Love DM, Domec J-C (2021) The roles of conduit redundancy and connectivity in xylem hydraulic functions. New Phytologist 231: 996–1007

Nagai S, Ohtani J, Fukazawa K, Wu J (1994) Sem Observations on Perforated Ray Cells. IAWA Journal 15: 293–300

Newbanks D (1983) Evidence for Xylem Dysfunction by Embolization in Dutch Elm Disease. Phytopathology 73: 1060

Newman KL, Almeida RPP, Purcell AH, Lindow SE (2003) Use of a green fluorescent strain for analysis of *Xylella fastidiosa* colonization of *Vitis vinifera*. AEM 69: 7319–7327

Pérez-Donoso AG, Greve LC, Walton JH, Shackel KA, Labavitch JM (2007) *Xylella fastidiosa* infection and ethylene exposure result in xylem and water movement disruption in grapevine shoots. Plant Physiol 143: 1024–1036

Pérez-Donoso AG, Lenhof JJ, Pinney K, Labavitch JM (2016) Vessel embolism and tyloses in early stages of Pierce's disease. Australian Journal of Grape and Wine Research 22: 81–86

Redak RA, Purcell AH, Lopes JRS, Blua MJ, Mizell III RF, Andersen PC (2004) The biology of xylem fluid–feeding insect vectors of *Xylella fastidiosa* and their relation to disease epidemiology. Annual Review of Entomology 49: 243–270

Riaz S, Tenscher AC, Rubin J, Graziani R, Pao SS, Walker MA (2008) Fine-scale genetic mapping of two Pierce's disease resistance loci and a major segregation distortion region on chromosome 14 of grape. Theor Appl Genet 117: 671–681

Roper MC, Greve LC, Warren JG, Labavitch JM, Kirkpatrick BC (2007) *Xylella fastidiosa* requires polygalacturonase for colonization and pathogenicity in *Vitis vinifera* grapevines. MPMI 20: 411–419

Sun Q, Greve LC, Labavitch JM (2011) Polysaccharide compositions of intervessel pit membranes contribute to Pierce's disease resistance of grapevines. Plant Physiol 155: 1976–1987

Sun Q, Sun Y, Juzenas K (2017) Immunogold scanning electron microscopy can reveal the polysaccharide architecture of xylem cell walls. Journal of Experimental Botany 68: 2231–2244

Sun Q, Sun Y, Walker MA, Labavitch JM (2013) Vascular occlusions in grapevines with Pierce's disease make disease symptom development worse. Plant Pathology 161: 1529–1541

Tyree MT, Zimmermann MH (2002) Xylem structure and the ascent of sap, 2nd edn. doi: 10.1007/978-3-662-04931-0

Varela LG, Smith RJ, Phillips PA (2001) Pierce's disease. University of California, Division of Agricultural and Natural Resources, Oakland, CA

Wason J, Bouda M, Lee EF, McElrone AJ, Phillips RJ, Shackel KA, Matthews MA, Brodersen C (2021) Xylem network connectivity and embolism spread in grapevine(*Vitis vinifera* L.). Plant Physiology 1–15

Wells JM, Raju BC, Hung H-Y, Weisburg WG, Mandelco-Paul L, Brenner DJ (1987) *Xylella fastidiosa* gen. nov., sp. nov: gram-negative, xylem-limited, fastidious plant bacteria related to *Xanthomonas* spp. International Journal of Systematic Bacteriology 37: 136–143

Zimmermann MH, Tomlinson PB (1966) Analysis of Complex Vascular Systems in Plants: Optical Shuttle Method. Science 152: 72–73

Table 1. Xylem traits of the studied grapevine genotypes and their level of resistance to Pierce diseases (PD). Data show means ±SD for the total number of vessel relays, pit fields, and pit field area by xylem volume; vessel relay diameter (RD), vessel diameter (VD), maximum vessel diameter (MVD), and the total number of vessels, solitary vessels, vessel pairs, and group of three or more vessels with their percentage. Data were processed on Aviso software and assessed through Tanax software.

		Traits by volume (mm^{-3})		Pit Field Area	RD	VD	MVD	Total number of			
Vitis	PD-level	Relays	Pit fields	($\mu m^2 mm^{-3}$)	(μm)	(μm)	(μm)	Vessels	Solitary	Pairs	+3 Group
Arizonica	Resistant	0.57 ± 0.16	17 ±4 ab	0.098 ±0.022 ab	36.5 ±14.0	56.0 ±5.8 ab	136.0 ±16 ab	319 ±73	190 ±18 (60%)	102 ±30 (32%)	27 ±8 (8%)
Hybrid	Resistant	0.28 ± 0.10	8 ±1 b	0.075 ±0.031 ab	33.4 ±10.7	60.7 ±5.0 a	138.4 ±11 a	349 ±99	245 ±26 (71%)	84 ±41 (23%)	20 ±9 (6%)
Lenoir	Resistant	0.46 ± 0.29	9±2 b	0.055 ±0.009 b	17.3 ±3.1	39.4 ±5.6 c	99.9 ±15 c	269 ±61	184 ±14 (59%)	107 ±11 (34%)	20 ±3 (6%)
B. du Bois	Resistant	0.31 ± 0.09	22 ±9 a	0.132 ±0.053 a	18.8 ±2.5	43.7 ±4.0 bc	110.6 ±9 abc	310 ±34	168 ±28 (62%)	78 ±22 (29%)	24 ±10 (9%)
Syrah	Susceptible	0.47 ± 0.10	13 ±4 ab	0.108 ±0.023 ab	32.7 ±6.5	56.5 ±8.4 ab	121.8 ±24 abc	377 ±155	209 ±30 (59%)	128 ±69 (32%)	40 ±25 (10%)
Chard.	Susceptible	0.48 ± 0.21	11 ±2 b	0.074 ±0.014 ab	30.3 ±22.2	42.3 ±6.6 c	102.4 ±13 bc	306 ±55	189 ±29 (61%)	93 ±3 (31%)	23 ±9 (8%)

Means ±SD. Within a column, traits with the same letter are not significantly different ($P < 0.05$) determined by post-hoc Tukey's HSD.

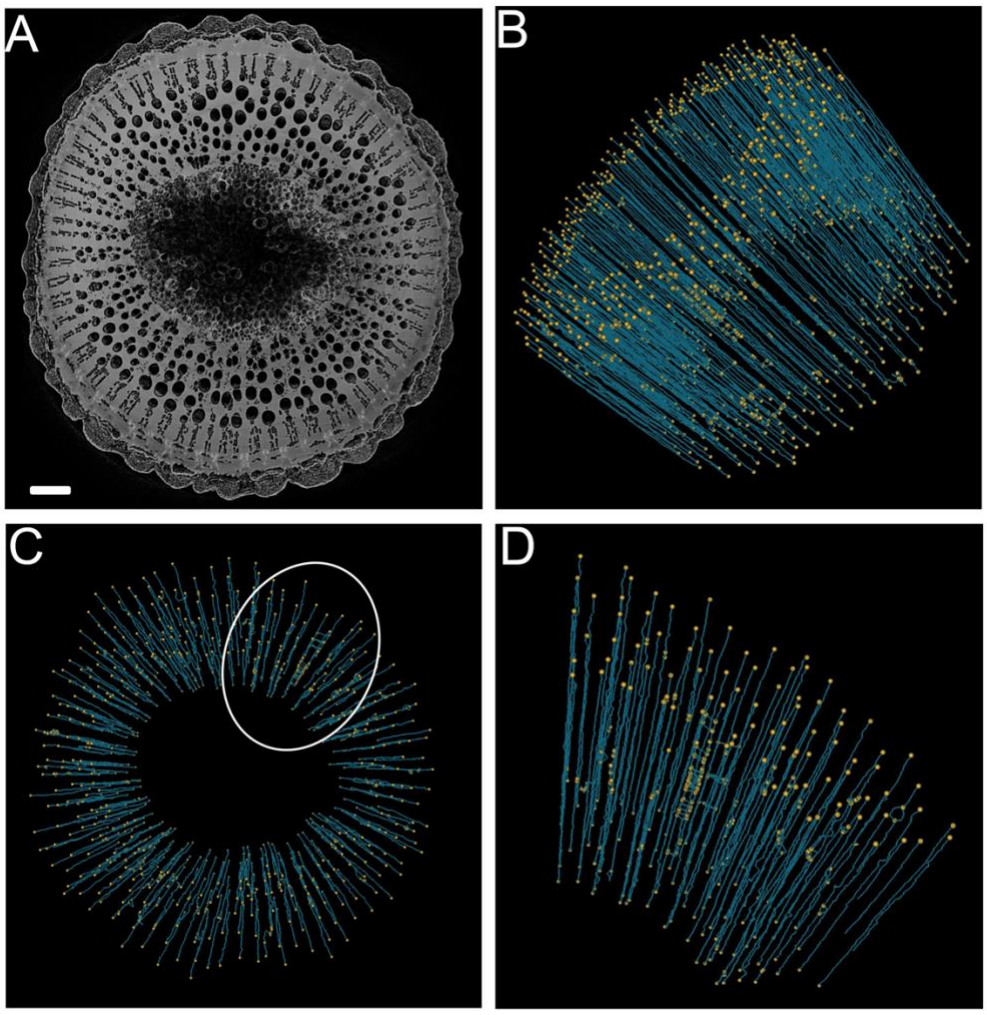

Figure 1. (A) Representative transverse volume rendering of the µCT dataset. Grapevine stem tissue is represented as light-gray pixels, while the vessel lumen is dark-gray pixels. Scale bar = 500 µm. (B) Diagonal visualization of the extracted vessel network and intervessel connections. Each blue line was positioned at the center of each vessel lumen representing a single vessel in the network. Yellow spheres denote nodes that are either at the end of the scan or between connected vessels. Light-blue horizontal lines represent an intervessel connection. (C) Higher magnification view of vessel network from a transverse perspective. (D) Magnified image of the area within the white box. (B-D) The scale varies with perspective.

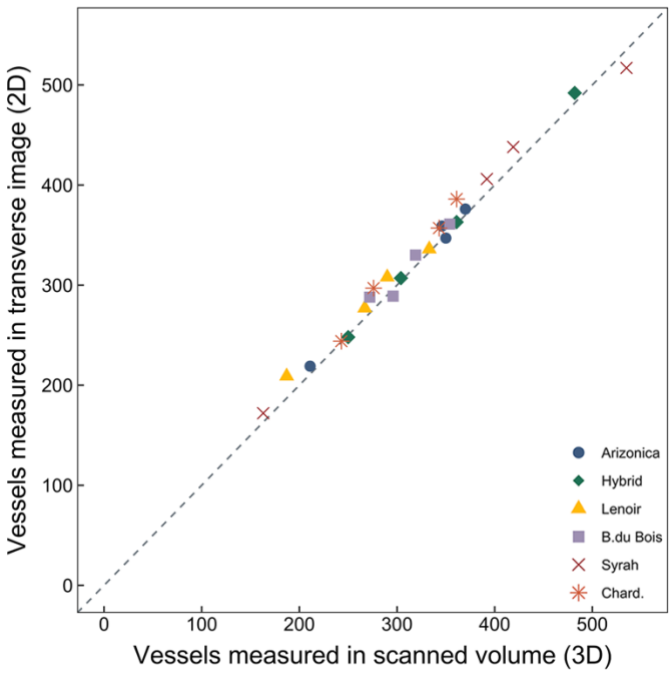

Figure 2. Linear relationship between the number of vessels measured in a transversal image and the number of vessels measured in the scanned volume for the six grapevines genotypes. The 2D-transverse measurements were taken from a slide in the center of stacked volume. The 1:1 relationship is represented by a dashed gray line. $R^2 = 0.986$, $p < 0.001$ (n=24 stems).

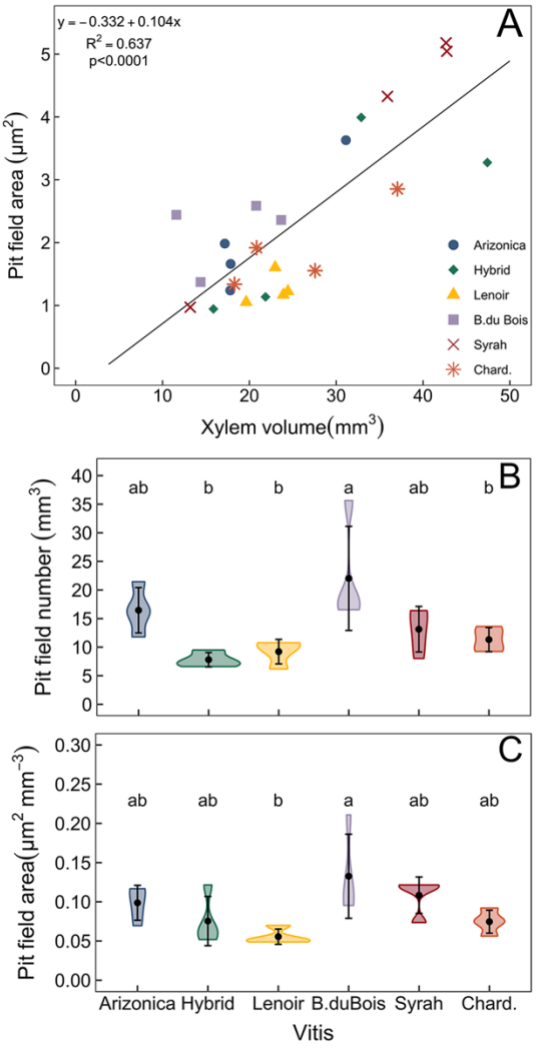

Figure 3. (A) Lineal relationship of total pit field area and xylem volume for the six grapevines genotypes. (B) Total number of pit fields by xylem volume. (B) Total pit field area by xylem volume. (B and C) Points represent the mean ±SD, violin shades are the data distribution, and Letters indicate significant differences between genotypes based on Tukey's HSD, α=0.05 (n=4 stems per genotype).

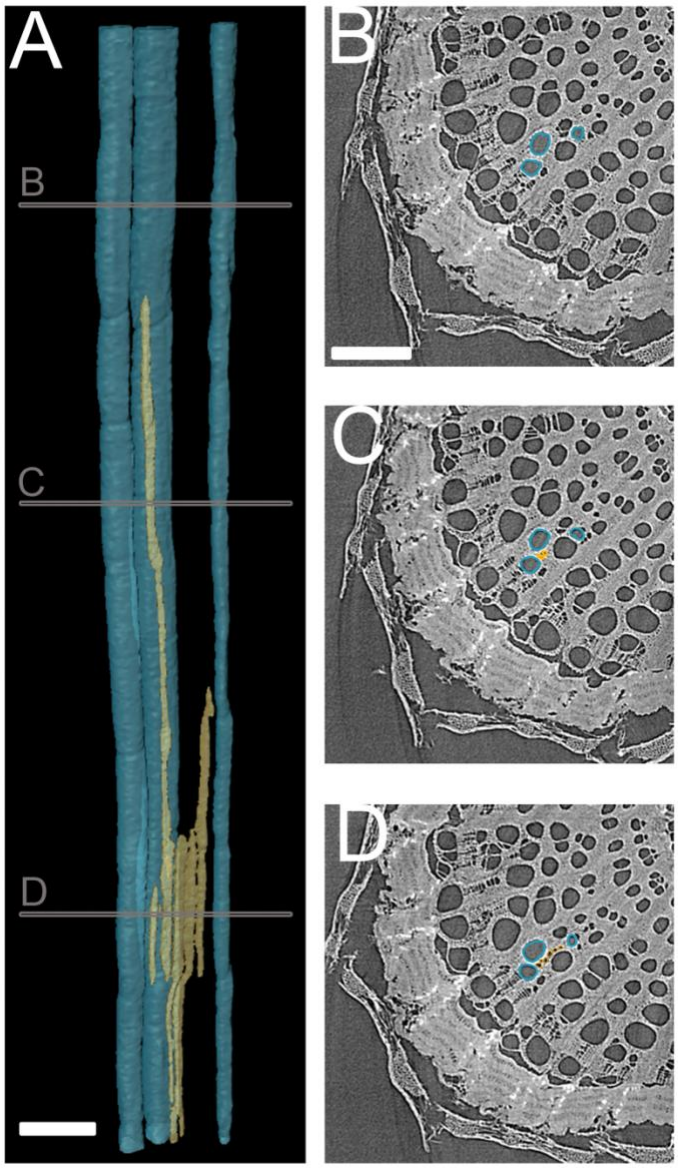

Figure 4. (A) 3D volume renderings showing vessel relay connecting large-diameter vessels within the same radial sector. Lines B to D correspond to the respective transverse microCT images in panels B to D, with vessel outlines in blue and vessel relay outlines in yellow. Bars = 250 μm.

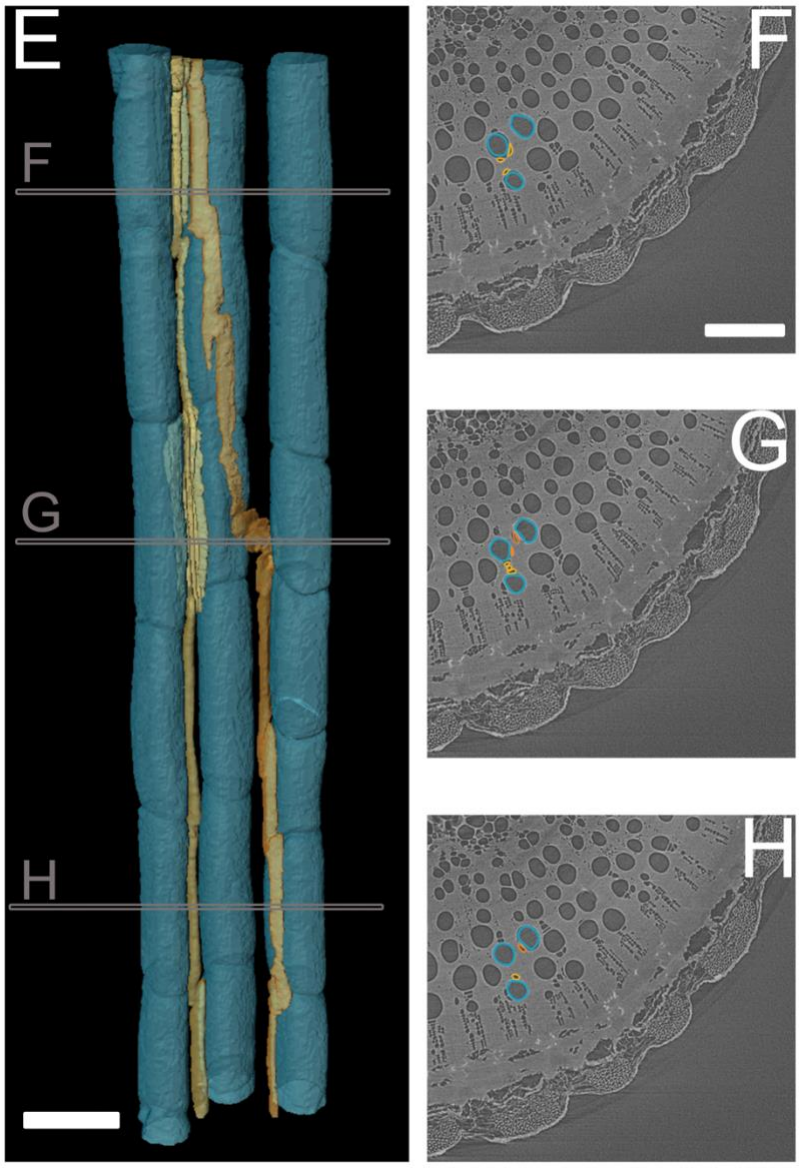

Figure 4. (E) 3D volume renderings showing vessel relay connecting large-diameter vessels within both the same radial sector and across ray sectors (e.g., radial and lateral connections, respectively). Lines F to H correspond to the respective transverse microCT images in panels F to H, with vessel outlines in blue and vessel relay outlines in yellow. Bars = 250 µm.

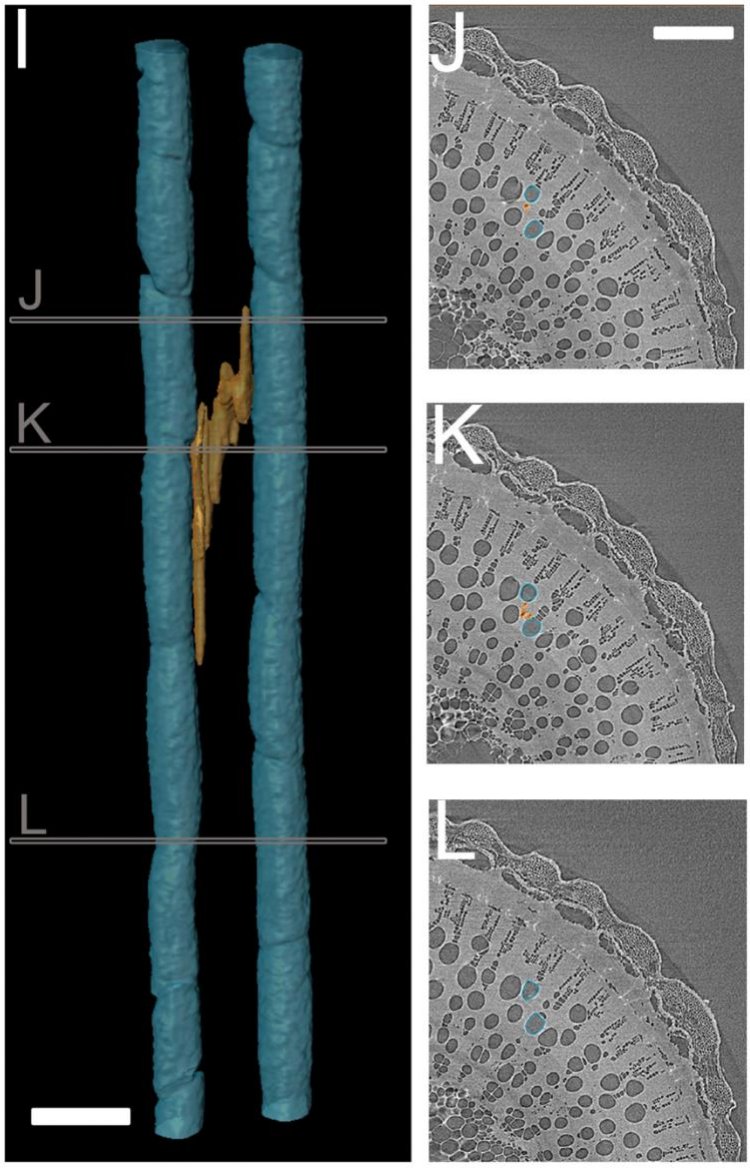

Figure 4. (I) 3D volume renderings showing a ‘zigzag’ shape vessel relay connecting large-diameter vessels across ray sectors. Lines J to L correspond to the respective transverse microCT images in panels J to K, with vessel outlines in blue and vessel relay outlines in yellow. Bars = 250 µm.

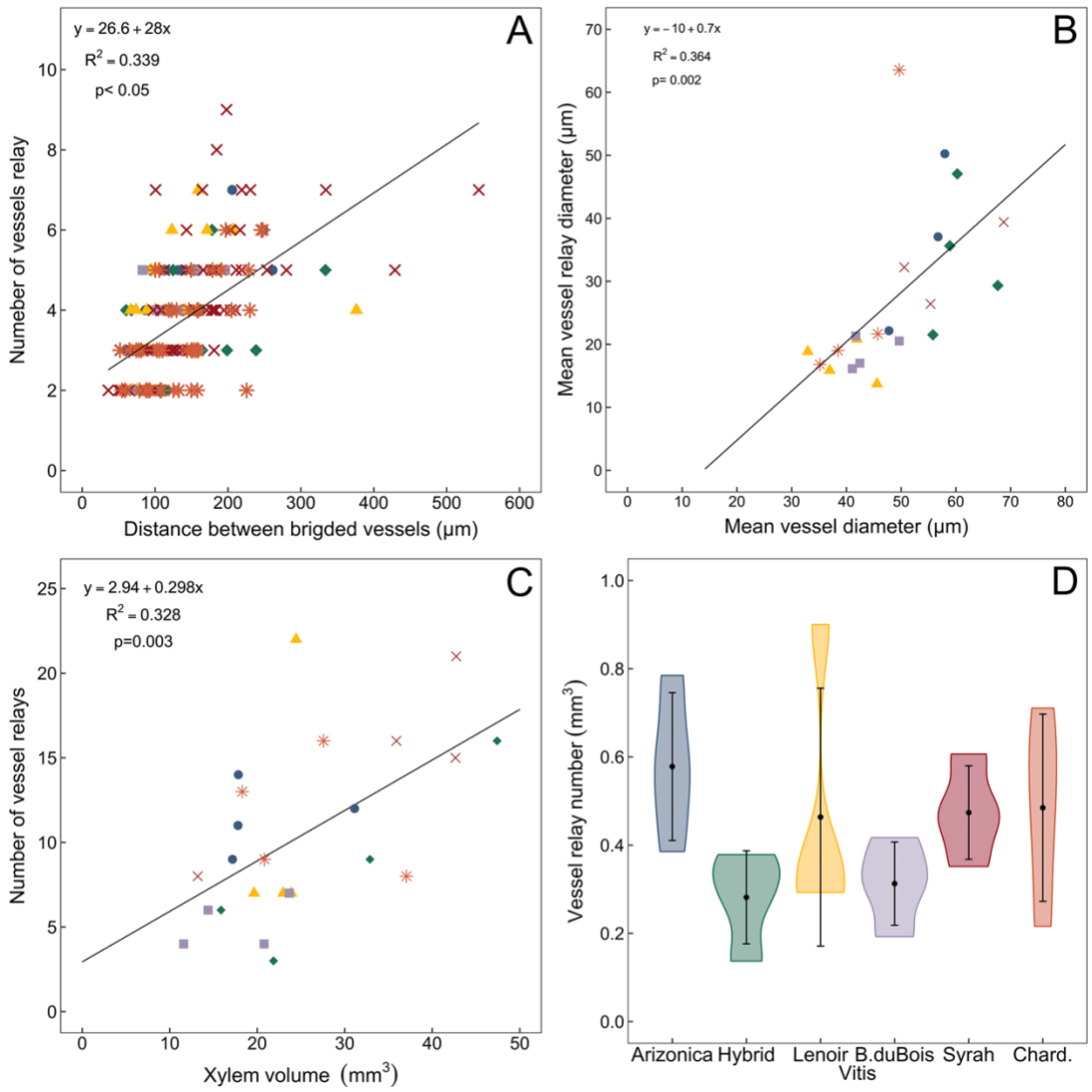

Figure 5. (A) Link between the distance separating two bridged vessels and the number of vessel relay elements spanning that distance among the six grapevines genotypes (n=1496 relays in 24 stems). (B) Linear relationship between the mean vessel relay diameter and the mean vessel diameter among the six grapevines genotypes. (C) Linear relationship of total number of vessel relays and xylem volume for the six grapevines genotypes. (D) Total number of vessels relays by xylem volume (p= 0.208). Points represent the mean ±SD, violin shades are the data distribution (n=4 stems per genotype).

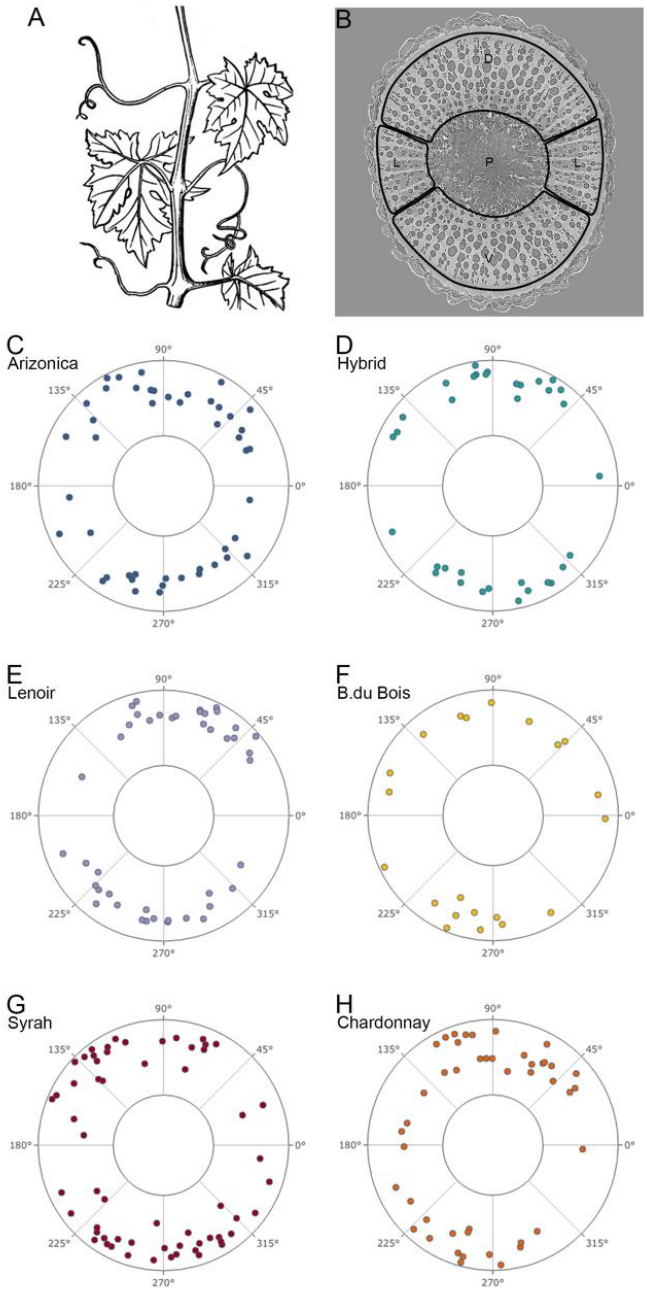

Figure 6. (A) Botanical drawing of a grapevine cane (one-year old stem). (B) Transversal µCT image showing secondary xylem dorsal 'D', ventral 'V', and lateral 'L' sectors surrounding the pith 'P'. Vessel relay locations in (C) Arizonica; (D) Hybrid; (E) Lenoir; (F) B. du Bois; (G) Syrah; and (H) Chardonnay compressed into a single transverse plane. Each symbol represents the location of one vessel relay chain. Inner ring is the approximate location pf the pith and outer ring, the epidermis. 0 ° and 180 ° are oriented to the lateral sides of the stem and 90 ° and 270 ° are oriented toward the dorsal and ventral sides of the stem, respectively.

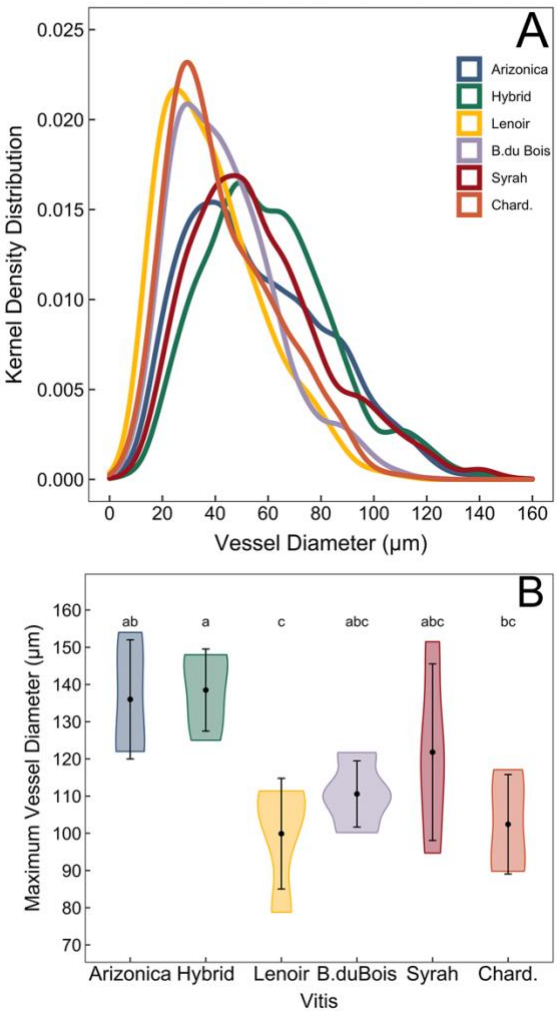

Figure 7. (A) Vessel diameter frequency distribution for the six grapevines genotypes. Kernel Density Bandwidth = 0.5. (B) Mean maximum vessels diameter for the six grapevines genotypes Points represent the mean ±SD, violin shades are the data distribution, and Letters indicate significant differences between genotypes based on Tukey's HSD, α=0.05 (n=4 stems per genotype).

Chapter 2

Hydraulic consequences of enzymatic breakdown of grapevine pit membranes

Abstract

Xylella fastidiosa (Xf) is the xylem-dwelling bacterial agent associated with Pierce's Disease (PD), which leads to significant declines in productivity in agriculturally important species like grapevine (*Vitis vinifera*). *Xf* spreads through the xylem network by digesting the pit membranes between adjacent vessels, thereby potentially changing the hydraulic properties of the stem. However, the effects of *Xf* on water transport varies depending on the plant host and the infection stage, presenting diverse outcomes. Here, we investigated the effects of polygalacturonase, an enzyme known to be secreted by *Xf* when it produces biofilm on the pit membrane surface, on stem hydraulic conductivity and pit membrane integrity. Experiments were performed on six grapevine genotypes with varying levels of PD resistance, with the expectation that pit membrane resistance to degradation by polygalacturonase may play a role in PD-resistance. Our objective was to study a single component of this pathosystem in isolation to better understand the mechanisms behind reported changes in hydraulics, thereby excluding the biological response of the plant to the presence of *Xf* in the vascular system. Pit membrane damage only occurred in stems perfused with polygalacturonase. Although the damaged pit membrane area was small (2-9% of the total pit aperture area), membrane digestion led to significant changes in the median air-seeding thresholds, and most importantly, shifted frequency

distribution. Finally, enzyme perfusion also resulted in a universal reduction in stem hydraulic conductivity, suggesting the development of tyloses may not be the only contributing factor to reduced hydraulic conductivity in infected grapevine.

Introduction

The ascent of sap through the xylem in vascular plants alternates between the low-resistance conduit lumina and the higher-resistance pit membranes (PMs) in the lateral and end walls between adjacent conduits. Vessel endings can represent 50% of the total resistance of xylem water transport (Sperry et al., 2005), forcing water to move through the pitted walls and the pit membranes. While PMs impose a resistance to the water flow, they also are believed to prevent the spread of air bubbles that may arise during extended periods of water deficit. Furthermore, PMs may also serve as a key physical structure that limits the spread of xylem-dwelling pathogens (Tyree and Zimmermann, 2002; Newman et al., 2003; Martín et al., 2009). As such, plant vascular systems may be compromised by either drought-induced embolism, vascular pathogens, or both, ultimately leading to hydraulic dysfunction.

PMs are the remnants of the primary cell walls and the middle lamella of adjacent secondary xylem vessel elements, comprising a three-dimensional matrix of interlaced cellulose microfibrils, hemicellulose, and pectic polysaccharides (Evert et al., 2006; Sun et al., 2017). This complex assemblage of PM constituents results in a tortuous pathway for the movement of water, air, or pathogens (Kaack et al., 2019) but is often approximated as a cylindrical pore for simplicity. Across many angiosperms, including grapevines (*Vitis sp*.), PM pore diameters are typically between 5-20 nm (Choat et al., 2008; Pérez-Donoso et al., 2010). The movement of gas bubbles across the air-water interface within PMs, known as air-seeding, is thought to related to PM porosity, and specifically the

diameter of the smallest pore in the membrane (Sperry and Tyree, 1988; Tyree and Zimmermann, 2002). Data indicate that the interface pressure between an embolized (air-filled) vessel and its adjacent functional vessel (containing sap under tension) can sustain a pressure differential set by the pore diameter and the viscosity of water (Choat et al., 2008). When xylem water potentials exceed the air-seeding threshold, gas bubbles can spread through the xylem network connections thereby blocking water transport and leading to subsequent declines in gas exchange (Sperry et al., 2002). If the plant is incapable of replacing the water lost during transpiration, these hydraulic failure and stomatal closure lead to lower plant productivity and ultimately plant death (McDowell et al., 2008; Choat et al., 2018).

Pathogens that systemically colonize the xylem network can affect PMs structure and, accordingly, disrupt the water transport. *Xylella fastidiosa* (*Xf*; Wells et al., 1987) is a xylem-dwelling bacterium transmitted by insects that feed on xylem sap (e.g., leafhopper sharpshooters; Superfamily Cercopoidea, Redak et al., 2004). To colonize the xylem network, *Xf* forms a biofilm within the intervessel pit fields and secrete cell wall-digesting enzymes to breach the PMs and then migrate to adjacent conduits (Newman et al., 2003; Roper et al., 2007; Chatterjee et al., 2008; Alves et al., 2009). As a consequence, the ability of *Xf* to multiply and spread within the vascular system has been associated with disease susceptibility. In susceptible grapevine genotypes (*Vitis vinifera* L.), *Xf* cells were found at greater distances from an inoculation point when compared to resistant grapevine genotypes (Fry and Milholland, 1990; Baccari and Lindow, 2011; Sun et

al., 2013). While pathogen resistance and subsequent disease susceptibility are complex and involve multiple traits, *Xf*-resistance is associated with low bacterial population levels in grapevines (Krivanek and Walker, 2005; Buzombo et al., 2006; Deyett et al., 2019). As such, small populations of *Xf* within the vascular system apparently trigger a systemic response. The overall resistance and tortuosity of the pathway that *Xf* must traverse when spreading through the xylem network should, therefore, influence the ability of the bacterium to become systemic (Lee et al., 2013; Wason et al., 2021). However, the subtle differences in xylem anatomy that limit the spread of *Xf* by inserting physical points of resistance along the vascular pathway, such as the spatial distribution of PMs and their chemical composition (Sun et al., 2011; Sun et al., 2017), may come with an associated cost of decreased hydraulic conductance.

Currently, the effects of *Xf* on water transport are not well understood and vary depending on the plant host and infection stage, which present diverse outcomes. Grapevine (*Vitis vinifera* L.) is a good model system for investigating the effects of *Xf* on hydraulic conductivity because it is both an important economic crop species where *Xf* has significant economic impacts on the industry (Hopkins and Purcell, 2002; Tumber et al., 2014), and usage as a model species for studying vascular transport (Brodersen et al., 2011; Bouda et al., 2019). Hydraulic conductivity (K_h) has been shown to decline in symptomatic host plants, but the underlying mechanisms for these differences are uncertain. Symptomatic grapevines, regardless of the genotype or level of resistance, typically have reduced K_h, yet susceptible genotypes have a greater reduction in K_h (Sun et al.,

2013; Deyett et al., 2019). This reductions in K_h have been associated with both the development of tyloses (Sun et al., 2011; Pérez-Donoso et al., 2016) and air-embolisms caused by the bacterium (McElrone et al., 2008; Pérez-Donoso et al., 2016). However, experiments imposing water stress on *Xf*-infected plants did not present significant differences in water transport compared to water-stressed control-plants (McElrone et al., 2003; Choat et al., 2009).

Given how *Xf* migrates through the vascular system (Lee et al., 2013), this bacterial spread may be associated with the same suite of anatomical traits that also influence drought-tolerance, such as the structure and spatial distribution of pit membranes. Resistance to the spread of gas bubbles via air-seeding has been shown to be related to both the porosity and thickness of the pit membrane (Choat et al., 2006; Kaack et al., 2019) and those same traits would also limit the spread of *Xf* (Lee et al., 2013). Yet, despite the potential similarities in physical barriers to the spread of *Xf* and embolism in the vascular system, the visual symptoms associated with PD are typically very different than those associated with prolonged drought stress. For example, the visible symptoms of PD include progressive leaf blade scorch along the margins, senescence at the petiole-lamina junction, and the irregular maturation of shoots (Varela et al., 2001; Thorne et al., 2006) In contrast, drought stress typically manifests as progressive leaf chlorosis, desiccation, and abscission at the stem-petiole junction (Thorne et al., 2006).

Experimental data suggest that following the formation of a biofilm on the PMs, cell-wall degrading enzymes enlarge the PM pores so they are large

enough to allow individual *Xf*-bacterium to move between adjacent vessels (Newman et al., 2003; Roper et al., 2007; Alves et al., 2009; Pérez-Donoso et al., 2010). With the PM pores enlarged, the effects on water transport should lead to both higher xylem hydraulic conductivity, due to the lowered resistance to axial flow, but also a decrease in the resistance to the spread of gas bubbles across the same membrane, assuming the biofilm leaves behind no significant residues. Additionally, the direct and indirect effects of *Xf* presence in xylem may trigger ethylene production and a subsequent production of tyloses (Pérez-Donoso et al., 2007). Therefore, it is difficult to determine the influence of PM degradation on its own. To eliminate the effects of both the presence of *Xf* in the xylem and the plant response to *Xf* (i.e., production of both ethylene and tyloses), we chose to perfuse the xylem with polygalacturonase, an enzyme known to be produced within the bacterial biofilm. In this way we aimed to simulate the effects of the enzymatic breakdown of the PMs and then monitored the resulting changes in K_h and the visual appearance of the PM using scanning electron microscopy. We hypothesized that PMs would be partially degraded in the presence of enzyme dissolved in the xylem sap, thereby enlarging the pores with two potential consequences. First, pore enlargement and membrane degradation should decrease the resistance of the intervessel connections to water transport, thereby increasing hydraulic conductivity. Second, pore enlargement should, in theory, also increase the vulnerability of the stems to air-embolism spread. The magnitude of these effects should be proportional to the degree of PM degradation, but air-seeding should be more strongly affected based on our understanding of how air

spreads through plant vascular systems (Choat et al., 2008; Christman et al., 2009).

To test these hypotheses and provide new insight into the influence of cell wall-degrading enzyme on hydraulic conductivity, we performed a series of experiments to measure changes in hydraulic conductivity following exposure to the enzyme polygalacturonase, and paired these measurements with anatomical observations of the PM after treatment. This allowed us to isolate a single component of this pathosystem in an effort to disentangle the mechanisms behind the reported changes in stem hydraulics and symptom development in grapevine. For this study, we selected grapevines with different degrees of reported *Xf*-resistance from discrete genetic pools: (1) two *Xf*-resistant genotypes, American native b43-17 *Vitis arizonica/candicans* used as a parent on the Pierce's Disease breeding program (Krivanek et al., 2006) and its daughter (2) hybrid 502-20[1], which is 88% *V. vinifera* cv. Chardonnay produced from the Pierce's Disease breeding program (A. Walker, 2016, personal communication). We then selected two commercial *Xf*-resistant hybrids with *Vitis aestivalis* parentage, (3) Lenoir (syn. Jacques or Black Spanish) and (4) Blanc du Bois, which are both popular in the American Southern wine industry where PD is problematic (Buzombo et al., 2006; Krivanek et al., 2006). Lastly, we selected two commercial wine grape varieties with reported *Xf*-susceptibility, *Vitis vinifera* L. cv. (5) Syrah and (6) Chardonnay (Varela et al., 2001).

[1] Hybrid 502-20 parents are: F8909-08=A. de Serres x b43-17 > 00-504-20= P79-101 x F8909-08 > A81-138=B52-89 x 00-504-20 > U0502-20=A81-138 x Chardonnay - Dr. Andrew Walker (Department of Viticulture and Enology, University of California Davis, *personal communication*).

Results

1) Enzyme perfusion and changes in hydraulic conductivity

Stem specific hydraulic conductivity values (K_s) in this study were between 0.56 and 20.64 Kg $s^{-1}m^{-1}MPa^{-1}$, well within the range reported for other potted *Vitis* genotypes (Fig. 1, Table 1; (Schultz and Matthews, 1988; Bavaresco and Lovisolo, 2000; Pérez-Donoso et al., 2007; Sun et al., 2013; Deyett et al., 2019). In the control treatment, mean K_s values were not significantly different among genotypes (Fig. 1, Table 1). Additionally, the percent different between the K_s means was 2.71% pre- and post-perfusion hydraulic measurements, indicating that the variation was small and perfusing stems with the 0.1M KCl solution with pH 4.0 had a negligible impact on K_s. This is a lower pH than what has been reported for grapevine xylem sap (pH 5.3-6.1; Andersen et al., 2007), however weak acidic solutions do not apparently affect K_s, whereas strong acidic solutions (pH ~2.5) can increase the hydraulic flow rates due to changes in hydrogels embedded in the pit membrane (Zwieniecki et al., 2001).

We observed a general trend showing that the enzyme perfusion caused K_s to decline in all grapevines regardless of their level of resistance to PD (Fig. 1, Table 1). The two PD-resistant commercial hybrids (Lenoir and B. du Bois) showed contrasting effects in K_s in response to the enzyme treatment (Fig. 1 C and D; Table 1). B. du Bois had the largest enzyme effect, where mean K_s declined by ~50% ($p = 0.0034$) (Fig. 1 D, Table 1). This reduction in K_s was similar to the susceptible genotype Syrah, which declined by ~40% ($p = 0.00345$) (Fig. 1 E, Table 1). In contrast, while Lenoir had the smallest enzyme effect, with mean K_s

reduced by 6% following the perfusion (Fig. 1 C, Table 1), we observed positive (n=5), negative (n=6), and neutral (n=1) responses. When compared with B. du Bois (Fig. 1 D) and Syrah (Fig. 1 E), where every stem showed a decline in K_s, we observed no obvious trend in the change in K_s based on reported susceptibility to *Xf* (Table 1, Fig. 1 A, B, and F).

One trait that may influence K_s is the mean maximum vessel length (MVL), and we predicted that grapevine genotypes with longer vessels, and therefore fewer end walls within the flow path, would be less affected by the enzyme perfusion. In all cases, the enzyme treatment did not significantly affect the length of the longest vessels ($p = 0.514$) but there were significant differences in MVL between genotypes ($p = 0.0017$). Hybrid had the greatest MVL mean of 0.63 ±0.07 m (Fig. 2 B, Table 1) differing from B. du Bois (0.44 ±0.06 m, $p = 0.0022$) (Fig. 2 D, Table 1) and Arizonica (0.49 ±0.04 m, p-value = 0.0408) (Fig. 2 A, Table 1). Interestingly, Hybrid and Chardonnay present close MVL means and very similar distribution of MVL (Fig. 2 B and F). Additionally, in our grapevine year-old-shoots (1.2 m), the maximum MVL measured was 1.04 m in a Chardonnay stem. Vessels above 0.9 m in length were found among *V. vinifera* genotypes only (Chardonnay, Syrah, and Hybrid), but their frequency was less than 10% (Fig. 2 B, E, and F).

We found a weak positive linear relationship between the percent change in K_s and the mean MVL ($R^2 = 0.1358$) (Fig. 3). Hybrid and Chardonnay stems had the longest MVL (0.63 and 0.62 m, respectively) (Fig. 2 B and F and Fig. 3) and a weak corresponding enzyme effect, where K_s decreased

approximately 25-30% (Table 1, Fig. 3). While B. du Bois had the shortest MVL mean (0.44 m) (Fig. 2 D and Fig 3) it had the greatest percent decline in K_s, decreasing by 50% (Table 1, Fig. 3).

2) Enzyme perfusion and pit membrane degradation

We measured the air-seeding threshold pressure (ASP) following the enzyme and control perfusion assays to assess intervessel PM vulnerability. ASPs in this study were between -0.1 and -6.1 MPa, within the range reported for other *Vitis* genotypes (Venturas et al., 2016). Mean ASP did not vary significantly between genotypes ($p = 0.1709$), but was significantly between treatments ($p = 2.95\ 10^{-05}$). The median ASP became less negative for the enzyme treatment in every genotype (Fig. 4, Table 1), being significant different in Arizonica ($p = 0.001$) (Fig. 4 A), Lenoir ($p = 0.004$) (Fig. 4 C), and marginally different in Syrah ($p = 0.079$) (Fig. 4 E). All genotypes showed a shift in the ASP distribution toward less negative values (i.e., less resistant to the spread of air). We found that the distribution of ASP thresholds changed from a bimodal distribution (control) to a right-skewed distribution with a higher proportion of less-negative air-seeding values after the enzyme treatment in Arizonica, Lenoir, B. Du Bois, and Syrah (Fig 4 A, C, D, and E). The contribution of low frequency, highly resistant ASP values kept the mean values from changing significantly. However, these data suggest a shift from a wider distribution of air-seeding values to less resistant PMs after the enzyme treatment.

Image analysis of ESEM micrographs showed PM damage in the intervessel pits and vessel-parenchyma pits only in enzyme-perfused stems. We examined a total of 531 vessels (nearly 85 vessels per genotype) and found no evidence of PM degradation in the control stems (Fig 5 A, C, E, G, I, and K). We observed that more fragments and unidentified debris particles appeared on the vessel walls (including within the pit aperture) in the enzyme-perfused stems than in the control treatment, but no tyloses or gels were found in any examined vessel. The three *V. vinifera* genotypes (Syrah, Chardonnay, and Hybrid) had a lower proportion of the vessel wall composed of pit fields compared to Arizonica or other *Xf*-resistant commercial genotypes (B. du Bois and Lenoir) (Fig 6 B, Table 1). These results showed a significant difference among the genotypes ($p = 4.46E-06$) (Fig 6 B), where Syrah (9.05 ±0.50 %) and Hybrid (9.24 ±0.67 %) have the lowest pit aperture area, followed by Chardonnay (10.45 ±0.61 %). In comparison, Arizonica (12.45 ±1.10 %), Lenoir (13.03 ±0.76 %), and B. du Bois (13.69 ±0.74 %) have larger pit aperture area.

Damage to the PMs took on a variety of forms (Fig. 5). In some vessels, PM damage appeared as a large pore (Fig 5 H, J, and L), while in others we observed a partial degradation of the PM (Fig 5 D, F). The total PM damaged area was small, less than 1% compared to the entire vessel wall (Fig 6 A) and between 2-9% of the pit aperture area (Fig 6 C). We found no significant differences in the damage to intervessel vs. vessel-parenchyma PMs regardless of genotype ($p = 0.788$); however, we did find significant differences between the genotypes ($p < 2e-16$) (Fig 6 C). The two *Xf*-resistant genotypes with *V. arizonica*

parentage (Arizonica and Hybrid) had the lowest PM damage of all the genotypes (2.43 ±0.31 and 2.76 ±0.42 %, respectively) (Fig 6 C, Table I). The other two resistant genotypes, Lenoir (7.80 ±0.61 %) and B. du Bois (6.25 ±0.61 %), had more extensive damage that was similar to the two susceptible genotypes, Syrah and Chardonnay (9.94 ±0.92 % and 7.30 ±0.52 %, respectively) (Fig 6 C, Table 1).

Discussion

PMs play an important role in xylem water transport; while they impose resistance to water flow, they can also act as a barrier to the spread of xylem-dwelling pathogens and air-embolism. Any alteration in the PM structure should influence the hydraulic functionality of the xylem. Our results show that the enzyme polygalacturonase partially degraded the PMs in all grapevine genotypes, but to a lesser degree in two resistant genotypes, Arizonica and Hybrid (Fig. 6). However, the hypothesis that PM degradation would increase K_s and simultaneously decrease PM resistance to embolism spread was not fully supported.

The pathway that the enzyme has to travel within the xylem network should influence the number of interactions between the enzyme and PMs. Thus, genotypes with shorter vessels, and therefore more points of resistance in the pathway, were expected to have higher K_s following the enzyme digestion and the removal of the end wall resistance. The opposite trend was observed (Fig. 2). For example, our data show that in B. du Bois the mean MLV increased (Fig. 3) and

the ASP became less negative (Fig. 4) after the enzyme treatment; with both measurements corroborating the visual evidence from the ESEM analysis (Fig. 5) that the PMs were indeed damaged. Yet, K_s consistently declined following the enzyme treatment (Fig 1). While we observed an increase in K_s in some stems, including the control samples, the general trend was a decline in K_s regardless of reported the PD-resistance.

The decline in K_s can be attributed to multiple factors. First, the chosen enzyme, its concentration in the perfusion solution, and the amount of time enzyme was allowed to interact with the xylem are likely to affect the results. We tested empirically that a concentration of 0.025 g of polygalacturonase in a KCl solution was sufficient to partially degrade the PMs based on our ESEM analysis. The enzyme degraded less then 10% of the total observable PM area, leaving more than 90% of PM intact across the different genotypes. Thus, the enzyme degradation affected a small proportion of the total PM area that would interact with water as a point of resistance to flow. Yet, we found significant declines in K_s, and changes in both the medians ASP and means MVL. In addition, the ESEM micrographs revealed the presence of unidentified debris particles that could contribute declines in K_s by creating an additional resistance to flow if the particles accumulate in the downstream vessel end walls. Indeed, we found that higher PM damage was associated with greater reductions in K_s (Table 1). This effect is likely due to the PM digestion by the enzymes and the flow of particulate debris downstream. We conclude that the particles were released into the vessel lumen during the enzymatic digestion as we did not see evidence of particles in the control

samples. In infected plants, *Xf* must digest the PMs to successfully spread through the xylem, and previous work suggests that the digested pit membranes may serve as a nutrient source for the bacteria (Roper et al., 2007; Chatterjee et al., 2008), as opposed to being flushed downstream and accumulating at the vessel end walls, and thereby obstructing flow as observed here. Given that we observed no debris particles in stems perfused with the control solution it is unlikely that they arose from cutting the stems and mounting them in the hydraulics apparatus. Another factor contributing to the K_s decline could be the different viscosities of the standard KCl solution and the enzyme solution (1.049 mPa s), which was 12.8 % more viscous than the KCl control solution (0.93 mPa s). However, our K_s calculations were corrected for the difference in viscosity between the two solutions, and it is unlikely that this difference made a significant contribution to the observed decline in Ks.

Our data suggest that neither mean ASP or MVL appear to be associated with PD resistance, even though the bacteria could achieve the longest unobstructed distance for migration in long-vessel species. Movement through these infrequent but long vessels would be dependent on the successful migration of the bacteria from the inoculation point, through the various intermediary vessels, and all of the PMs in between. Given the low frequency of long vessels the probability of their role in PD susceptibility is therefore low in the genotypes we studied here.

The overall effect of the enzymatic digestion leads to two notable changes in the vascular system of grapevines that would become problematic

during periods of water deficit. First, the hydraulic conductivity declines, which would limit the amount of water available to the foliage for transpiration. While this trend has been shown previously in *Xf*-infected plants (McElrone et al., 2003; Choat et al., 2009), our data show that the enzymatic treatment alone can induce significant reductions in flow, and the development of tyloses may not be the only contributing factor to reduced hydraulic conductivity in grapevine. Our ESEM observations revealed no evidence of tyloses production, and we attribute the declines in K_s to changes in PM permeability. Second, the enzyme digestion weakened PM resistance to air-seeding, which would only require a small change in pore diameter to lead to significantly lower the resistance to air movement. In combination with the decline in K_s, this would severely limit xylem water transport and put *Xf*-infected grapevines in a more vulnerable position when exposed to drought.

Interestingly, the two genotypes with *V. arizonica* parentage (Arizonica and Hybrid) showed the least amount of damage to the PMs in the ESEM images, but that damage led to significant changes in the mean ASP for Arizonica, and a shift in the ASP frequency distribution for both genotypes (Fig. 4). Previous work suggests that there are significant differences in the PM composition between grapevine species and genotypes that could lead to such results. For example, Sun et al., (2017) found that both the chemical composition and structure of PMs were significantly different in *V. arizonica* and *V. vinifera* cv. 'Chardonnay'. In the present study, Hybrid's parentage includes *V. arizonica* and a gene associated with PD-resistance (Krivanek and Walker, 2005; Krivanek et al.,

2006). The presence of the gene is associated with low bacterial levels and no symptom development (Krivanek and Walker, 2005), yet it is unclear of the specific role of the gene. In developing a more complete understanding of PD resistance, it will be critical to compare not only the physiological response but also anatomical traits among different genotypes, such as xylem network connectivity that would prevent or facilitate the systemic spread of *Xf* (Lee et al., 2013). Here, the overall effect of the damage that did occur may be the result of differences in the chemical composition of the PM (Sun et al., 2011; Ingel et al., 2021), but this effect may be minimized by other network properties like shorter vessel lengths (Wason et al., 2021).

These data also suggest that the different empirical measurements used in this study clearly target changes in PM permeability at different scales. The MLV and ASP measurements rely on the pressurization of the vascular system either as a whole (MLV) or in individual conduits (ASP), where air needs to pass through few membranes to complete a measurement. This is in contrast to the K_s measurements, which tests the resistance of most of the end wall PMs in the stem. Thus, small changes in PM permeability can lead to significant changes in the performance and vulnerability of the grapevine xylem network. Our ASP measurements showed that the enzyme treatment made the PMs less resistant to air-seeding, but also led to a change in the ASP distribution from a bimodal distribution (control) to a right-skewed distribution. Given that we observed a low percentage of damaged PMs overall, this trend is notable and suggests that longer exposure could result even greater losses in resistance to air-seeding. Future work

focused on ASP measurements in in *Xf*-infected stems would confirm an association of these events.

Overall, our study shows that the enzymatic component of *Xf* colonization alone can lead to significant changes in how the vascular system functions. The enzymatic digestion leads to significant declines in hydraulic conductivity, but also makes the PMs more susceptible to air-seeding. When coupled with the bacterial biofilm accumulation on the PMs associated with *Xf* vessels colonization (Newman et al., 2003; Alves et al., 2009), these factors would significantly affect the water transport capacity of infected grapevines, and put them at greater risk to the effects of drought.

Material and Methods

1) Plant material

We selected six grapevines (*Vitis sp.*) genotypes with different degrees of resistance to Pierce's Disease: four PD-resistant (1) b43-17 *Vitis arizonica/candica*ns hereafter designated as Arizonica, (2) Hybrid 502-20, 88% *V. vinifera* cv. Chardonnay, hereafter designated as Hybrid, (3) Lenoir and (4) Blanc du Bois; and two PD-susceptible *Vitis vinifera* L. cv. (5) Syrah and (6) Chardonnay. All cuttings were kindly provided by Dr. Andrew Walker (Department of Viticulture and Enology, University of California Davis). The grapevine plants were grown and maintained in a greenhouse on the Yale University campus from self-rooted cuttings in 4 L pots filled with a peat-based growing medium with perlite and vermiculite (Premier Pro-Mix BX, Premier Horticulture Inc). All grapevine

genotypes were trained with a primary trunk with two vertical one year-old-shoots (one growth ring) that were held at 1.2 m height. Plants were irrigated daily, fertilized with slow-release fertilizer (Osmocote Plus Outdoor and Indoor, 15-09-12), and provided with supplemental lighting (1,000 μmol (photons) m^{-2} s^{-1} at the top of canopy) on a 16 h day - 8 h night cycle.

2) Effect of enzyme perfusion on stem hydraulic conductivity

2.1) Stem specific hydraulic conductivity (K_s)

Grapevine plants were brought into the lab and cut under water at the base of the current year shoot. We used 12 stems for the enzyme treatments and 8 stems for control treatments, totaling 120 stems across the six genotypes. We first verified that there were no open xylem vessels from the base to the tip of the stem (described below) so the enzyme had to move through at least one PM. Then, we measured stem hydraulic conductivity (K_h) before and after perfusing stem segments with an enzyme or control solutions into the xylem. The leaves were removed at the stem-petiole junction, and the cut surfaces were sealed with superglue and accelerant (Loctite, Henkel North America, Rocky Hill, CT, USA) to force all flow through vessels that have a continuous pathway through the stem segment. Next, the stem segment-ends were smoothed with a sharp razor blade and fitted tightly to flexible Tygon tubing under water. The stem segment basal-end was attached to an elevated Mariotte bottle (which maintains a constant upstream pressure, (McCarthy, 1934) and the stem apical-end was connected via tubing to a balance (Sartorius Practum 224-1s) that collected and weighed the KCl

solution. Hydraulic conductivity (K_h) was measure using gravity induced flow rate (F, kg s^{-1}) created by pressure differential (8.34 10^{-3} MPa) across the stem segment (m) (Sperry et al., 1988). For all experiments, the hydraulics apparatus was filled with 0.1M KCl made with deionized and filtered water (0.22 µm, Millipore Millipak, MilliporeSigma, USA). The flow of solution through the segments was in the same direction as in the intact plant.

The perfused solutions (enzyme and KCl control) used in this experiment had different dynamic viscosities (η). We took into account this difference in viscosity by measuring the kinematic viscosity (v) of both solutions using a glass capillary viscometer (Cannon-Fenske Instrument Company, size 25 CFRC Series). This equipment uses gravity to determine the flow rate (in seconds) that a liquid takes to drain through a glass capillary. Measurements of this time and knowledge of the glass capillary dimensions yield v since the drainage through the glass is governed by the viscous flow in it (laminar flow). Finally, η was estimated by dividing v to the solution density.

Hydraulic conductivity is a measurement of water flow through the xylem which is dependent on the medium permeability (ρ) and the water viscosity (µ). We used two steps equations where in first we estimate the xylem permeability (ρ) using η of each solution and considering the stem length (L, m) and area (A, m^2) (equation 1). Then we estimated the hydraulic conductivity by normalizing to the water viscosity (µ) (equation 2). This resulted in two different calculations for specific stem hydraulic conductivity (K_s) for each treatment, one measured before the enzyme perfusion, and the other, after. A repeated measurement ANOVA (R

package) was used to determine the effect of the enzyme treatment on xylem water transport.

$$\rho = \frac{\mathrm{F\ L\ \eta}}{\Delta \mathrm{P}} / A \quad (1)$$

$$Ks = \frac{\rho}{\mu} \quad (2)$$

2.2) Enzyme perfusion

To simulate the effects of an enzyme produced in the *Xf* biofilm we applied a solution of commercially available Polygalacturonase, from *Aspergillus niger* (EC 3.2.1.15 - Fisher Scientific ICN 19897901). Polygalacturonase is one of the cell wall-degrading enzymes present in the *Xf* genome that is required for colonization and pathogenicity in grapevines (Agüero et al., 2005; Roper et al., 2007; Chatterjee et al., 2008), however the quantity of enzymes in the xylem sap or the capacity of bacterium production is still unknown. This commercial enzyme is a lyophilized powder with specific enzyme activity of 1,000 units per gram, meaning that 1 unit will liberate 10^{-6} mole of galacturonic acid from polygalacturonic acid per minute at pH 4 and 25˚ C, according to the manufacturer analysis. We determined empirically that 0.025 g of enzyme dissolved 1 mL of 0.1 M KCl ionic solution with pH 4 was sufficient to degrade the PMs, which was visually confirmed with ESEM imaging. However, different concentrations or perfusion times could yield to different results (Figure S1). We also used the same 0.1 M KCl ionic solution with pH 4 as control treatment. The weak acidic KCl solution was reached with a 0.01 M citric acid buffer. Using a syringe, we applied the 1 mL of the enzyme or control solutions through a three-way stopcock added

into a standard hydraulics apparatus. After solution insertion, the apparatus was pressurized (0.06 MPa) allowing the added solution to perfuse throughout the grapevine stem until 1 g of perfusion solution was recorded on the balance, which typically occurred in approximately 20 minutes for enzyme solution and 7 minutes for control solution. This assay was performed at lab ambient temperature 23˚C (optimum temperature for enzyme activity is 25˚C, according to the manufacturer).

3) Stem characterization

3.1) Stem segment length

Before performing the hydraulics assay, we cut the grapevine year-old-shoots to a length longer than the maximum vessel length, meaning that there was no open xylem vessel from the base to the tip of the stem segment, thus the perfused enzyme solution had to move through at least one intervessel PM. To verify that, the basal-end was connected to a tubing attached to a compressed air source and the distal-end was submerged in a water-filled tray. We then pressurized the stem at 0.1 MPa. If no air bubbles were seen exiting the submerged end, we assumed there were no open vessels in that stem segment. Next, samples were flushed with 0.1 M KCl solution for 25 min at 0.1 MPa to remove residual gas bubbles in the xylem.

3.2) Maximum vessel length

To test the effects of the enzyme on the permeability of PMs, we used the air injection method (Zimmermann and Jeje, 1981) to measure the

maximum vessel length (MVL), with the expectation that enlargement of the PM pores would effectively increase the maximum vessel length by removing PM in the vessel end walls. After enzyme or control perfusion assays, stem segments were air-flushed (0.1 MPa) with the stem basal-end attached to a compressed air source and the distal-end submerged in water-filled tray. The sample was progressively cut back, in 1 cm increments, until air bubbles could be seen exiting the submerged end and indicating that a vessel was open through the entire length of that sample. The remaining stem length was measured as the equivalent MVL. This test was performed on total 20 stems from each genotype and for stems with and without a perfusion of the enzyme. The means between genotypes were compared using ANOVA (R package). We applied the Silverman's function to predict the bandwidth into Kernel density estimation (R package).

3.3) Xylem cross-section area

The twenty stems from each genotype were cut using a microtome (GSL1-microtome Zurich, Switzerland) to produce transverse cross sections from the basal and apical internodes. The thin sections were then stained with Safranin-O and imaged with a compound microscope (Olympus BX60, Olympus America). Anatomical traits were measured from the images using ImageJ software (https://imagej.net/Fiji/Downloads) to isolate and calculate the mean xylem cross-section area (A, m^2).

4) Pit membrane characterization

4.1) Single vessel air-seeding threshold pressure

To determine if the enzyme had any influence on the PM resistance to embolism spread, we used the single vessel air injection method (Choat et al., 2006) to assess the vulnerability of inter-vessel PM to air-seeding pressure (ASP) after the enzyme or the control perfusion assay. Measurements were performed immediately after the hydraulics assay or within 24-48hrs; stem segments were stored at 4˚ C, a temperature at which enzyme used in the experiments should not be active, according to the manufacturer.

Stem segments measured consisted of the second, third, and fourth internode counting from the basal-end. We therefore measured three internodes per stem from each of the six genotypes for a total of 36 measurements for enzyme treatment and 24 measurements for control, and mean segment length was 5.88 ±0.27 cm. Samples were cut in the air with a razor blade and mounted in a multi-position vice (Panavise model 201, Medford, OR, USA). The distal-end was positioned so that it was immersed in water and basal-end was observed under a dissecting microscope (Leica S6 Stereo; Leica Microsystems Buffalo Grove, IL, USA), therefore enabling identification of a vessel-pair for measurement. Next, we inserted a glass capillary pipette (World Precision Instrument, 1B150-4; WPI Inc, Sarasota, FL, USA) pulled to a tip ~15-20 µm in diameter (Vertical Micropipette Puller P-30, Sutter Instrument, Novato, CA, USA) into a selected vessel-pair using a micromanipulator. The capillary tube was then glued in place using superglue and accelerant (Loctite, Henkel North America, Rocky Hill, CT, USA). The other end of the capillary pipette was attached to a polyetheretherketone tubing

(Extreme-Pressure PEEK Tubing, 1.59 mm outer diameter, 0.4mm wall thickness) connected to a pressure chamber (PMS Instruments, Corvallis, OR, USA). We pressurized the system at a constant rate (0.4 MPa min^{-1}) until air bubbles were visible exiting the submerged sample-end. The recorded pressure value is equal to, but opposite the sign, to the air-seeding threshold of the aspirated intervessel PM. The means between genotypes were compared using ANOVA (R package). The difference deciles (Q 0.1-0.9) between the treatment distributions were compared using Harrell-Davis Quantile Estimator (R package). We applied the Silverman's function to predict the bandwidth into Kernel density estimation (R package).

4.2) Pit membrane integrity

We used an environmental scanning electron microscope (ESEM) to investigate PM integrity in the enzyme and control perfusion stems, specifically searching for visible enlargement of pores in the PM surface. Fresh stem samples from the third and fourth internodes were dissected using a razor blade under a dissecting microscope (Leica ICC50 HD; Leica Microsystems Buffalo Grove, IL, USA), to expose longitudinal sections of shared walls (vessels-pair and vessel-parenchyma pair). We cut and imaged two samples per internode, totaling 48 and 32 samples from enzyme perfused and control stems, respectively. Next, we observed the integrity of the PM using an ESEM at an accelerating voltage 10 kV (FEI-XL30, Hillsboro, Oregon, USA). ESEM micrographs were analyzed using ImageJ software (https://imagej.net/Fiji/Downloads). We used ESEM micrographs

with a scale of 20 µm to measure the visible vessel walls, pit apertures, and the damage PMs areas of enzyme perfused stems. Then we calculated the relative areas, thus normalizing the differences between pixels within the scale provided by the ESEM (4.56 to 9.86 pixels μm^{-1}). The calculated relative areas are between (1) pit aperture and visible vessel wall and (2) damaged PMs and visible vessel wall, and (3) damaged PMs and pit aperture. We measured 10 vessel-pairs and 25 vessel-parenchyma pairs per genotype (totaling 210 vessel walls). The means between genotypes were compared using ANOVA followed by a Tukey's post-hoc analysis (R package).

Acknowledgements

I would like to thank the coauthor Craig R. Brodersen. I thank Dr. Andy Walker for providing the grapevines plants and for corresponding with the authors, as well as Adriana Rubinstein for her help with data collection of stem area. Additionally, we thank our funding source, the Yale Institute for Biospheric Studies (YIBS) for financially supporting this study.

doi:10.1093/plphys/kiab191

References

Agüero CB, Uratsu SL, Greve C, Powell ALT, Labavitch JM, Meredith CP, Dandekar AM (2005) Evaluation of tolerance to Pierce's disease and *Botrytis* in transgenic plants of *Vitis vinifera* L. expressing the pear PGIP gene. Molecular Plant Pathology 6: 43–51

Alves E, Leite B, Pascholati SF, Ishida ML, Andersen PC (2009) *Citrus sinensis* leaf petiole and blade colonization by *Xylella fastidiosa*: details of xylem vessel occlusion. Sci agric (Piracicaba, Braz) 66: 218–224

Andersen PC, Brodbeck BV, Oden S, Shriner A, Leite B (2007) Influence of xylem fluid chemistry on planktonic growth, biofilm formation and aggregation of *Xylella fastidiosa*. FEMS Microbiology Letters 274: 210–217

Baccari C, Lindow SE (2011) Assessment of the process of movement of *Xylella fastidiosa* within susceptible and resistant grape cultivars. Phytopathology 101: 77–84

Bavaresco L, Lovisolo C (2000) Effect of grafting on grapevine chlorosis and hydraulic conductivity. Vitis: Journal of Grapevine Research 39: 89–92

Bouda M, Windt CW, McElrone AJ, Brodersen CR (2019) In vivo pressure gradient heterogeneity increases flow contribution of small diameter vessels in grapevine. Nat Commun 10: 5645

Brodersen CR, Lee EF, Choat B, Jansen S, Phillips RJ, Shackel KA, McElrone AJ, Matthews MA (2011) Automated analysis of three-dimensional xylem networks using high-resolution computed tomography. New Phytologist 191: 1168–1179

Buzombo P, Jaimes J, Lam V, Cantrell K, Harkness M, McCullough D, Morano L (2006) An American hybrid vineyard in the Texas Gulf Coast: analysis within a Pierce's disease hot zone. Am J Enol Vitic 57: 347–355

Chatterjee S, Almeida RPP, Lindow S (2008) Living in two worlds: the plant and insect lifestyles of *Xylella fastidiosa*. Annu Rev Phytopathol 46: 243–271

Choat B, Brodie TW, Cobb AR, Zwieniecki MA, Holbrook NM (2006) Direct measurements of intervessel pit membrane hydraulic resistance in two angiosperm tree species. Am J Bot 93: 993–1000

Choat B, Brodribb TJ, Brodersen CR, Duursma RA, López R, Medlyn BE (2018) Triggers of tree mortality under drought. Nature 558: 531–539

Choat B, Cobb AR, Jansen S (2008) Structure and function of bordered pits: new discoveries and impacts on whole-plant hydraulic function. New Phytologist 177: 608–626

Choat B, Gambetta GA, Wada H, Shackel KA, Matthews MA (2009) The effects of Pierce's disease on leaf and petiole hydraulic conductance in *Vitis vinifera* cv. Chardonnay. Physiologia Plantarum 136: 384–394

Christman MA, Sperry JS, Adler FR (2009) Testing the 'rare pit' hypothesis for xylem cavitation resistance in three species of *Acer*. New Phytologist 182: 664–674

Deyett E, Pouzoulet J, Yang J -I., Ashworth VE, Castro C, Roper MC, Rolshausen PE (2019) Assessment of Pierce's disease susceptibility in *Vitis vinifera* cultivars with different pedigrees. Plant Pathol 68: 1079–1087

Evert RF, Esau K, Esau K (2006) Esau's plant anatomy: meristems, cells, and tissues of the plant body: their structure, function, and development, 3rd ed. Wiley-Interscience, Hoboken, N.J

Fry SM, Milholland RD (1990) Multiplication and translocation of *Xylella fastidiosa* in petioles and stems of grapevine resistant, tolerant, and susceptible to Pierce's disease. Phytopathology 80: 61

Hopkins DL, Purcell AH (2002) *Xylella fastidiosa*: cause of Pierce's disease of grapevine and other emergent diseases. Plant Disease 86: 1056–1066

Ingel B, Reyes C, Massonnet M, Boudreau B, Sun Y, Sun Q, McElrone AJ, Cantu D, Roper MC (2021) *Xylella fastidiosa* causes transcriptional shifts that precede tylose formation and starch depletion in xylem. Mol Plant Pathol 22: 175–188

Kaack L, Altaner CM, Carmesin C, Diaz A, Holler M, Kranz C, Neusser G, Odstrcil M, Jochen Schenk H, Schmidt V, et al (2019) Function and three-dimensional structure of intervessel pit membranes in angiosperms: a review. IAWA J 40: 673–702

Krivanek AF, Riaz S, Walker MA (2006) Identification and molecular mapping of PdR1, a primary resistance gene to Pierce's disease in *Vitis*. Theor Appl Genet 112: 1125–1131

Krivanek AF, Walker MA (2005) *Vitis* resistance to Pierce's disease is characterized by differential *Xylella fastidiosa* populations in stems and leaves. Phytopathology 95: 44–52

Lee EF, Matthews MA, McElrone AJ, Phillips RJ, Shackel KA, Brodersen CR (2013) Analysis of HRCT-derived xylem network reveals reverse flow in some vessels. Journal of Theoretical Biology 333: 146–155

Martín JA, Solla A, Esteban LG, de Palacios P, Gil L (2009) Bordered pit and ray morphology involvement in elm resistance to *Ophiostoma novo-ulmi*. Can J For Res 39: 420–429

McDowell N, Pockman WT, Allen CD, Breshears DD, Cobb N, Kolb T, Plaut J, Sperry J, West A, Williams DG, et al (2008) Mechanisms of plant survival and mortality during drought: why do some plants survive while others succumb to drought? New Phytol 178: 719–739

McElrone AJ, Jackson S, Habdas P (2008) Hydraulic disruption and passive migration by a bacterial pathogen in oak tree xylem. Journal of Experimental Botany 59: 2649–2657

McElrone AJ, Sherald JL, Forseth IN (2003) Interactive effects of water stress and xylem-limited bacterial infection on the water relations of a host vine. Journal of Experimental Botany 54: 419–430

Newman KL, Almeida RPP, Purcell AH, Lindow SE (2003) Use of a green fluorescent strain for analysis of *Xylella fastidiosa* colonization of *Vitis vinifera*. AEM 69: 7319–7327

Pérez-Donoso AG, Greve LC, Walton JH, Shackel KA, Labavitch JM (2007) *Xylella fastidiosa* infection and ethylene exposure result in xylem and water movement disruption in grapevine shoots. Plant Physiol 143: 1024–1036

Pérez-Donoso AG, Lenhof JJ, Pinney K, Labavitch JM (2016) Vessel embolism and tyloses in early stages of Pierce's disease. Australian Journal of Grape and Wine Research 22: 81–86

Pérez-Donoso AG, Sun Q, Roper MC, Greve LC, Kirkpatrick B, Labavitch JM (2010) Cell wall-degrading enzymes enlarge the pore size of intervessel pit membranes in healthy and *Xylella fastidiosa*-infected grapevines. Plant Physiology 152: 1748–1759

Redak RA, Purcell AH, Lopes JRS, Blua MJ, Mizell III RF, Andersen PC (2004) The biology of xylem fluid–feeding insect vectors of *Xylella fastidiosa* and their relation to disease epidemiology. Annual Review of Entomology 49: 243–270

Roper MC, Greve LC, Warren JG, Labavitch JM, Kirkpatrick BC (2007) *Xylella fastidiosa* requires polygalacturonase for colonization and pathogenicity in *Vitis vinifera* grapevines. MPMI 20: 411–419

Schultz HR, Matthews MA (1988) Resistance to water transport in shoots of Vitis vinifera L.: relation to growth at low water potential. Plant Physiol 88: 718–724

Sperry JS, Hacke UG, Oren R, Comstock JP (2002) Water deficits and hydraulic limits to leaf water supply. Plant, Cell & Environment 25: 251–263

Sperry JS, Hacke UG, Wheeler JK (2005) Comparative analysis of end wall resistivity in xylem conduits. Plant Cell Environ 28: 456–465

Sperry JS, Tyree MT (1988) Mechanism of water stress-induced xylem embolism. Plant Physiol 88: 581–587

Sun Q, Greve LC, Labavitch JM (2011) Polysaccharide compositions of intervessel pit membranes contribute to Pierce's disease resistance of grapevines. Plant Physiol 155: 1976–1987

Sun Q, Sun Y, Juzenas K (2017) Immunogold scanning electron microscopy can reveal the polysaccharide architecture of xylem cell walls. Journal of Experimental Botany 68: 2231–2244

Sun Q, Sun Y, Walker MA, Labavitch JM (2013) Vascular occlusions in grapevines with Pierce's disease make disease symptom development worse. Plant Pathology 161: 1529–1541

Thorne ET, Stevenson JF, Rost TL, Labavitch JM, Matthews MA (2006) Pierce's disease symptoms: comparison with symptoms of water deficit and the impact of water deficits. American Journal of Enology and Viticulture 57: 11

Tumber KP, Alston JM, Fuller KB (2014) Pierce's disease costs California $104 million per year. Cal Ag 68: 20–29

Tyree MT, Zimmermann MH (2002) Xylem structure and the ascent of sap, 2nd edn. doi: 10.1007/978-3-662-04931-0

Varela LG, Smith RJ, Phillips PA (2001) Pierce's disease. University of California, Division of Agricultural and Natural Resources, Oakland, CA

Venturas MD, Rodriguez-Zaccaro FD, Percolla MI, Crous CJ, Jacobsen AL, Pratt RB (2016) Single vessel air injection estimates of xylem resistance to cavitation are affected by vessel network characteristics and sample length. Tree Physiol 36: 1247–1259

Wason J, Bouda M, Lee EF, McElrone AJ, Phillips RJ, Shackel KA, Matthews MA, Brodersen C (2021) Xylem network connectivity and embolism spread in grapevine(*Vitis vinifera* L.). Plant Physiology 1–15

Wells JM, Raju BC, Hung H-Y, Weisburg WG, Mandelco-Paul L, Brenner DJ (1987) *Xylella fastidiosa* gen. nov., sp. nov: gram-negative, xylem-limited, fastidious plant bacteria related to *Xanthomonas* spp. International Journal of Systematic Bacteriology 37: 136–143

Zimmermann MH, Jeje AA (1981) Vessel-length distribution in stems of some American woody plants. Can J Bot 59: 1882–1892

Zwieniecki MA, Melcher PJ, Holbrook NM (2001) Hydrogel control of xylem hydraulic resistance in plants. Science 291: 1059–1062

Table I. Xylem traits of the studied grapevine genotypes and their level of resistance to Pierce diseases (PD). The perfusion effect in the K_s calculated as the percentage between before and after measurements. Maximum vessels length (MVL), and air-seeding threshold pressure (ASP) were measured after the perfusion assay. Relative pit aperture area and damage PM area to the vessel wall area measured from ESEM micrographs of enzyme perfused assay.

Vitis Genotype	PD-level	Perfusion effect in Ks (%)		MVL (m)	MVL[1] (m)		ASP[2] (MPa)		Relative area to vessel wall[1] (%)	
		Control	Enzyme		Control	Enzyme	Control	Enzyme	Pit aperture	Damaged PM
Arizonica	Resistant	1.67±2.39	-23.40±6.87	0.79	0.43±0.05	0.49±0.04	-2.56 (-3.4, -1.4)	-0.92 (-1.3, -0.7)*	12.45±1.1 a	0.28±0.04 a
Hybrid	Resistant	-0.82±3.15	-29.86±10.13	1.01	0.71±0.07	0.63±0.07	-1.94 (-2.6, -1.1)	-1.48 (-2.0, -1.2)	9.94±0.6 b	0.29±0.05 b
Lenoir	Resistant	5.56±3.98	-6.16±10.17	0.82	0.45±0.04	0.53±0.04	-2.33 (-3.2, -1.2)	-1.00 (-1.7, -0.6)*	13.03±0.7 bc	1.05±0.1 ab
B. du Bois	Resistant	4.33±7.57	-50.53±6.34	0.81	0.35±0.01	0.44±0.06	-1.99 (-2.8, -1.1)	-1.47 (-2.2, -1.1)	13.69±0.7 bd	0.78±0.07 ab
Syrah	Susceptible	6.60±2.53	-40.28±2.71	0.96	0.56±0.06	0.56±0.06	-2.02 (-2.8, -1.2)	-1.34 (-1.8, -0.9)	9.05±0.5 acd	0.94±0.1 ab
Chard.	Susceptible	-2.27±5.29	-24.30±7.58	1.04	0.63±0.10	0.62±0.07	-1.17 (-2.0, -0.7)	-0.99 (-1.8, -0.7)	10.45±0.6 d	0.74±0.06 ab

[1]Means ±SE. Different letters within columns indicate a significant difference ($P < 0.05$) between the species' means determined by post-hoc Tukey's HSD.
[2]Medians (95%CI). Stars indicate a significant difference ($P < 0.05$) between the species' medians determined by Harrell-Davis Quantile Analysis.

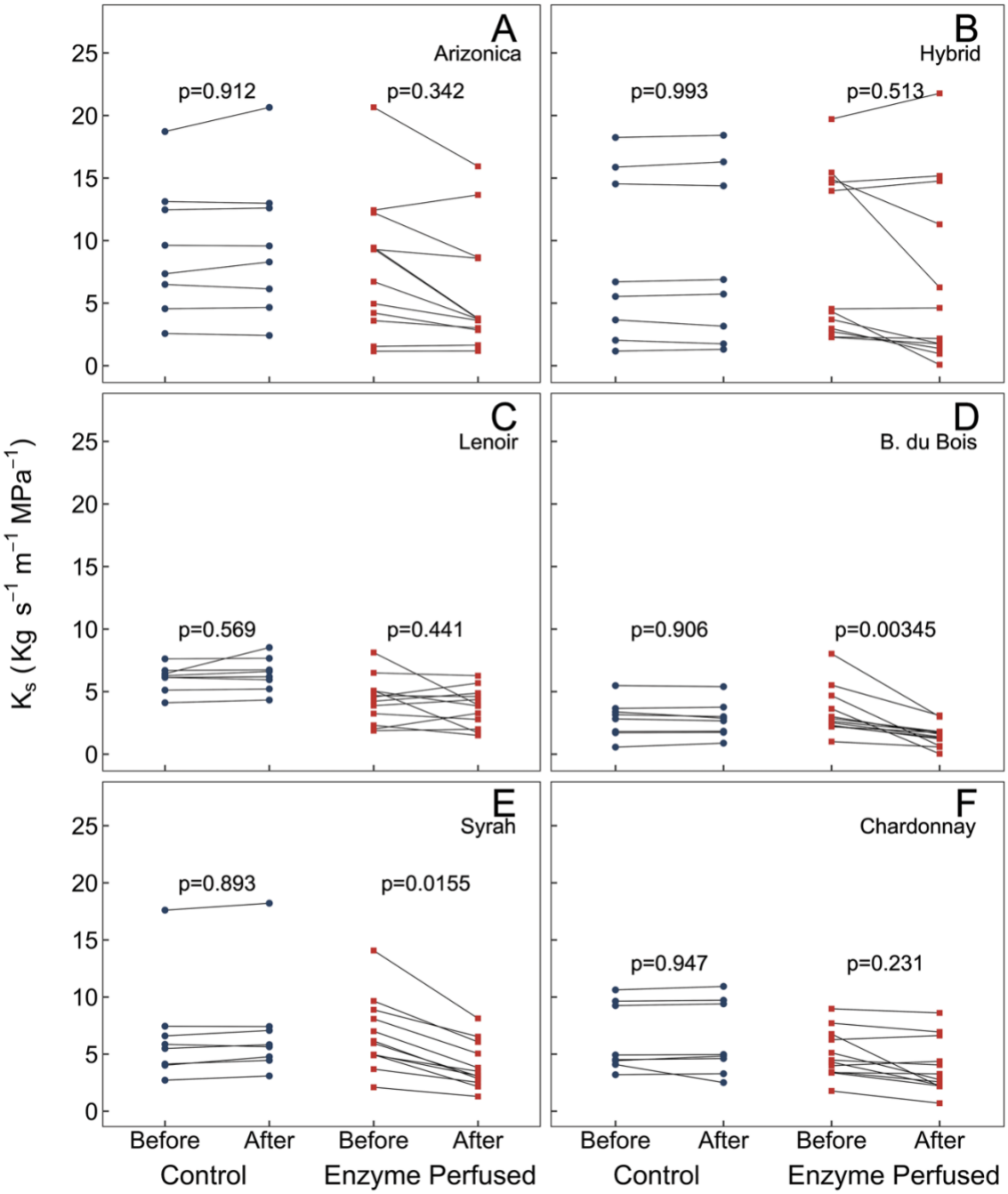

Figure 1. Changes in specific hydraulic conductivity (K_s) of grapevine stems before and after treatment with the cell wall digesting enzyme polygalacturonase (n=20 stems per genotype). The blue connected points (left) show each stem for the control treatment with non-significant K_s change after control solution perfusion. The red connected points (right) show each stem for the enzyme treatment presenting a general trend of K_s decrease after perfusion. Reported Pierce's Disease resistance decreases in the genotypes from A to F. P-values are from Repeated Measurements ANOVA within treatments ($P < 0.05$).

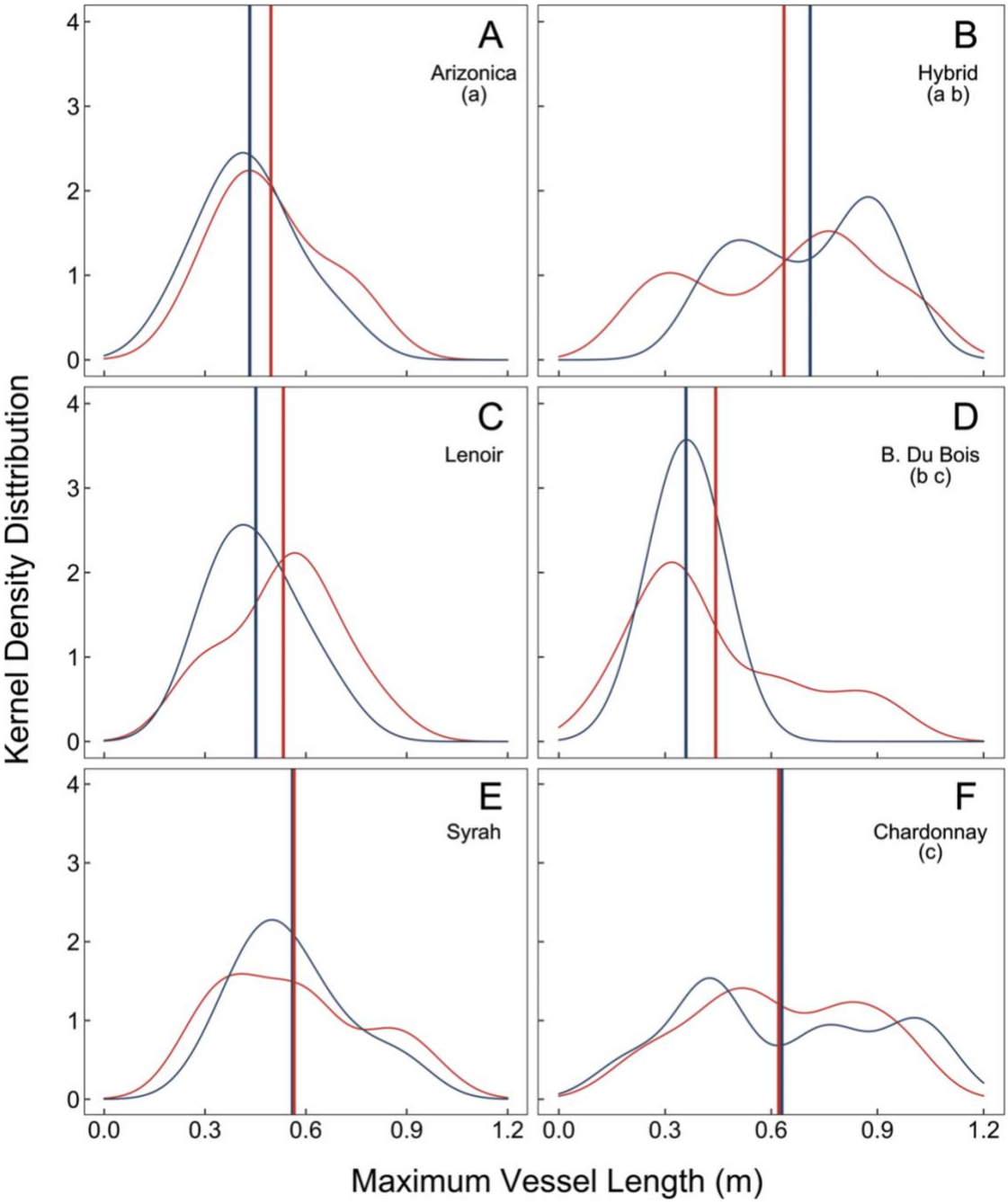

Figure 2. Maximum vessel length (MVL) frequency distribution for the six grapevines genotypes for control (blue) and enzyme (red) treatments (n=20 stems per genotype). Reported Pierce's Disease resistance decreases in the genotypes from A to F. Vertical lines indicate calculated means. The enzyme treatment did not significantly affect the length of the longest vessels ($p = 0.514$) but there were significant differences in MVL means between genotypes. Same letter shows significant differences ($P < 0.05$) according to Tukey's post-hoc analysis among genotypes. Kernel Density Bandwidth = 0.1

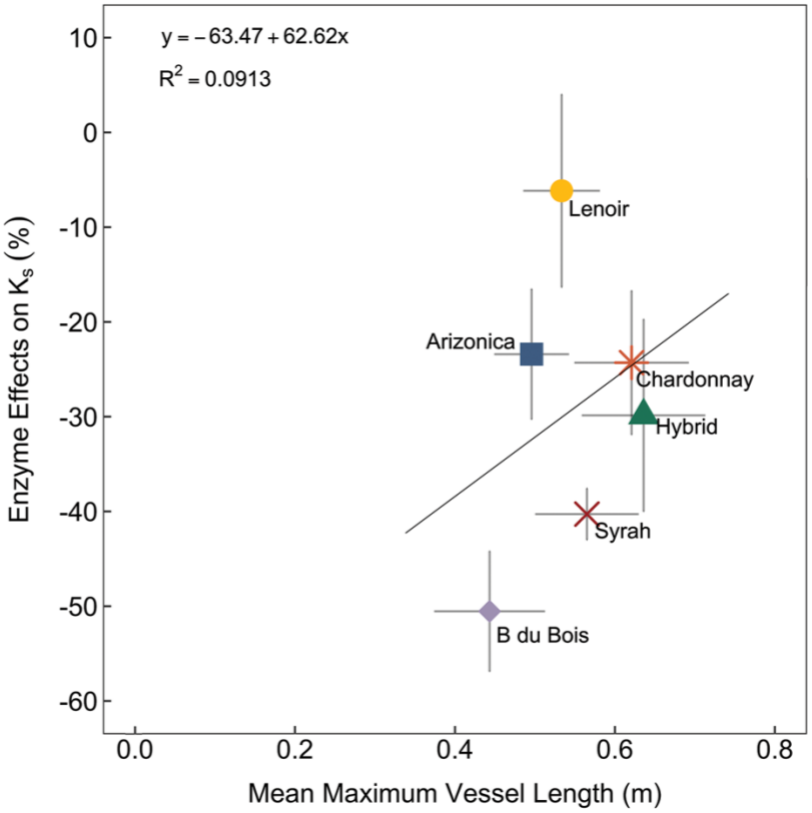

Figure 3. Relationship between mean maximum vessel length (MLV) and the percent change in Ks following the enzyme treatment. Data represent means ±SE (n=12 stems per genotype).

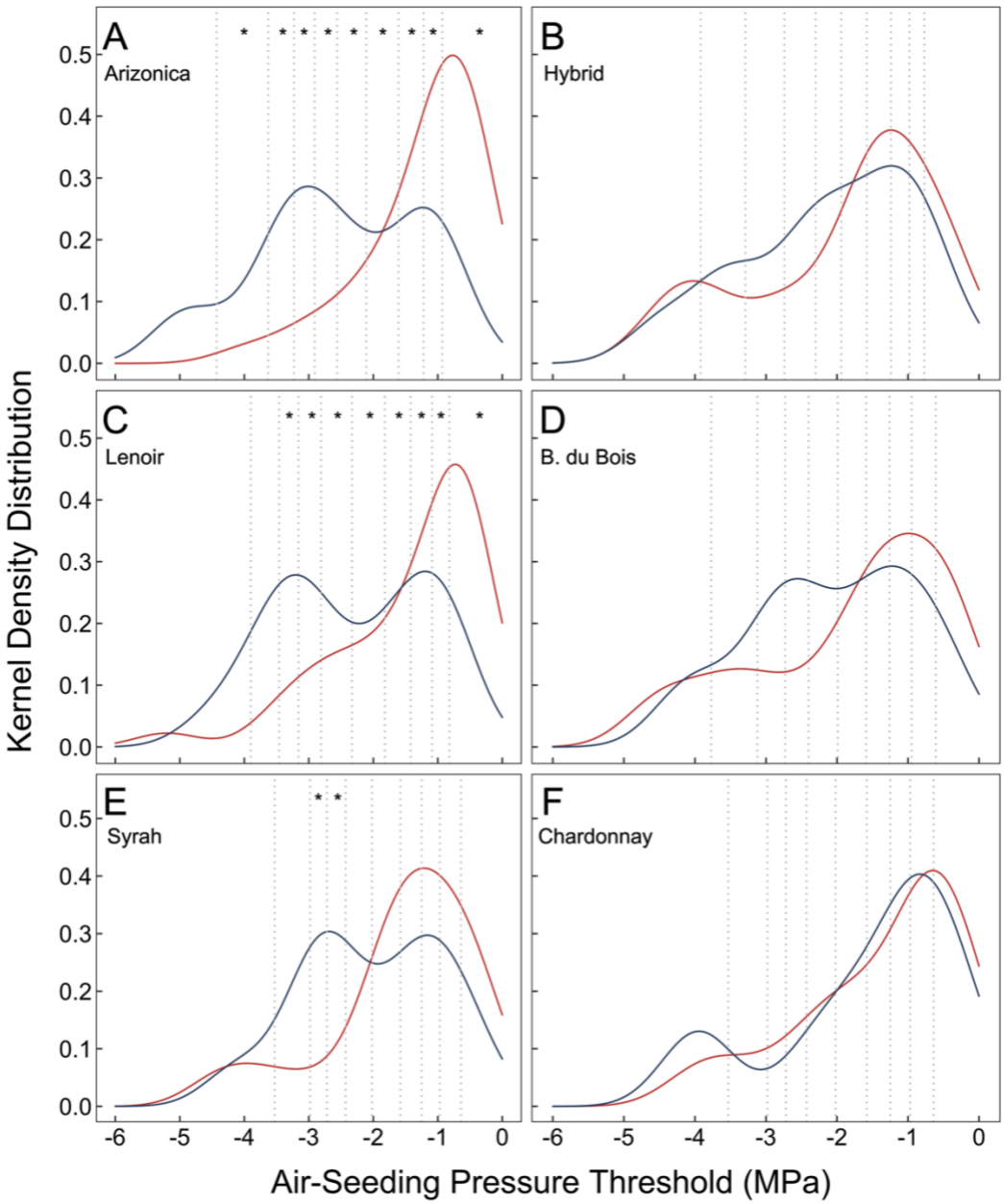

Figure 4. Air-seeding threshold pressure (ASP) frequency distribution for the six grapevine genotypes for control (blue) and enzyme (red) treatments (n=60 ASP per genotype). Reported Pierce's Disease resistance decreases in the genotypes from A to F. Vertical lines indicate deciles, and stars show significant differences ($P < 0.05$) between each quantile for both treatments according to Harrell-Davis Quantile Analyses. Kernel Density Bandwidth = 0.5

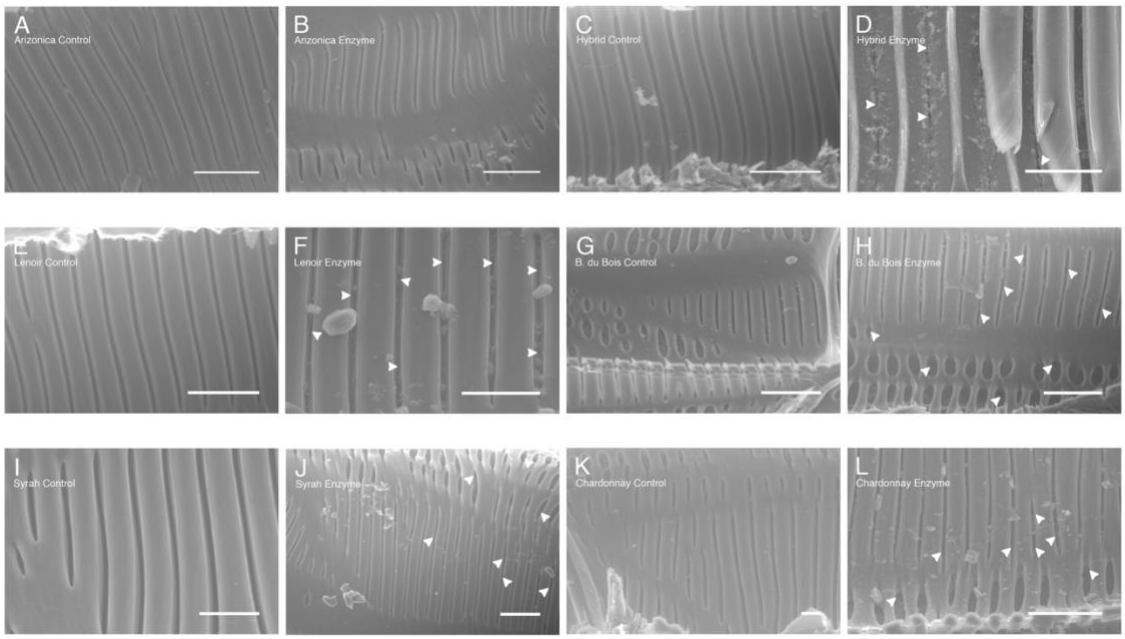

Figure 5. Representative longitudinal environmental scanning electron micrographs of the vessel walls and pit membranes of the six genotypes for control and enzyme treatments. A-B, Arizonica. C-D, Hybrid. E-F, Lenoir. G-H, B. du Bois. I-J, Syrah. K-L, Chardonnay. First and third columns show the control treatment samples. Second and fourth columns show samples after the enzyme perfusion. Arrowheads indicate areas with significant PM damage (e.g., pore enlargement). Bar = 25 µm; except in D and F (10µm).

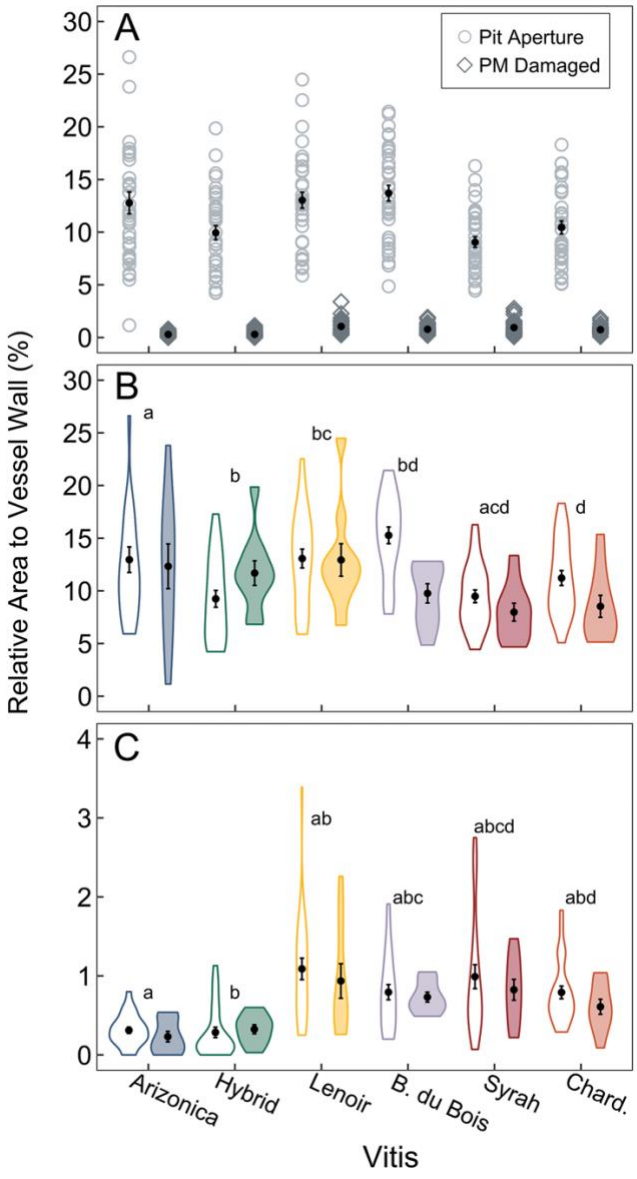

Figure 6. (A) Pit aperture area (grey circles) and damaged PM area (black diamonds) relative to the measured vessel wall area. (B) Area of the intervessel (open) and vessel-parenchyma (filled) pits relative to the measured vessel wall area. (C) Damaged PM area in either the intervessel (open) or vessel-parenchyma (filled) pits. Reported Pierce's Disease resistance decreases in the genotypes from left to right. Data points represent means ±SE and violin shades are data distribution (n=35 areas per genotype). Same letter shows significant differences ($P < 0.05$) according to Tukey's post-hoc analysis among genotypes.

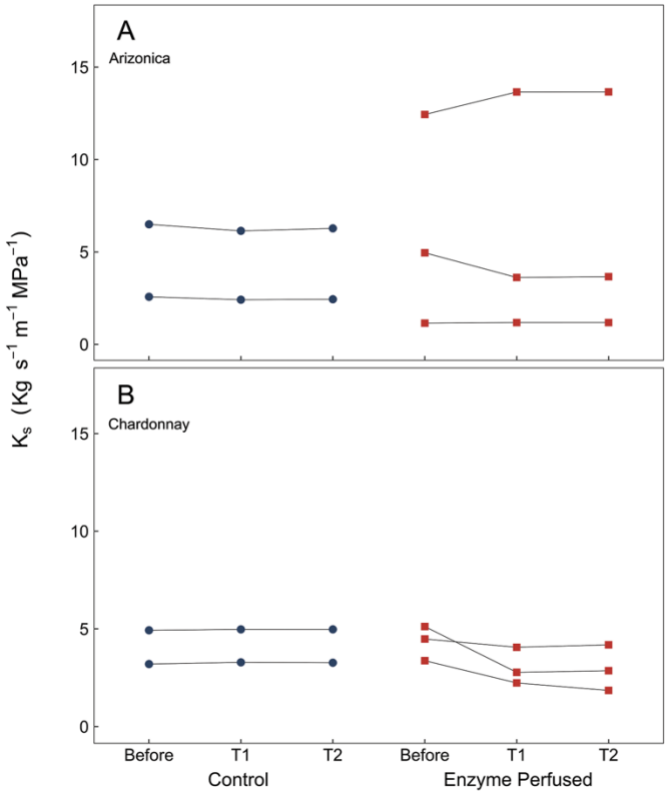

Supplemental Figure 1. Empirical test of two different perfusion times of polygalacturonase enzyme solution on Arizonica and Chardonnay stems. T1 is equivalent to the time for the solution added to perfuse (at 0.06 MPa) throughout the grapevine stem until 1 g of solution was recorded on the balance, which typically occurred in approximately 20 minutes for enzyme solution and 7 minutes for control solution. T2 correspond to additional 20 minutes after the T1-perfusion but without pressurization. In this test, there was non-significant Ks changes between T1 and T2 (n=5 stems per genotypes).

Chapter 3

Pathogen-induced hydraulic decline limits photosynthesis and nonstructural carbohydrate storage in grapevines (*Vitis spp.*)

Abstract

- *Xylella fastidiosa* (*Xf*) is the bacterial pathogen responsible for Pierce's Disease (PD) in grapevine (*Vitis vinifera* L.) and numerous diseases in agriculturally and ecologically important species. Localized inoculations spread systemically through the xylem, reducing water transport capacity which leads to declines in productivity and ultimately plant death. Yet, the underlying mechanisms of *Xf*-induced mortality are not fully understood, with a specific knowledge gap linking the cascading effects of vascular impairment on photosynthesis and the subsequent impact on nonstructural carbohydrate production and storage.
- After *Xf*-inoculation, we documented the development of PD symptoms after 12-13 weeks incubation period and assessed photosynthetic capacity, starch storage, and stem hydraulics in four grapevine genotypes (two PD-resistant and two PD-susceptible), comparing those changes to control plants.
- PD-susceptible genotypes showed a coordinated decline in photosynthesis, starch storage, and stem hydraulics. *Xf*-inoculation led to no change in starch and stem hydraulics in the PD-resistant genotypes.
- We demonstrated a systematic link between loss of hydraulic conductivity with the production of tyloses in response to *Xf* inoculation, and the downstream effects on photosynthesis and starch depletion in the PD-susceptible

genotypes. Our data support the theory that hydraulic failure and carbon starvation underlie plant mortality resulting from PD.

Introduction

Xylella fastidiosa (*Xf*; Wells *et al.*, 1987) is a xylem-limited bacterium transmitted by insects that feed on xylem sap (e.g., leafhopper sharpshooters; Superfamily Cercopoidea; Redak *et al.*, 2004). *Xf* causes diseases in economically important crops, including grapevines (Pierce's Disease), citrus (Citrus Variegated Chlorosis), coffee (Coffee Leaf Scorch), and olive (Olive Quick Decline Syndrome), and other ecologically important species can serve as alternative hosts, such as oak (*Quercus* spp.) and maple (*Acer* spp.) (EFSA, 2020). Pierce's Disease (PD) of grapevine (*Vitis vinifera* L.) is chronic in the USA, responsible for the limited production of European vinifera wine grapes in the Southern US, and leads to significant yield declines in California vineyards (Hopkins & Purcell, 2002; Tumber *et al.*, 2014).

After *Xf* is introduced into the xylem, it migrates with the transpiration stream or by physical movement with its pili (Meng *et al.*, 2005) until it reaches vessel end walls, where the intervessel pit membranes temporarily obstruct its movement. It then forms a biofilm capable of secreting cell wall digesting enzymes that breach the pit membrane (Newman *et al.*, 2003; Roper *et al.*, 2007; Chatterjee *et al.*, 2008; Ingel *et al.*, 2019). The bacteria can then migrate between adjacent vessels, spreading within the xylem network. Susceptibility to PD has been associated with the ability of *Xf* to multiply and sustain large colonies *in planta* and

systematically colonize the xylem tissue. The ability of *Xf* to migrate long distances through the xylem is a key weakness of susceptible hosts, and PD-susceptible *Vitis* genotypes have been shown to have bacterial cells present further from the inoculation site when compared to PD-resistant genotypes (Fry & Milholland, 1990; Krivanek & Walker, 2005; Baccari & Lindow, 2011; Sun *et al.*, 2013). While PD-resistance is complex and involves multiple traits, it has been associated with low bacterial population levels in grapevine tissues (Fry & Milholland, 1990; Krivanek & Walker, 2005; Buzombo *et al.*, 2006; Deyett *et al.*, 2019). However, small *Xf* populations within the xylem can trigger a systemic response that includes the production of ethylene which triggers the formation of tyloses that occlude vessel elements in the xylem (Pérez-Donoso *et al.*, 2007; Sun *et al.*, 2013). The production of tyloses presents a physical barrier to the movement of *Xf*, but also blocks water transport to the foliage. This response leads to internal symptoms that mimic drought stress, which could limit gas exchange and carbon gain. The direct effect of *Xf* on water transport is not well understood and varies depending on the genotype and infection stage, which present diverse outcomes (McElrone *et al.*, 2003, 2008; Pérez-Donoso *et al.*, 2007, 2016; Choat *et al.*, 2009; Deyett *et al.*, 2019; Ingel *et al.*, 2021).

Symptomatic grapevines show reduced stem hydraulic conductivity (K_h), regardless of the genotype or level of PD-resistance, yet PD-susceptible genotypes generally have a greater reduction in K_h (Sun *et al.*, 2013; Deyett *et al.*, 2019). These reductions in K_h have been associated with xylem occlusions, including tyloses and air-embolisms (Pérez-Donoso *et al.*, 2007, 2016; Sun *et al.*,

2013). Tyloses production can take days to weeks to complete (Sun *et al.*, 2007), ultimately leading to a reduction in K_h and an increase in leaf senescence (Choat *et al.*, 2009). The *Xf*-induced decline in K_h is variable, with susceptible *Xf*-inoculated plants showing reduced K_h compared to control plants, but not greater than water-stressed control plants (McElrone *et al.*, 2003; Choat *et al.*, 2009). In each case, however, tyloses appear to be one cause of K_h decline even though they may not completely prevent the systemic spread of *Xf* (Sun *et al.*, 2013). This is likely because the active response of susceptible grapevines to the presence of *Xf* in the xylem is not targeted (i.e., ethylene is volatile) and thus more damaging to the plant than the direct effects of the bacteria (Pérez-Donoso *et al.*, 2007). Consequently, the mechanisms underlying grapevine mortality due to the *Xf*-infection process are not fully understood, with a specific gap in our knowledge regarding the link between stem hydraulic constraints caused by *Xf* limiting the supply of water delivered to the foliage to support gas exchange and the production and storage of nonstructural carbohydrates (NSCs).

Xylem transport is directly connected to gas exchange and carbon uptake and utilization (Pinheiro & Chaves, 2011; McDowell, 2011). Through carbon assimilation (A_N), carbon dioxide (CO_2) is taken up from the atmosphere through stomata and converted into NSCs during photosynthesis. NSCs, primarily soluble sugars and insoluble starch, serve a variety of roles in primary and secondary metabolism to maintain proper plant function and NSCs can also be stored in parenchyma cells for later use (Pinheiro & Chaves, 2011; Hartmann & Trumbore, 2016). When conditions arise where insufficient soil moisture is available to

replenish the water lost during transpiration, water potentials decline and trigger stomatal closure to minimize subsequent water loss (Sperry *et al.*, 2002). This response is widespread in angiosperms despite the lost opportunity cost for carbon gain because of the catastrophic effects of hydraulic failure and systemic embolism spread in the xylem (Choat *et al.*, 2018). Stomatal closure then limits CO_2 uptake to sustain photosynthesis, ultimately leading to lower production of NSCs and a potential depletion of previously stored NSCs due to a negative carbohydrate balance (McDowell *et al.*, 2011; Sala *et al.*, 2012; Sevanto *et al.*, 2014; Hartmann & Trumbore, 2016; Adams *et al.*, 2017). Specifically, starch has been shown to serve as the main source to support plants during and following stressful periods (Earles *et al.*, 2018; Smith *et al.*, 2018). When considering the existing data on known declines in hydraulic conductivity resulting from the *Xf*-infection process (McElrone *et al.*, 2003, 2008; Pérez-Donoso *et al.*, 2007; Choat *et al.*, 2009; Sun *et al.*, 2013; Deyett *et al.*, 2019) and the often slow, multi-year decline in productivity (Varela *et al.*, 2001; Hopkins & Purcell, 2002), the causal link between *Xf* and mortality is likely the systemic hyper-immune response (Roper *et al.*, 2019) that triggers a cascade of events that ultimately blocks water transport and then initiates a period of negative carbon balance and carbon starvation. However, this direct mechanistic link has not been established for this bacterial infection in the same way that it has been done for drought (Martínez-Vilalta *et al.*, 2016; Adams *et al.*, 2017).

Here, our objective was to determine the mechanisms underlying grapevine mortality due to the *Xf* infection process. After *Xf*-inoculation and

development of symptoms, we measured photosynthetic capacity, instantaneous gas exchange, and stem hydraulics in grapevine genotypes with different degrees of reported *Xf*-resistance (Varela *et al.*, 2001; Krivanek & Walker, 2005). For this study, we selected two *Xf*-resistant genotypes, (1) American native b43-17 *Vitis arizonica/candicans* that is used as a parent in PD-resistance breeding programs (Krivanek *et al.*, 2006) and its daughter (2) Hybrid 502-20, which is 88% *V. vinifera* cv. 'Chardonnay' produced from the PD breeding program at University of California Davis (A. Walker, 2016; personal communication). We also selected two commercial wine grape varieties with reported *Xf*-susceptibility, *V. vinifera* L. cv. (3) 'Chardonnay' and (4) c.v. 'Syrah'. Fanton & Brodersen (2021) recently showed a differential response to artificial enzymatic digestion of the pit membranes of these same genotypes, where small changes in the porosity of the pit membranes led to significantly reduced air-seeding resistance. Yet, the declines in hydraulic conductivity and gas exchange associated with the *Xf* infection process have not been clearly determined. Within this resistance/susceptibility framework, we aimed to pinpoint the key anatomical or physiological traits that lead to mortality, with a specific focus on tyloses and starch in the xylem. We hypothesized that PD-susceptible grapevines would show a greater production of tyloses in response to *Xf*-inoculation, followed by a greater decline in hydraulic conductivity which would then limit gas exchange and the overall NSC balance of the plants as measured by starch in the xylem ray parenchyma of the stem.

Material and Methods

1) Plant material and growing conditions

We selected four grapevine genotypes with different degrees of resistance to Pierce's Disease: two PD-resistant (1) b43-17 *Vitis arizonica/candica*ns hereafter designated as Arizonica and (2) Hybrid 502-20 - 88% *V. vinifera* cv. Chardonnay, hereafter designated as Hybrid; and two PD-susceptible *V. vinifera* L. (3) cv. Chardonnay and (4) cv. Syrah. All cuttings were kindly provided by Dr. Andrew Walker (Department of Viticulture and Enology, University of California Davis).

Before inoculation, plants (n=12 per genotype, n=48 total) were grown in a greenhouse on the Yale University campus from self-rooted cuttings in 4 L pots filled with a peat-based growing medium containing perlite and vermiculite (Premier Pro-Mix BX, Premier Horticulture Inc). Plants were trained to have a primary trunk with a single vertical one-year-old shoot (one growth ring), irrigated daily, and fertilized with slow-release fertilizer (Scotts Miracle-Gro, Osmocote 15-09-12). After inoculation (see below), the plants were moved into three growth chambers (model E-41L2, Percival Scientific, Perry, IA, USA), pruned to 100 cm height to fit in the growth chambers, and maintained under the same conditions over the 12-13 weeks incubation period. The growth chambers were set to a 16h diurnal photoperiod, photosynthetic photon flux density (PPFD) of 650 mmol m^{-2} s^{-1}, and constant 70% relative humidity. The temperature regime was 28 (day) / 25(night) ºC (Feil & Purcell, 2001) and irrigation was provided daily until soil

saturation was reached to prevent water deficit that might lead to drought symptoms.

2) Inoculation experiment and confirmation of *Xf*-cells in the xylem

The green-fluorescent protein marked Temecula strain of *Xf* (GFP-*Xf*, Newman *et al.*, 2003) was cultured on PD3 agar-medium at 28 °C for 5 days (Davis *et al.*, 1981). These GFP-*Xf* cells were kindly provided by Dr. Caroline Roper (Department of Microbiology & Plant Pathology, University of California Riverside) and hereafter referred to as *Xf*. The bacterium cells were harvested and suspended in phosphate-buffered saline solution. The *Xf*-solution was quantified by reading $OD_{600\ nm}$ with a spectrophotometer (Ocean Insights, USB4000 Fiber Optic Spectrometer) and adjusted to 0.25 concentration to correspond to 10^8 colony-forming units (CFU) mL^{-1} (Hill & Purcell, 1995). To inoculate the plants, we placed a 10 µL droplet of *Xf*-suspension or buffered solution (control) on the stem, then pierced through the droplet with a sterile hypodermic needle. The droplet was sucked into the xylem when the needle was removed due to the tension of the transpiration flow. We did this twice on opposite sides (dorsal-ventral) of the second internode of the one-year-old shoot (n=48 plants total; n=6 *Xf*-inoculated plants per genotype and n=6 mock-inoculated plants per genotype).

We verified the presence of GFP-*Xf* cells in the xylem tissue of all plants using a fluorescence microscope, after having conducted the carbon assimilation and hydraulic measurements. We cut transverse fresh stem cross sections using a microtome (GSL1-microtome Zurich, Switzerland) at the

inoculation site (0 cm), and then at 10, 25, and 50 cm from the inoculation site towards the shoot apex. The 10 µm thin sections were mounted in water and then imaged with a fluorescence microscope (Olympus BX40, Olympus America). The GFP-*Xf* cells were visualized using the FITC filter set (excitation 475/50; emission 540/50).

3) *Xf* effects on carbon dynamics

3.1) Carbon assimilation

After susceptible plants displayed PD symptoms (all leaves with some level of marginal scorching and basal leaf blades abscised, leaving the petioles attached to the cane; Varela *et al.*, 2001), we used a LICOR-6400 equipped with a Leaf Chamber Fluorometer (6400-40, Li-Cor, Lincoln, NE) to measure chlorophyll fluorescence, CO_2 assimilation (A_N), and stomatal conductance (g_s) to assess if there was any difference in carbon assimilation between *Xf*-inoculated and control plants. We performed light response curves (LRC) on fully expanded and mature leaves near the stem apex for both *Xf*-inoculated and control plants (n=6 leaves per genotype per treatment). The leaves on *Xf*-inoculated plants were symptomatic, but the Leaf Chamber Fluorometer was still able to be attached to a green, presumably photosynthetic area. The LRCs were conducted to compare the photosynthetic capacity between *Xf*-inoculated and control plants, as well as to determine the rate of dark respiration and the maximum rate of photosynthetic assimilation. We started the LRC at an intensity of 0 µmol (photons) m^{-2} s^{-1} to record dark respiration and photosynthetic

assimilation and the values were logged after the leaf achieved stability. We then repeated this process at increasing light intensity (10, 25, 50, 100, 200, 400, 600, and 1,000 µmol (photons) m^{-2} s^{-1}). To fit the data points into a LRC, we applied the Microsoft Excel-Solver Tool developed by Lobo *et al.*, (2013).

We also assessed chlorophyll fluorescence on 3 dark-adapted leaves per plant (n=18 leaves per genotype per treatment). The leaves were dark-adapted for 1 h using dark adapting clips (9964-091, Li-Cor). We used the Leaf Chamber Fluorometer to measure F_0 (baseline) before sending a quick and saturating flash of light to measure F_m (maximal fluorescence level). The F_v/F_m ratio (maximum quantum efficiency of PSII photochemistry) was calculated and used to characterize the efficiency of photosystem II (Baker, 2008; Murchie & Lawson, 2013).

3.2) Histological quantification of starch in xylem ray parenchyma

To visualize and quantify starch in the xylem ray parenchyma of stem cross-sections, we used a 2%-iodine tincture USP as stain since starch readily reacts with iodine and results in a purple/black stained granule. We sectioned the 48 stems from both treatments at four points above the inoculation site (0, 10, 25, and 50 cm, with 0 being the inoculation site) using a microtome (GSL1-microtome Zurich, Switzerland) (N=192 xylem cross-sections). The 10µm thin sections were then immersed for 60 seconds in an iodine tincture (diluted 1:5 Vol. in DI water), rinsed in DI water, and immediately photographed (Canon 6D DSLR camera) with a compound microscope (Olympus BX40, Olympus America). Iodine-stained

starch granules in the ray parenchyma were assessed from the images using ImageJ software (https://imagej.net/Fiji/Downloads). For each image, we selected the rays in the xylem, thus creating a region of interest (ROI). Next, we cropped the images leaving only the ROI, and converted this subsequent image to an 8-bit image format. We used the image thresholding tool to identify starch in each xylem ray; the threshold range (0-60) was applied across all images. This threshold range was determined based on the mean grey value from the control images (96 cross-sections). We then calculated the area of the ROI (in pixels) and the area of thresholded-starch (in pixels), yielding the percent starch in the rays.

3.3) Quantification of starch concentration in the xylem tissue

In addition to visualizing and imaging starch via iodine staining, starch concentrations were quantified enzymatically. We cut three segments (1.5 cm each) from the internodes between 0 and 10 cm (3rd internode), 10 and 25 cm (4th or 5th internode), and 25 and 50 cm (7th or 8th internode). We removed the bark of these stem segments and combined them to produce one homogenous sample of the xylem tissue for each plant (n=18 stem segments per genotype per treatment). We followed the commonly used method of Landhäusser *et al.* (2018) to quantify starch concentrations, expressed as mg starch per g dry wood. Briefly, samples were oven-dried at 100 ^{o}C for the first hour and then at 70 ^{o}C for 36 h until the samples were completely dried. The dried samples were then ground (Thomas Scientific Wiley Mini-Mill model 3383P29; mesh 40) and approximately 30 mg of each sample was weighed out for starch analysis. The samples were extracted

with hot ethanol and the remaining dried pellet was sequentially digested with α-amylase and amyloglucosidase solution to produce a glucose hydrolysate solution. Peroxidase-glucose oxidase color reagent was then added to the digested samples and absorbance readings ($A_{525\ nm}$) were taken with a spectrophotometer (Ocean Insights, USB4000 Fiber Optic Spectrometer). Starch concentrations were calculated based on a glucose standard curve.

4) *Xf* effects on water transport

4.1) Stem specific hydraulic conductivity (K_s)

To assess the plant's capacity to move water in response to *Xf*-inoculation, we measured stem hydraulic conductivity (K_h) on 48 stem segments (n=6 stem segments per genotype per treatment). We used a gravimetric "Sperry Apparatus" (Sperry *et al.*, 1988) filled with 0.1M KCl solution prepared with deionized and filtered water (0.22 µm, Millipore Millipak, MilliporeSigma, USA). The day before hydraulic measurements, all plants were watered to saturation to ensure maximum stem hydration. Leaves were then removed at the stem-petiole junction, and the cut surfaces were sealed with superglue and accelerant (Loctite, Henkel North America, Rocky Hill, CT, USA) to force all flow through vessels that had a continuous pathway through the stem segment. Next, the one-year-old shoots were cut underwater at the base and the stem segment-ends were smoothed with a sharp razor blade and fitted tightly to flexible Tygon tubing. The basal-end of the stem segment was attached to an elevated Mariotte bottle (which maintained a constant upstream pressure, McCarthy, 1934) and the stem apical-

end was connected via tubing to a balance (Sartorius Practum 224-1s) that collected and weighed the KCl solution. The flow of solution through the stem segments was in the same direction as in the intact plant. K_h was measured as the quotient of gravity-induced flow rate (F, kg s^{-1}) created by pressure differential (8.34 10^{-3} MPa) by the stem segment (m).

As plants were held at 100 cm height to fit in the growth chambers, the mean stem segment length was 84 ±0.01 cm. The xylem cross-section area (A, m^2) was determined based on the mean of four points (0, 10, 25, and 50 cm above the inoculation site) along each stem. Lastly, K_h was normalized by xylem cross-sectional area to obtain specific hydraulic conductivity (K_s).

4.2) Percentage of vessels occluded by tyloses

To assess whether tyloses formation occluded vessels and interfered with water transport, we analyzed the quantity and distribution of tyloses at 10 cm from the inoculation site in all 48 stems (n=6 plants per genotype per treatment). Stems were cut using a microtome (GSL1-microtome Zurich, Switzerland) to produce cross-sections. The 10 µm thin sections were then stained with Toluidine blue, a stain for general anatomical study, and imaged with a compound microscope (Olympus BX40, Olympus America). The total vessel number and the number of tyloses-occluded vessels were measured from the images using ImageJ software to calculate the percent of tyloses in the xylem cross-section.

5) Statistical Analyses

We used two-sample t-tests to compare the means of F_v/F_m, A_{max}, RD, I_{comp}, A_N, g_s, iodine-stained starch, starch concentration, and K_s between *Xf*-inoculated and control plants for each genotype. Further, we performed a one-way ANOVA to determine whether (a) the percent of tyloses differed between genotypes and (b) there were any differences between the four sampling points (0, 10, 25 and 50cm) along the stem for iodine-stained starch, followed by a Tukey's HSD post hoc test. We also assessed whether the percent of tyloses influenced K_s using linear regression (LM model); those variables were first $\log_{10}$ transformed to test normality assumptions. Finally, we used linear regression to evaluate (a) the relationship between the percent of starch in the xylem ray parenchyma determined via iodine staining/imaging and the starch concentration (mg g^{-1}) in the stem determined enzymatically and (b) the relationship between the percent change of A_N and iodine-stained starch variables between the control and *Xf*-inoculated plants. All statistical analyses were performed in R Studio (Version 1.4.1717).

Results

1) *Xylella fastidiosa* spread in the xylem

We noted visual symptom development only on the *Xf*-inoculated PD-susceptible genotypes Chardonnay and Syrah. Symptoms presented as necrotic, scorched tissue along the margins on all leaf blades. Basal leaves dropped at the petiole-lamina junction and we also observed irregular maturation

of shoots. No visual symptoms were present in *Xf*-inoculated PD-resistant genotypes and control plants. The control plants (mock-inoculated) were free of *Xf*-cells (Fig. **1 a, c, e, g**), whereas all *Xf*-inoculated plants had *Xf*-cells at 0 cm (0 being just above the inoculation site) on both sides of the xylem (Table 1; Fig. **1 b, d, f, h**). In general, the *Xf*-cells were attached to vessel walls and not always occluding the vessel lumen. If they did occlude a vessel lumen, it was more likely to be a combination of *Xf*-cells with tyloses development.

Xf migrated a greater distance from the inoculation site in the susceptible genotypes Chardonnay and Syrah, compared to the Arizonica and Hybrid genotypes, with *Xf*-cells present at all harvest points 0, 10, 25 and, 50 cm on both inoculated sides of all stems (Table 1; Fig. **1 f, h**). In the PD-resistant genotypes Arizonica and Hybrid, the number of stems with *Xf*-cells decreased as the distance from the inoculation site increased, and in many cases, the *Xf*-cells were observed on only one side of the stem. At 10 cm, the number of stems with *Xf*-cells decreased by almost half (67% dorsal and 50% ventral) in Arizonica, while in Hybrid, this decrease was on only one side of the stem (100% dorsal and 67% ventral; Table 1; Fig. **1 b, d**). At 50 cm, we detected *Xf*-cells on only one side of Hybrid stem (17% dorsal and 0% ventral, Table 1).

2) *Xf* effects on carbon dynamics

The mean F_v/F_m values among all grapevines were between 0.77 - 0.79, with no significant difference between the *Xf* and control treatments except for the *Xf*-inoculated Chardonnay which had a mean F_v/F_m of 0.70 $\pm$0.009 which

was 9.8% lower than the control Chardonnay (0.77 ±0.004) ($T(32.7)= 6.6$, $p<0.05$, Fig. **2**). We were unable to obtain F_v/F_m values for the necrotic, scorched leaf margins.

The leaf capacity to fix carbon as PPFD increases, represented by the light response curves (LRC), was reduced in all *Xf*-inoculated grapevines (Fig. **3**). Likewise, the parameters estimated from the LRC model (Lobo *et al.*, 2013) were also one way or another affected in all *Xf*-grapevines. The predicted A_{max} was lower for all *Xf*-plants (Fig. **3**). *Xf*-inoculated Arizonica leaves had a lower mean dark-respiration (RD) and mean light compensation point (I_{comp}) compared to control leaves (RD $T(9.9)= 0.07$, $p= 0.94$; I_{comp} $T(9.9)= 0.9$, $p= 0.34$), contrasting with what was observed for the vinifera genotypes (Fig. **3**). Hybrid, Chardonnay, and Syrah tended to have higher mean RD and I_{comp} for the *Xf*-leaves compared to control leaves (Fig. **3**; Hybrid RD $T(6.3)= 2.2$, $p= 0.06$, I_{comp} $T(5.6)= 1.3$, $p= 0.23$; Chardonnay RD $T(5.9)= 0.2$, $p= 0.8$, I_{comp} $T(5.7)= 1.1$, $p= 0.28$; Syrah RD $T(7.4)= 1.0$, $p= 0.34$, I_{comp} $T(5.1)= 1.9$, $p= 0.11$). It is worth noting that the I_{comp} for the two PD-susceptible genotypes, Chardonnay and Syrah, were 32.1 ±11 and 58.0 ±19 μmol m^{-2} s^{-1}, respectively, being above the I_{comp} standard range for healthy, sun adapted leaves (10 to 20 μmol (photons) m^{-2} s^{-1}; Taiz *et al.*, 2015) whereas the controls and *Xf*-resistant genotypes leaves were mainly within the range.

We observed a general trend in which the mean net carbon assimilation rate (A_N) declined in all *Xf*-inoculated grapevines compared to their controls regardless of their level of resistance to PD (Fig. **4 a**). However, this reduction was greater for the PD-susceptible genotypes, with the mean A_N

decreasing by 65% in *Xf*-Chardonnay ($T(7.6)= 4.2$, $p<0.05$) and 54% in *Xf*-Syrah ($T(8.3)= 3.5$, $p<0.05$), compared to 18% in Arizonica ($T(9.9)= 0.9$, $p= 0.36$), and 39% in Hybrid ($T(9.4)= 3.0$, $p<0.05$). In addition, for *Xf*-inoculated Chardonnay and Syrah, the A_N reduction was accompanied by a decline in stomatal conductance (g_s), which means were reduced by 90% ($T(5.4)= 3.8$, $p<0.05$) and 52% ($T(6.7)= 4.6$, $p<0.05$) mmol m^{-2} s^{-1}, respectively (Fig. **4 b**). The *Xf*-resistant genotypes, however, had a contrasting g_s behavior, where the mean g_s of Arizonica and Hybrid increased by 14% ($T(5.4)= 0.39$, $p= 0.70$) and 3% ($T(9.2)= 0.008$, $p= 0.93$), respectively, compared to their controls (Fig. **4 b**). We found a positive association between A_N and g_s ($R^2 = 0.801$, $p< 0.01$; Fig. **4 c**). Both A_N and g_s declined in *Xf*-inoculated Chardonnay and Syrah compared to their controls; in contrast, A_N was reduced, but g_s increased in the *Xf*-inoculated Arizonica and Hybrid compared to their controls (Fig. **4 c**). Thus, indicating different responses to *Xf*-inoculation according to PD-resistance levels.

We quantified starch storage by two different methods, iodine-stained starch (histological) and enzymatically-measured starch concentrations (biochemical) and found a positive association between them ($R^2 = 0.566$, $p= 0.018$; Fig. **5 c**). This validates starch quantification via threshold imaging and suggests that both methods could be complementary to each other. The stem cross-sections showed that starch granules were almost exclusively stored in the ray parenchyma with very little starch granules present in the axial parenchyma in the xylem for all four genotypes (Fig. **6**). In the control cross-sections, the xylem ray parenchyma was fully stained, with starch filling the cells from the pith towards

the phloem (Fig. **6 a, c, e, g**), and the mean iodine-stained starch percent was 78 ±1.9 % across genotypes. For control cross-sections of individual genotypes, Hybrid and Chardonnay had the highest percentages of iodine-stained starch (91 ±0.7 and 92 ±0.8 %, respectively), followed by Arizonica (65 ±3.1 %), and then Syrah (64 ±4.7 %) (Fig. **5 a**). This same pattern was assessed with the biochemical assay; Hybrid and Chardonnay had the largest starch concentrations (122.7 ±2.8 and 117.4 ±5.2 mg g^{-1}, respectively), followed by Arizonica (25.8 ±6.9 mg g^{-1}), and then Syrah (16.1 ±7.7 mg g^{-1}) (Fig. **5 b**).

Xf-inoculated Arizonica and Hybrid cross-sections also had xylem ray parenchyma largely stained with starch (Figs. **6 b, d**). However, starch was sparse or absent in ray parenchyma of *Xf*-inoculated Chardonnay and Syrah cross-sections, with mean values of 45% ±4.3 ($T(24.5)= 10.6$, $p<0.05$) and 31% ±4.6 ($T(45.8)= 3.7$, $p<0.05$), respectively (Figs. **5 a** and **6 f, h**). Likewise, starch concentration decreased only in the PD-susceptible genotypes *Xf*-inoculated Chardonnay ($T(8.0)= 3.9$, $p<0.05$) and Syrah ($T(5.2)= 1.6$, $p= 0.14$, Fig. **5 b**) compared to their controls. Besides, *Xf*-inoculation led to increased starch concentrations in Arizonica (43.5 ±4.6 mg g^{-1} $T(8.7)= 2.1$, $p= 0.06$ Fig. **5 b**), which was also detected with the histological method (77 ±2.9 % ($T(45.8)= 2.6$, $p<0.05$, Fig. **5 a**). Lastly, the transverse sections between the four harvest points (0, 10, 25, and 50 cm, with 0 being the inoculation site) showed no difference in the iodine-stained starch percent for *Xf*-stems ($F(187)= 0.01$, $p= 0.89$), indicating that starch depletion was consistent along the length of the stem.

To determine whether the reduction in photosynthesis was

accompanied by starch depletion in the xylem, we calculated the percent change between the control and *Xf*-inoculated genotypes for the variables A_{max} and iodine-stained starch. Subsequently, we found a strong relationship between the percent change in A_{max} and the percent change of starch in the stem (R^2 = 0.798, p= 0.069; Fig. **7**). While the PD-resistant genotypes showed a distinct relationship, stored starch remained mostly unchanged (close to the point-zero) in Hybrid and increased in Arizonica. *Xf*-inoculation led to a decrease in both A_{max} and percent starch in both PD-susceptible genotypes Chardonnay and Syrah (both points on the negative percent change).

3) *Xf* effects on water transport

Mean xylem specific stem hydraulic conductivity (K_s) for control grapevine stems ranged from 3.66 $\pm$ 0.73 to 5.29 $\pm$1.53 Kg $s^{-1}m^{-1}MPa^{-1}$ (Fig. **8 a**); a relatively small statical variance of 6.81, when compared to the variance of 34.32 in the *Xf*-stems. The greatest variability in K_s was found in the *Xf*-inoculated Arizonica and Hybrid stems. Mean K_s in *Xf*-inoculated Chardonnay and Syrah were reduced by 69% (T(6.4)= 3.2, p<0.05) and 77% ((T(5.3)= 2.2, p<0.05), respectively, compared to their controls (Fig. **8 a**). In contrast, mean K_s increased in the *Xf*-inoculated Arizonica and Hybrid by 67% (T(8.2)= -1.3, p=0.20) and 68% (T(5.3)= 0.99, p=0.36), respectively, compared to their controls (Fig. **8 a**). Thus, indicating different responses to *Xf*-inoculation according to PD-resistance levels. We found a weak positive linear relationship between K_s and g_s for *Xf*-stems (R^2 = 0.192, p= 0.227; Fig. **8 b**). While *Xf* led to an increase in both K_s and g_s in *Xf*-

inoculated Arizonica, Hybrid only showed an increase in K_s, and the g_s did not change. Both PD-susceptible genotypes Chardonnay and Syrah showed significant declines in K_s and g_s after *Xf*-inoculation.

At 10 cm from the inoculation site, we found no evidence for tyloses in the control plants for any genotype, but tyloses production diverged according to PD-resistance in the *Xf*-inoculated plants ($F(44)= 2.1$, $p= 0.11$). Tyloses production was lower in Arizonica (11 ±2.9 %) and Hybrid (10 ±1.9 %) compared to Chardonnay (23 ±4.4 %) and Syrah (33 ±5.1% Fig **9**). A negative linear relationship between log-transformed K_s and the percentage of vessels occluded by tyloses ($R^2 = 0.926$, $p= 0.024$; Fig. **8 c**) indicated a strong association between the production of tyloses and decline in K_s for the PD-susceptible genotypes.

Discussion

The data presented here show the first conclusive relationship between the infection of grapevine stems by the bacterial pathogen *Xf* and the subsequent occlusion of the vascular system and its direct effects on hydraulic conductivity, photosynthesis, and stored starch. Our data build on a growing body of knowledge characterizing the various effects of this pathogen on the vascular system (Pérez-Donoso *et al.*, 2007, 2016; Choat *et al.*, 2009; Sun *et al.*, 2013; Deyett *et al.*, 2019; Ingel *et al.*, 2021; Fanton & Brodersen, 2021).

Fanton & Brodersen (2021) found that the mean maximum vessel length was nearly the same for Chardonnay and Hybrid (62 cm and 66 cm respectively) and support the data presented here on the distance that *Xf* was

observed from the inoculation site. *Xf*-cells were observed in Syrah, Chardonnay, and Hybrid at the most distal measurement of 50 cm from the inoculation site, suggesting that bacteria could achieve the longest unobstructed distance for migration in these long-vessel genotypes. Despite that the mean maximum vessel length for Arizonica was smaller (47 cm); in Hybrid and Arizonica, the presence of *Xf*-cells decreased as the distance from the inoculation site increased (Table 1), supporting the idea that *Xf* spreads systematically within the xylem network of only PD-susceptible genotypes (Fry & Milholland, 1990; Baccari & Lindow, 2011; Sun *et al.*, 2013).

In terms of photosynthetic capacity, chlorophyll fluorescence was only reduced compared to control plants in Chardonnay. Maximum efficiency of photosystem II (measured by the dark-adapted F_v/F_m) normally indicates abiotic stress level (Baker, 2008; Murchie & Lawson, 2013) and F_v/F_m declines has been shown under intense drought stress in grapevines (Pou *et al.*, 2012; Hochberg *et al.*, 2013). The F_v/F_m reduction for Chardonnay was not surprising given that it is highly susceptible to PD (Varela *et al.*, 2001; Krivanek & Walker, 2005), although the exact mechanism for this decline is still unknown and further investigations are needed regarding, for example, PSII electron transport rate. We found that the *Xf*-inoculated grapevines showed declines in A_N compared to the controls (Figs. **3** and **4**). Furthermore, respiration rates were increased in Chardonnay, Syrah, and Hybrid, suggesting that greater resources were required to produce a hyper-immune response.

These lower A_N findings are ultimately reflected in starch storage in

the stem, specifically for the *Xf*-inoculated Chardonnay and Syrah which showed declines in both the percent of iodine-stained starch and enzymatically-derived starch concentrations. Overall, we found a strong relationship between A_N and iodine-stained starch in the stem (Fig. **7**). Recent work has shown that *Xf*-inoculated PD-susceptible Cabernet Sauvignon down-regulated the genes related to the photosynthetic metabolism (i.e., chlorophyll biosynthesis and thylakoid organization and biogenesis) and up-regulated genes related to carbohydrate, starch, and sucrose metabolism (Ingel *et al.*, 2021). Together, these data support the idea that reductions in hydraulic conductivity impose stomatal limitations, which then in turn lead to reduced photosynthesis, and ultimately leads to starch depletion in the xylem of the PD-susceptible genotypes Chardonnay and Syrah. The grapevines were able to use stored starch to compensate for reduced carbon assimilation and to support C-demanding processes like the higher rates of respiration associated with *Xf* infection. Indeed, this mechanistic link has been well established for abiotic stress, such as drought stress when xylem water transport is hampered and initiates a period of negative carbon balance and ultimately carbon starvation (McDowell, 2011; Hartmann & Trumbore, 2016; Martínez-Vilalta *et al.*, 2016)), but has been less studied in the context of biotic stress like pests and disease. However, starch depletion is not unique to PD, as similar responses have been reported in grapevines with the vascular fungal pathogen *Phaeomoniella chlamydospora* (Pouzoulet *et al.*, 2017).

Our K_s data showed two distinct responses to the *Xf* infection process. The increase in K_s in the *Xf*-inoculated Arizonica and Hybrid compared to

their controls can be attributed to two factors. First, stem length; we used the complete stem (mean 84 ±0.01 cm) in our hydraulics experiments, while in other studies, the stem segment length was much shorter (15 to 30 cm; Sun *et al.*, 2013; Deyett *et al.*, 2019). This difference in stem length could change the measured K_s since most of the tyloses were observed close to the inoculation site in all studies. Second, the lower production of tyloses in *Xf*-inoculated Arizonica and Hybrid led to more open xylem conduits that were apparently more hydraulically efficient. We also observed the greatest variability in *Xf*-stems of Arizonica and Hybrid, suggesting that there may be a more delayed or variable response to the presence of *Xf* in these PD-resistance genotypes. In addition, the increase in K_s was perhaps due to pit membrane pore enlargement that was more effectively accomplished by *Xf* than by experimental digestion in Fanton & Brodersen, (2021). *Xf* is capable of secreting different cell wall digesting enzymes on its biofilm that breach the pit membrane, and it has been suggested that it can use the pit membrane debris as a nutrient source on its migration path (Roper *et al.*, 2007; Chatterjee *et al.*, 2008; Ingel *et al.*, 2019). Consequently, it leaves behind an enlarged pit membrane pore that decreases the resistance of the intervessel connections to water transport, thereby increasing K_s.

Conclusion

We have taken a comprehensive approach to examine the different mechanisms of *Xf*-induced mortally in grapevine genotypes. These data supported our proposed hypothesis regarding the systematic link between loss of hydraulic

conductivity with the production of tyloses and the downstream effects on photosynthesis and net carbon gain. Therefore, we conclude that there is a direct link between the disruption in xylem transport limiting water supplies to the foliage for photosynthesis and gas exchange in the PD-susceptible genotypes. However, additional work is needed to better understand the dynamics of starch and other NSCs (e.g., sugars and lipids) in the xylem in response to the *Xf*-infection process. Our results suggest that one reason for starch depletion is to sustain the infected plants under reduced carbon assimilation and increased respiration rates. Overall, future research efforts that compare resistant and susceptible genotypes, especially those combining tools from physiology and molecular biology, will help determine the mechanism of *Xf*-induced mortality and *Xf*-resistance in grapevines and other important crops.

Acknowledgements

I would like to thank the coauthors: Morgan Furze and Craig Brodersen. I thank Dr. Andy Walker for providing the grapevines plants and Dr. Carolina Roper for providing the *Xylella fastidiosa* cells and both for corresponding with the authors. As well as Dr. Claudia Castro and Dr. Cintia Sagawa for their support with *X. fastidiosa* handling.

References

Adams HD, Zeppel MJB, Anderegg WRL, Hartmann H, Landhäusser SM, Tissue DT, Huxman TE, Hudson PJ, Franz TE, Allen CD, et al. 2017. A multi-species synthesis of physiological mechanisms in drought-induced tree mortality. Nature Ecology & Evolution 1: 1285–1291.

Baccari C, Lindow SE. 2011. Assessment of the process of movement of *Xylella fastidios*a within susceptible and resistant grape cultivars. Phytopathology 101: 77–84.

Baker NR. 2008. Chlorophyll fluorescence: a probe of photosynthesis in vivo. Annual Review of Plant Biology 59: 89–113.

Buzombo P, Jaimes J, Lam V, Cantrell K, Harkness M, McCullough D, Morano L. 2006. An American hybrid vineyard in the Texas Gulf Coast: analysis within a Pierce's disease hot zone. Am. J. Enol. Vitic 57: 347–355.

Chatterjee S, Almeida RPP, Lindow S. 2008. Living in two worlds: the plant and insect lifestyles of *Xylella fastidiosa*. Annual Review of Phytopathology 46: 243–271.

Choat B, Brodribb TJ, Brodersen CR, Duursma RA, López R, Medlyn BE. 2018. Triggers of tree mortality under drought. Nature 558: 531–539.

Choat B, Gambetta GA, Wada H, Shackel KA, Matthews MA. 2009. The effects of Pierce's disease on leaf and petiole hydraulic conductance in *Vitis vinifera* cv. Chardonnay. Physiologia Plantarum 136: 384–394.

Davis MJ, French WJ, Schaad NW. 1981. Axenic culture of the bacteria associated with phony disease of peach and plum leaf scald. Current Microbiology 6: 309–314.

Deyett E, Pouzoulet J, Yang J -I., Ashworth VE, Castro C, Roper MC, Rolshausen PE. 2019. Assessment of Pierce's disease susceptibility in *Vitis vinifera* cultivars with different pedigrees. Plant Pathology 68: 1079–1087.

Earles JM, Knipfer T, Tixier A, Orozco J, Reyes C, Zwieniecki MA, Brodersen CR, McElrone AJ. 2018. In vivo quantification of plant starch reserves at micrometer resolution using x-ray microCT imaging and machine learning. New Phytologist 218: 1260–1269.

EFSA. 2020. Update of the Xylella spp. host plant database. EFSA Journal 18.

Fanton AC, Brodersen C. 2021. Hydraulic consequences of enzymatic breakdown of grapevine pit membranes. Plant Physiology: kiab191.

Feil H, Purcell AH. 2001. Temperature-dependent growth and survival of *Xylella fastidiosa* in vitro and in potted grapevines. Plant Disease 85: 1230–1234.

Fry SM, Milholland RD. 1990. Multiplication and translocation of *Xylella fastidiosa* in petioles and stems of grapevine resistant, tolerant, and susceptible to Pierce's disease. Phytopathology 80: 61.

Hartmann H, Trumbore S. 2016. Understanding the roles of nonstructural carbohydrates in forest trees – from what we can measure to what we want to know. New Phytologist 211: 386–403.

Hill BL, Purcell AH. 1995. Multiplication and movement of *Xylella fastidiosa* within grapevine and four other plants. Phytopathology 85: 1368.

Hochberg U, Degu A, Fait A, Rachmilevitch S. 2013. Near isohydric grapevine cultivar displays higher photosynthetic efficiency and photorespiration rates under drought stress as compared with near anisohydric grapevine cultivar. Physiologia Plantarum 147: 443–452.

Hopkins DL, Purcell AH. 2002. *Xylella fastidiosa*: cause of Pierce's disease of grapevine and other emergent diseases. Plant Disease 86: 1056–1066.

Ingel B, Jeske DR, Sun Q, Grosskopf J, Roper MC. 2019. *Xylella fastidiosa* endoglucanases mediate the rate of Pierce's disease development in Vitis vinifera in a cultivar-dependent manner. Molecular Plant-Microbe Interactions 32: 1402–1414.

Ingel B, Reyes C, Massonnet M, Boudreau B, Sun Y, Sun Q, McElrone AJ, Cantu D, Roper MC. 2021. *Xylella fastidiosa* causes transcriptional shifts that precede tylose formation and starch depletion in xylem. Molecular Plant Pathology 22: 175–188.

Krivanek AF, Riaz S, Walker MA. 2006. Identification and molecular mapping of PdR1, a primary resistance gene to Pierce's disease in *Vitis*. Theoretical and Applied Genetics 112: 1125–1131.

Krivanek AF, Walker MA. 2005. *Vitis* resistance to Pierce's disease is characterized by differential *Xylella fastidiosa* populations in stems and leaves. Phytopathology 95: 44–52.

Landhäusser SM, Chow PS, Dickman LT, Furze ME, Kuhlman I, Schmid S, Wiesenbauer J, Wild B, Gleixner G, Hartmann H, et al. 2018. Standardized protocols and procedures can precisely and accurately quantify non-structural carbohydrates (M Mencuccini, Ed.). Tree Physiology 38: 1764–1778.

Lobo F de A, de BARROS MP, Dalmagro HJ, Dalmolin ÂC, Pereira WE, de SOUZA ÉC, Vourlitis GL, Ortíz CER. 2013. Fitting net photosynthetic light-response

curves with Microsoft Excel – a critical look at the models. Photosynthetica 51: 445–456.

Martínez-Vilalta J, Sala A, Asensio D, Galiano L, Hoch G, Palacio S, Piper FI, Lloret F. 2016. Dynamics of non-structural carbohydrates in terrestrial plants: a global synthesis. Ecological Monographs 86: 495–516.

McCarthy EL. 1934. Mariotte's bottle. Science 80: 100–100.

McDowell NG. 2011. Mechanisms linking drought, hydraulics, carbon metabolism, and vegetation mortality. Plant Physiology 155: 1051–1059.

McDowell NG, Beerling DJ, Breshears DD, Fisher RA, Raffa KF, Stitt M. 2011. The interdependence of mechanisms underlying climate-driven vegetation mortality. Trends in Ecology & Evolution 26: 523–532.

McElrone AJ, Jackson S, Habdas P. 2008. Hydraulic disruption and passive migration by a bacterial pathogen in oak tree xylem. Journal of Experimental Botany 59: 2649–2657.

McElrone AJ, Sherald JL, Forseth IN. 2003. Interactive effects of water stress and xylem-limited bacterial infection on the water relations of a host vine. Journal of Experimental Botany 54: 419–430.

Meng Y, Li Y, Galvani CD, Hao G, Turner JN, Burr TJ, Hoch HC. 2005. Upstream migration of *Xylella fastidiosa* via pilus-driven twitching motility. Journal of Bacteriology 187: 5560–5567.

Murchie EH, Lawson T. 2013. Chlorophyll fluorescence analysis: a guide to good practice and understanding some new applications. Journal of Experimental Botany 64: 3983–3998.

Newman KL, Almeida RPP, Purcell AH, Lindow SE. 2003. Use of a green fluorescent strain for analysis of *Xylella fastidiosa* colonization of Vitis vinifera. Applied and Environmental Microbiology 69: 7319–7327.

Pérez-Donoso AG, Greve LC, Walton JH, Shackel KA, Labavitch JM. 2007. *Xylella fastidiosa* infection and ethylene exposure result in xylem and water movement disruption in grapevine shoots. Plant Physiology 143: 1024–1036.

Pérez-Donoso AG, Lenhof JJ, Pinney K, Labavitch JM. 2016. Vessel embolism and tyloses in early stages of Pierce's disease. Australian Journal of Grape and Wine Research 22: 81–86.

Pinheiro C, Chaves MM. 2011. Photosynthesis and drought: can we make metabolic connections from available data? Journal of Experimental Botany 62: 869–882.

Pou A, Medrano H, Tomàs M, Martorell S, Ribas-Carbó M, Flexas J. 2012. Anisohydric behaviour in grapevines results in better performance under moderate water stress and recovery than isohydric behaviour. Plant and Soil 359: 335–349.

Pouzoulet J, Scudiero E, Schiavon M, Rolshausen PE. 2017. Xylem vessel diameter affects the compartmentalization of the vascular pathogen *Phaeomoniella chlamydospora* in grapevine. Frontiers in Plant Science 8: 1442.

Redak RA, Purcell AH, Lopes JRS, Blua MJ, Mizell III RF, Andersen PC. 2004. The biology of xylem fluid–feeding insect vectors of *Xylella fastidiosa* and their relation to disease epidemiology. Annual Review of Entomology 49: 243–270.

Roper C, Castro C, Ingel B. 2019. *Xylella fastidiosa*: bacterial parasitism with hallmarks of commensalism. Current Opinion in Plant Biology 50: 140–147.

Roper MC, Greve LC, Warren JG, Labavitch JM, Kirkpatrick BC. 2007. *Xylella fastidiosa* requires polygalacturonase for colonization and pathogenicity in Vitis vinifera grapevines. Molecular Plant-Microbe Interactions 20: 411–419.

Sala A, Woodruff DR, Meinzer FC. 2012. Carbon dynamics in trees: feast or famine? Tree Physiology 32: 764–775.

Sevanto S, Mcdowell NG, Dickman LT, Pangle R, Pockman WT. 2014. How do trees die? A test of the hydraulic failure and carbon starvation hypotheses. Plant, Cell & Environment 37: 153–161.

Smith MG, Arndt SK, Miller RE, Kasel S, Bennett LT. 2018. Trees use more non-structural carbohydrate reserves during epicormic than basal resprouting (M Ryan, Ed.). Tree Physiology 38: 1779–1791.

Sperry JS, Donnelly JR, Tyree MT. 1988. A method for measuring hydraulic conductivity and embolism in xylem. Plant, Cell and Environment 11: 35–40.

Sperry JS, Hacke UG, Oren R, Comstock JP. 2002. Water deficits and hydraulic limits to leaf water supply. Plant, Cell & Environment 25: 251–263.

Sun Q, Rost TL, Reid MS, Matthews MA. 2007. Ethylene and not embolism is required for wound-induced tylose development in stems of grapevines. Plant Physiology 145: 1629–1636.

Sun Q, Sun Y, Walker MA, Labavitch JM. 2013. Vascular occlusions in grapevines with Pierce's disease make disease symptom development worse. Plant Pathology 161: 1529–1541.

Taiz L, Zeige E, Moller I, Murphy A. 2015. Plant physiology and development. Sunderland, Massachusetts: Sinauer Associates Inc.

Tumber KP, Alston JM, Fuller KB. 2014. Pierce's disease costs California $104 million per year. California Agriculture 68: 20–29.

Varela LG, Smith RJ, Phillips PA. 2001. Pierce's disease. Oakland, CA: University of California, Division of Agricultural and Natural Resources.

Wells JM, Raju BC, Hung H-Y, Weisburg WG, Mandelco-Paul L, Brenner DJ. 1987. *Xylella fastidiosa* gen. nov., sp. nov: gram-negative, xylem-limited, fastidious plant bacteria related to *Xanthomonas* spp. International Journal of Systematic Bacteriology 37: 136–143.

Table 1. Percentage of plants (n=6 plants per genotype) that had *Xf*-cells present at four different distances above the inoculation site (0, 10, 25, 50 cm, with 0 being the inoculation site) following inoculation with *Xf* on the dorsal and ventral sides of the stem.

Distance	Arizonica		Hybrid		Chardonnay		Syrah	
(cm)	dorsal	ventral	dorsal	ventral	dorsal	ventral	dorsal	ventral
0	100%	100%	100%	100%	100%	100%	100%	100%
10	67%	50%	100%	67%	100%	100%	100%	100%
25	50%	17%	83%	0%	100%	100%	100%	100%
50	0%	0%	17%	0%	100%	100%	100%	100%

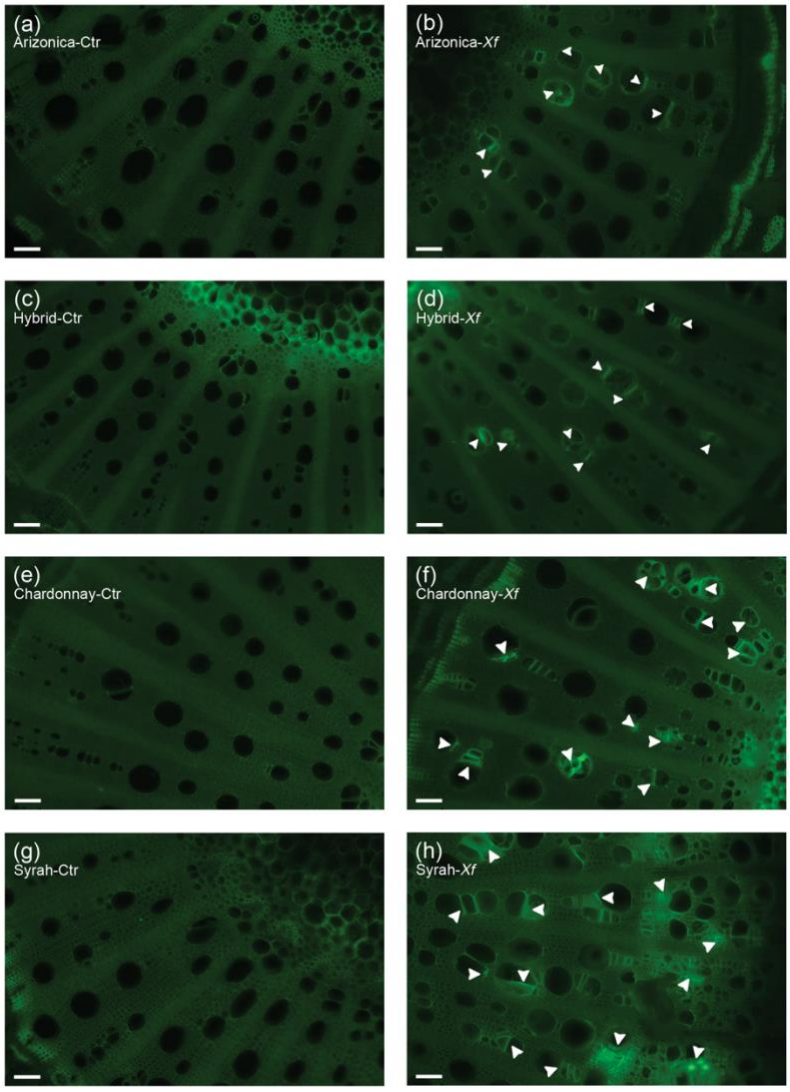

Figure 1. Representative xylem cross-sections of mock-inoculated (left column) and *Xf*-inoculated (right column) stems at 10 cm above the inoculation site for the four grapevine genotypes (**a-b**) Arizonica, (**c-d**) Hybrid, (**e-f**) Chardonnay, and (**g-h**) Syrah. (**a-d)** are PD-resistant, and (**e-h)** are PD-susceptible. Arrowheads indicate GFP-*Xf* cells (n=48 plants). Bar = 100 µm.

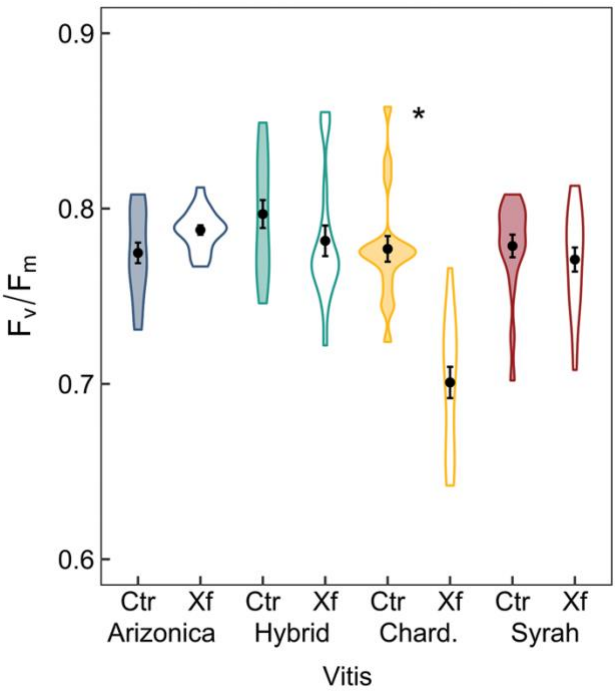

Figure 2. Mean photosynthetic efficiency (F_v/F_m) for control (filled) and *Xf*-inoculated (open) grapevine leaves. *Xf*-leaves were only symptomatic in the PD-susceptible genotypes (Chardonnay and Syrah). Points represent the mean ±SE, violin shades are the data distribution (n=18 leaves per genotype per treatment). Asterisks indicate a significant difference between *Xf*-inoculated and control plants for each genotype based on two sample t tests.

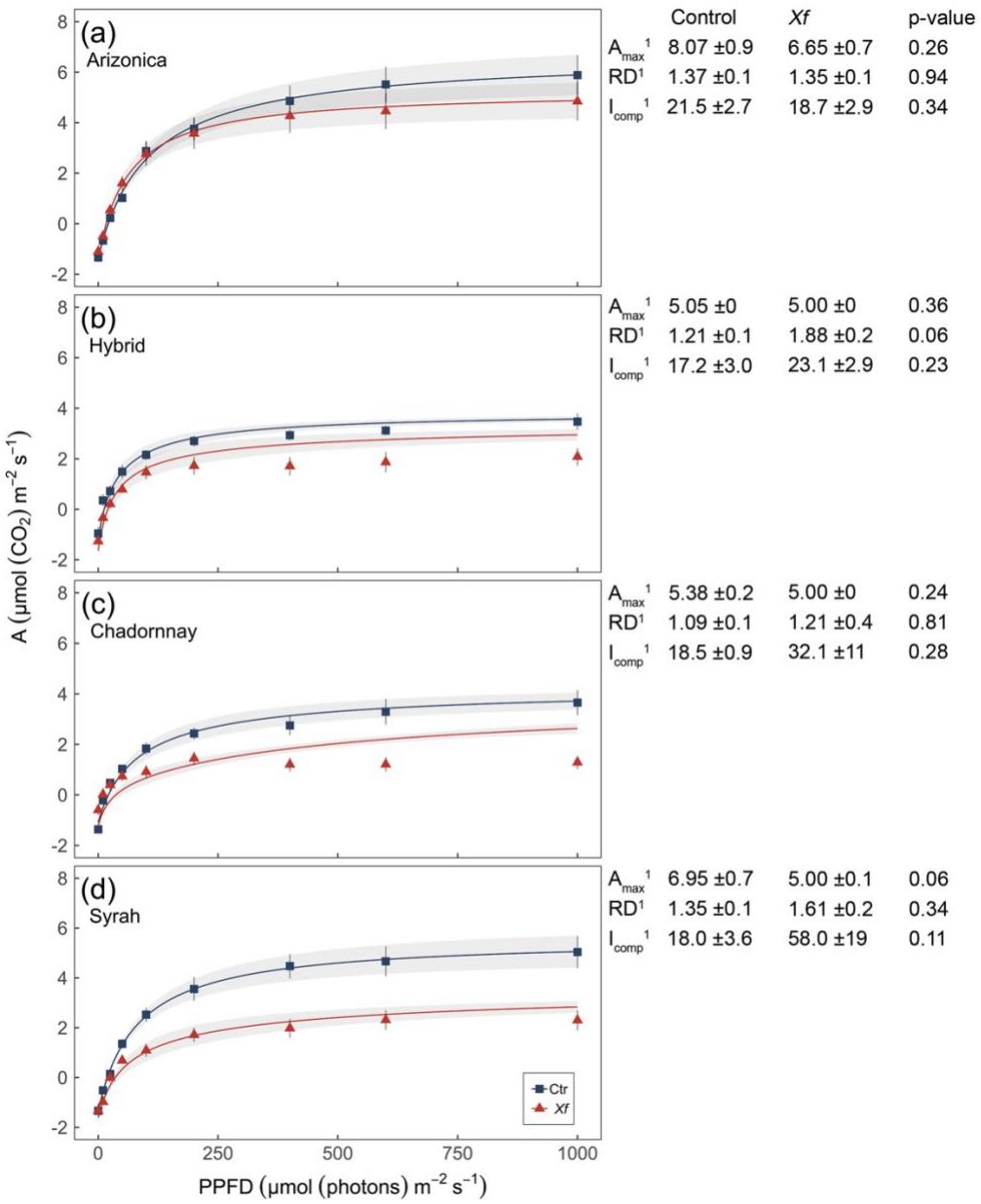

Figure 3. Response of photosynthesis (A) to increasing light intensity (PPFD) for control (blue) or *Xf*-inoculated (red) grapevines for four genotypes (**a**) Arizonica, (**b**) Hybrid, (**c**) Chardonnay, and (**d**) Syrah. Points are measured A (mean ±SE) and lines are modelled curves (mean ±SE). On the right, parameters estimated from the LRC model are displayed; A_{max} is the maximum photosynthetic rate in μmol (CO_2) m^{-2} s^{-1}, RD is the dark respiration rate in μmol (CO_2) m^{-2} s^{-1}, and I_{comp} is the light compensation point in μmol (photons) m^{-2} s^{-1}. *Xf*-leaves were symptomatic in PD-susceptible genotypes (Chardonnay and Syrah). [1]Mean ±SE (n=6 leaves per genotype per treatment), and p-values are from two sample t tests between *Xf*-inoculated and control plants for each genotype.

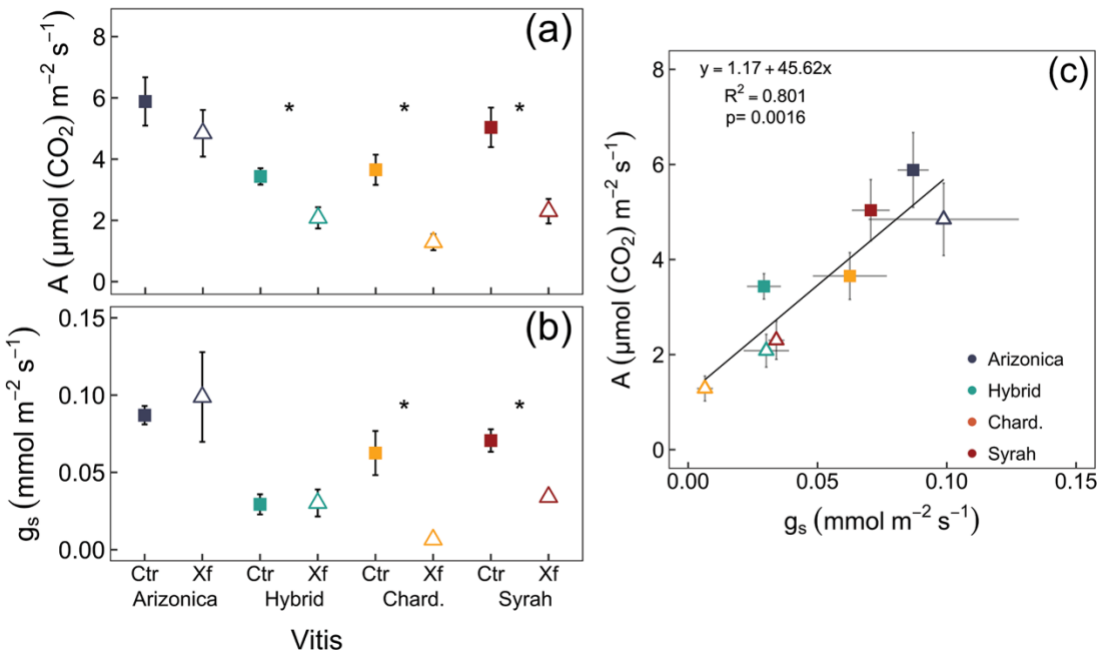

Figure 4. (**a**) Mean carbon assimilation rate (A); (**b**) mean gas exchange rate (g_s); and (**c**) relationship between A_N and gs for control (squares) and *Xf*-inoculated (triangles) grapevines. *Xf*-leaves were symptomatic in the PD-susceptible genotypes (Chardonnay and Syrah). Points represent the mean ±SE (n=6 plants per genotype per treatment). In (**a**) and (**b**), asterisks indicate a significant difference between *Xf*-inoculated and control plants for each genotype based on two sample t tests.

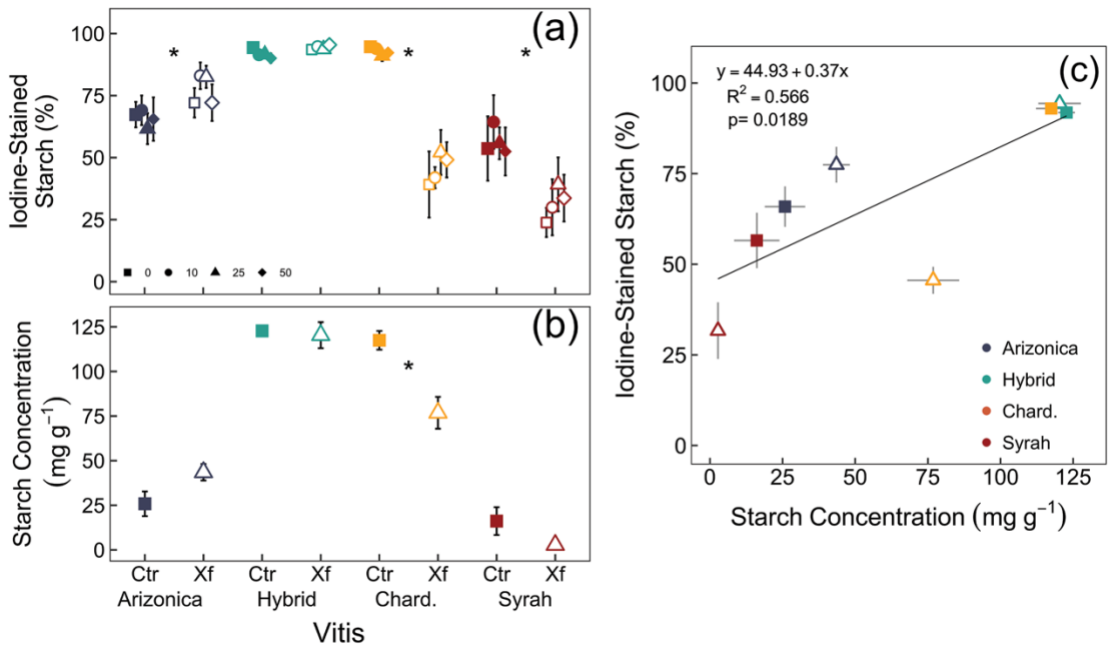

Figure 5. (**a**) Mean percent iodine-stained starch in xylem ray parenchyma at four different distances above the inoculation site (0, 10, 25, and 50 cm, with 0 being the inoculation site) quantified via threshold imaging. (**b**) Mean starch concentration in the xylem tissue measured enzymatically. (**c**) Relationship between both methods histological and biochemical (iodine-stained starch and starch concentration, respectively) on control (squares) and *Xf*-inoculated (triangles) grapevines. Points represent the mean ±SE (n=6 plants per genotype per treatment). In (**a**) and (**b**), asterisks indicate a significant difference between *Xf*-inoculated and control plants for each genotype based on two sample t test.

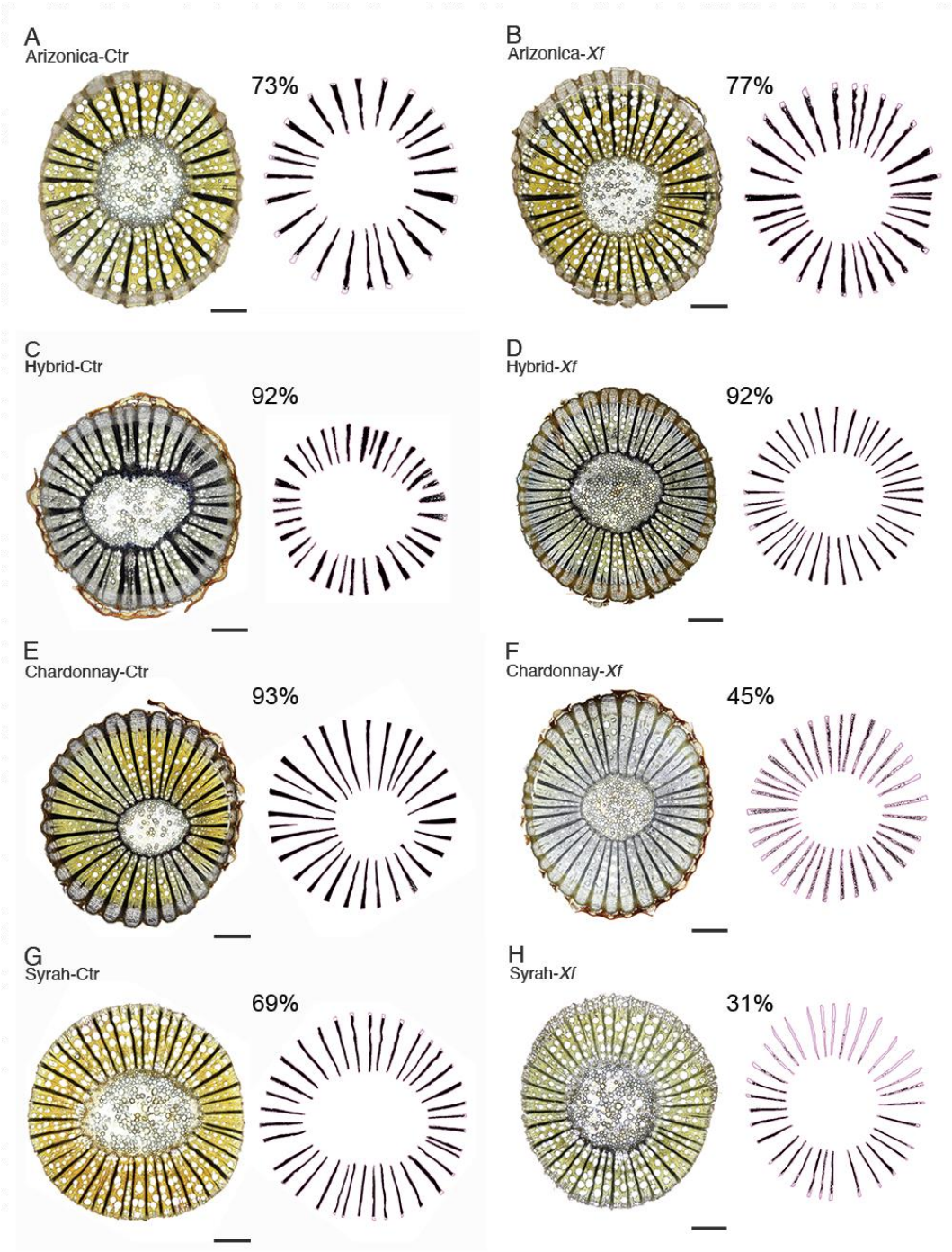

Figure 6. Representative xylem cross-section of control (left) and *Xf*-inoculated (right) stems at 10 cm above the inoculation site four grapevine genotypes (**a-b**) Arizonica, (**c-d**) Hybrid, (**e-f**) Chardonnay, and (**g-h**) Syrah. First and third columns show the imaged cross-sections. Second and fourth columns show the same images with ray traced and starch identified via thresholding in Image J. This thresholding procedure was used to quantify the percent of starch in ray cells in the xylem. Bar = 500 µm.

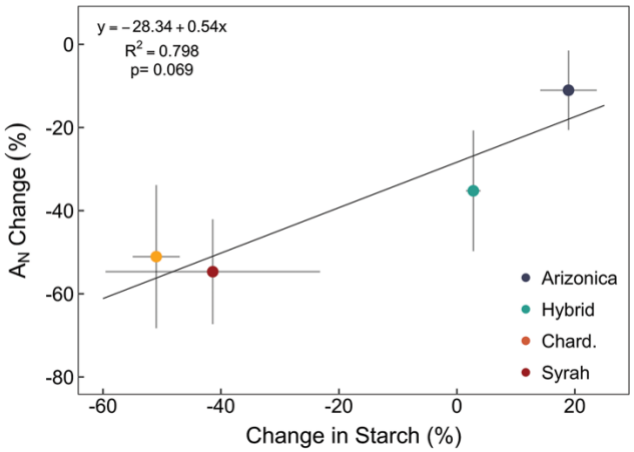

Figure 7. Relationship between the *Xf*-induced percent change in both A_{max} and iodine-stained starch. Points (circles) represent the percent changes between both treatments ±SE (n=12 plants per genotype).

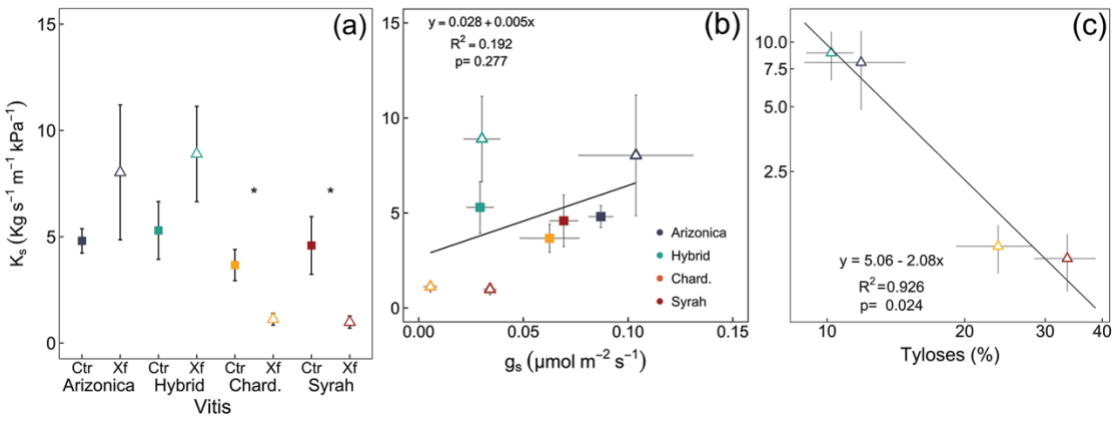

Figure 8. (**a**) Mean specific stem hydraulic conductivity (K_s); (**b**) relationship between K_s and g_s for control (squares) and *Xf*-inoculated (triangles) grapevines; and (**c**) relationship between K_s and percent of tyloses for *Xf*-inoculated (triangles) grapevines, both axes are in log-scale. Points represent the mean ±SE (n=6 plants per genotype per treatment). In (**a**), asterisks indicate a significant difference between *Xf*-inoculated and control plants for each genotype based on two sample t test.

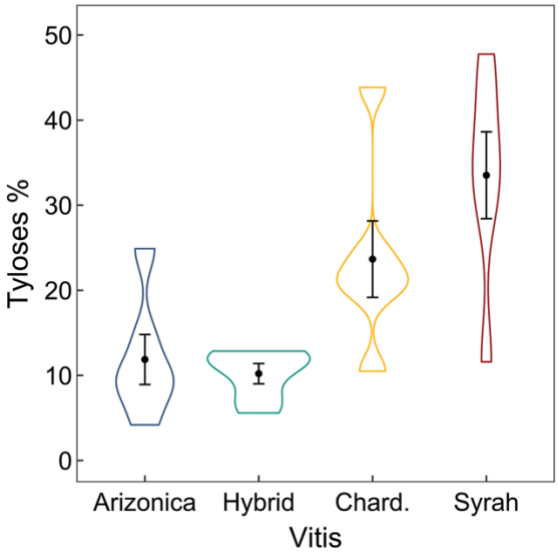

Figure 9. Percent of tyloses in the xylem vessels at 10 cm above the inoculation site of *Xf*-inoculated grapevines. Points represent the mean ±SE, violin shades are the data distribution (n=6 plants per genotype).

Concluding Remarks

Pierce's Disease (PD) is chronic problem in the wine and table grape industry in the USA. Managing PD in vineyards is very difficult as a variety of unsuccessful control measures have been attempted, such as, insecticides targeting the vectors, removal of sick grapevines and 'alternative hosts', and minimization of abiotic stresses (e.g., drought and nutrient deficiency). Nevertheless, these management strategies are unsustainable for long-term use and not effective. As we do not have an effective remedy against the *Xylella fastidiosa* (*Xf*) bacterium, a more accurate understanding of how some grapevines resist to the infection process is one piece of this very important puzzle.

My dissertation explored the roles of the xylem structure and function on the PD mechanisms of resistance. It investigated the mechanisms behind grapevine mortality, by showing a conclusive relationship between *Xf*-infection and a coordinated decline in photosynthesis, starch storage, and stem hydraulics only on the PD-susceptible grapevines genotypes. It also targeted xylem anatomical traits that could have led to PD resistance by restricting the *Xf* spread.

Collectively this work provided knowledge characterizing the PD resistance traits, thus building on a growing body of knowledge on the understanding of this pathosystem. It is my hope that my dissertation work motivates further research into expanding our knowledge in this complex pathosystem. As such, I suggest two key areas for future research:

(1) as the mechanisms of resistance are more like to be connected to the living cells of the xylem, future studies should focus on flavonoids or proteins present in the xylem sap. Comparing then whether a new production of secondary compounds followed inoculation among different grapevines genotypes.

(2) additional work is also needed to better understand the dynamics of starch and other NSCs (e.g., sugars and lipids) in the xylem in response to the *Xf*-infection process. Whether starch was depleted to support to photosynthesis decline or to support tyloses formation.

Overall, future research efforts should compare resistant and susceptible genotypes, especially those combining tools from physiology and molecular biology, will help determine the mechanism of *Xf*-induced mortality and *Xf*-resistance in grapevines and other important crops.